AD A014496

Report No. G-D-34-75
Task No. 4111.6.5

12

LB

DEVELOPMENT OF FAST CURRENT OIL RESPONSE SYSTEM

N. P. TRENTACOSTE

DDC
RECEIVED
SEP 15 1975
C

MARCH 1975

FINAL REPORT

Document is available to the public through the
National Technical Information Service,
Springfield, Virginia 22161

Prepared for

DEPARTMENT OF TRANSPORTATION
UNITED STATES COAST GUARD
Office of Research and Development
Washington, D.C. 20590

This document is disseminated under the sponsorship of the Department of Transportation in the interest of information exchange. The United States Government assumes no liability for its content or use thereof.

The contents of this report do not necessarily reflect the official view or policy of the Coast Guard, and they do not constitute a standard, specification or regulation.

This report, or portions thereof, may not be used for advertising publication, or promotional purposes. Citation of trade names and manufacturers does not constitute endorsements or approval of such products.

W. L. KING
Captain, U. S. Coast Guard
Chief, Environmental and
Transportation Technology Division
Office of Research and Development
U. S. Coast Guard Headquarters
Washington, D. C. 20590

Technical Report Documentation Page

1. Report No.	2. Government Accession No.	3. Recipient's Catalog No.
USCG-D-34-75	N/A	

4. Title and Subtitle
Development of Fast Current Oil Response System
Phase I - Concept Feasibility Study

5. Report Date
Mar 75

6. Performing Organization Code
N/A

7. Author(s)
Nicholas P. Trentacoste

8. Performing Organization Report No.
SAI-74-638-WA

9. Performing Organization Name and Address
Science Applications, Inc.
1600 Anderson Road
McLean, Virginia 22101

10. Work Unit No. (TRAIS)
4111.6.5

11. Contract or Grant No.
DOT-CG-40216-A

13. Type of Report and Period Covered
Final Report.

12. Sponsoring Agency Name and Address
Department of Transportation
United States Coast Guard
Office of Research and Development
Washington, D.C. 20590

14. Sponsoring Agency Code
G-DET-1

15. Supplementary Notes

DDC
SEP 15 1975

16. Abstract

The primary objective of this work was to demonstrate the feasibility of a new oil control/recovery system concept in a fast current environment. This system consists of two basic components, the control function (a vented hydrofoil) and a recovery function (a rotating belt of polyurethane foam). The system is operated in the following manner: A thin layer of oil and water is separated by and passes over the top of the lead hydrofoil. A large portion of the remaining water in the oil/water layer is vented through a slot which separates the leading hydrofoil from the main hydrofoil. The remaining oil/water flow, which now contains a higher concentration of oil, passes over the main hydrofoil and is directed by a small ramp, placed at the rear of the main hydrofoil, tangentially onto the rotating belt of polyurethane foam. The water drains through the foam belt while retaining the oil until it is squeezed out and pumped to a storage container. Numerous experiments were performed with both small and full scale models in calm, wavy and choppy water conditions. Deficiencies in the full scale hardware design limited the device's operation to a small range of velocities (4.0 ± 0.5 fps); however, an 80% overall throughput efficiency (oil recovered/oil delivered) was achieved with this particular model design. Therefore, the results of this study have shown that the vented hydrofoil/polyurethane foam belt oil control/recovery system is a viable one.

17. Key Words	18. Distribution Statement
Oil control and recovery, currents, waves	Document is available to the public through the National Technical Information Service, Springfield, Virginia 22151

19. Security Classif. (of this report)	20. Security Classif. (of this page)	21. No. of Pages	22. Price
UNCLASSIFIED	UNCLASSIFIED	175	

Form DOT F 1700.7 (8-72) Reproduction of completed page authorized

408 404

TABLE OF CONTENTS

TABLE OF CONTENTS

LIST OF FIGURES

LIST OF FIGURES (Continued)

LIST OF FIGURES (Continued)

LIST OF FIGURES (Continued)

LIST OF FIGURES (Continued)

LIST OF FIGURES (Continued)

LIST OF FIGURES (Continued)

LIST OF TABLES

LIST OF SYMBOLS

$F = V_1/\sqrt{gL}$ (Froude number)

V_1 = Free stream velocity

g = Acceleration of gravity

L = Characteristic length of the hydrofoil (thickness, chord, etc.)

T = Maximum thickness of hydrofoil

$G_B = gB/V_1^2$

B = Freeboard - height of the highest point on the hydrofoil above the undisturbed free surface far upstream

$G_{11} = gY_1/V_1^2$

Y_1 = Depth of stagnation streamline beneath the free surface far upstream

$G_{13} = gY_3/V_1^2$

Y_1 = Depth of stagnation streamline beneath the free surface far upstream

$G_{13} = gY_3/V_1^2$

Y_3 = Depth of flow over highest point on hydrofoil

m = Meters

mm = Millimeters

cm = Centimeters

l = Liters

cs = Centistokes

ft = Feet

in = Inches

sec = Seconds

fps = Feet per second

GPM = Gallons per minute

Hg = Mercury

SECTION 1

Introduction

1.1 Background

During the past several years, numerous concepts have been proposed to control and recover oil slicks. However, existing technology has only been successful in controlling and recovering oil slicks in an environment for which the water current does not exceed approximately 1.0 knot. Recent experience has shown that many oil spills have occurred in environments (coastal waters, rivers, bays, harbors, estuaries, etc.) for which the current has been in excess of 1.0 knot and usually less than 10.0 knots. These oil spill events have resulted in considerable damage to the local environment because adequate technology was not available to ameliorate the spill. The primary purpose of the present program is to develop a fast current oil response system to deal with these latter oil spill situations.

After reviewing much of the literature[1] concerned with the control and recovery of fast current oil slicks, it was found that no single technique was completely successful over a wide range of test conditions. Several of the oil slick control and recovery mechanisms relied principally on dissipating or diverting a significant fraction of the

---

[1] Hale, L. A., Norton, D. J., and Rodenberger, C. A., "The Effects of Current and Waves on an Oil Slick Retained By a Barrier," USCG Report CG-D-53-75, April, 1974.

mean kinetic energy of the oil-water flow. Even if this task could be accomplished with a device of reasonable length, a large fraction of the mean kinetic energy of the flow would be converted into turbulence. This turbulence in the flow would induce mixing and entrainment of the oil in the water column, thus inhibiting the control/recovery function. Moreover, such devices are cumbersome and present handling and logistics problems in their deployment. Other techniques such as the oleophilic belt and surface penetrating blade belong to a class of devices that actively utilize a portion of the oil-water flow energy to perform the control/recovery function. The oleophilic belt relies upon the kinetic energy of the flow to force the oil into the pores of the foam belt. In a similar sense, the kinetic energy of the flow is converted into potential energy by the lifting mechanism associated with the surface penetrating blade. The fundamental concept of utilizing a portion of the kinetic energy of the oil-water stream, rather than dissipating it, is attractive from the standpoint of control/recovery device development. However, a fast current oil control/recovery system that utilizes the most favorable aspects of a combination of mechanisms appears to have the best chance of operating successfully in a fast current environment. This eclectic approach is the basis for the proposed fast current oil response system.

1.2 Discussion of the Control/Recovery Concepts

The primary objective of the Phase I program was to demonstrate concept feasibility in the fast current ($\leq$10.0 knots) environment. In order to achieve this objective, the SAI system has evolved, through a series of

modifications, to a device substantially different in operating principle from what was initially proposed.

1.2.1 Original Control/Recovery System - The originally proposed fast current oil control/recovery device was composed of four basic subsystems: (1) hydrofoil, (2) air jet, (3) rotating belt of oleophilic and hydrophobic material and (4) oil storage and water drain system. These four subsystems are shown schematically in Figure 1.1. The complete system operates in the following way: a thin layer of water and oil is removed from the larger body of water by the presence of the hydrofoil; as the layer of water and oil traverses the hydrofoil, a portion of the remaining water is aspirated through the hydrofoil and is deposited in the flow region on the bottom rear of the hydrofoil. The remaining oil-water flow (on the top surface) continues down the hydrofoil until it is intercepted by the air jet which separates it from the surface and produces a fine droplet oil/water spray. The spray is then directed toward the rotating oleophilic and hydrophobic belt where the oil is adsorbed onto the surface and the water drains through and is collected in a drain pipe and deposited into the main body of water. The oil that has been collected by the rotating belt is then squeezed out and pumped to a storage container. The following is a detailed discussion of each subsystem.

(a) Hydrofoil

The hydrofoil has been designed so that its stagnation streamline is located below the oil-water interface; in this way, no flow from above can vertically traverse the stagnation streamline. This feature serves a dual purpose in that only a limited quantity of flow will move across

FIGURE 1.1: SCHEMATIC OF ORIGINALLY PROPOSED
FAST CURRENT CONTROL/RECOVERY SYSTEM

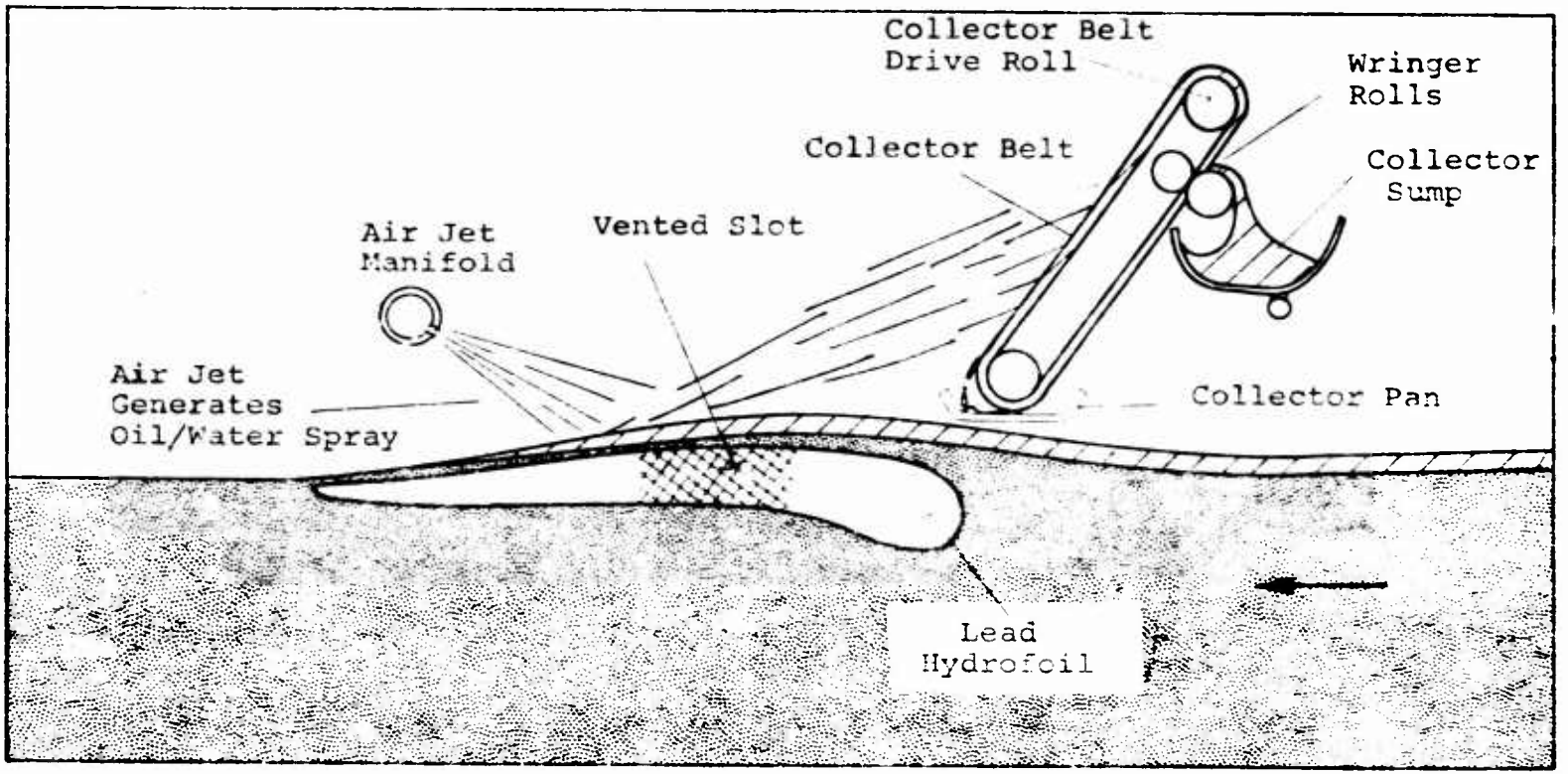

the top of the hydrofoil as well as limiting the amount of water that the oil can mix with if turbulence were introduced into the flow system. As the flow moves across the hydrofoil, a hydraulic jump is observed to occur; its position and properties with respect to the hydrofoil design is the subject of U.S. Environmental Protection Agency (EPA) research presently nearing completion. One qualitative result of this research is that the oil layer has been observed to thicken while traversing the hydraulic jump. A slightly unstable oil-water interface may also result from this phenomenon. As the oil-water layer moves across the top of the hydrofoil, its mean kinetic energy is continuously being dissipated through the action of surface friction. This effect will become more important as the thickness of the oil-water layer decreases and will tend to thicken the oil layer. Before traversing the entire length of hydrofoil a significant fraction of the water layer is aspirated through a carefully designed flow channel to a region in the lower rear portion of the hydrofoil. The remaining layer of oil and water over the top of the hydrofoil (after passing downstream of the aspirator section) is now rich in oil, increased in thickness and reduced in speed as it approaches the impact point of the air jet.

(b) Air Jet

The purpose of the air jet is to separate the surface layer of oil and water from the hydrofoil and to lift it into the air in the form of a fine spray of oil/water droplets. The angle of the air jet with respect to the hydrofoil surface will be designed in such a fashion that the spray is directed toward the rotating belt of oleophilic and hydrophobic

material. The fact that a very thin layer of oil and water is presented to the air jet precludes the use of an enormous amount of power to lift the oil-water layer from the hydrofoil.

(c) Rotating Belt of Oleophilic and Hydrophobic Material

The momentum of the oil/water spray combined with its small droplet size distribution will insure that the oil penetrates deeply into the porous belt material. This will allow the belt material to absorb more oil than is normally recovered when the oleophilic material is rolled into a flowing stream of water with oil on its surface.

(d) Oil Storage and Water Drain Systems

Once the oil has been collected on the rotating oleophilic and hydrophobic belt material, it is squeezed out and pumped to storage tanks. The water, on the other hand, drips down into a drain pipe and is allowed to return, by gravity, to the stream of water or be collected for further processing to remove oil that has drained into the water.

1.2.2 Final Control/Recovery System - The final control/recovery system which evolved during the Phase I program is shown schematically in Figure 1.2. This system is similar to that shown in Figure 1.1 with the exception that the air jet has been discontinued from use and that a small ramp has been placed at the trailing edge of the hydrofoil. The hydrofoil operates in the same manner as previously discussed; however, as the oil-water flow proceeds toward the trailing edge of the main hydrofoil, the ramp converts

FIGURE 1.2: SCHEMATIC OF FINAL CONTROL/RECOVERY CONCEPT

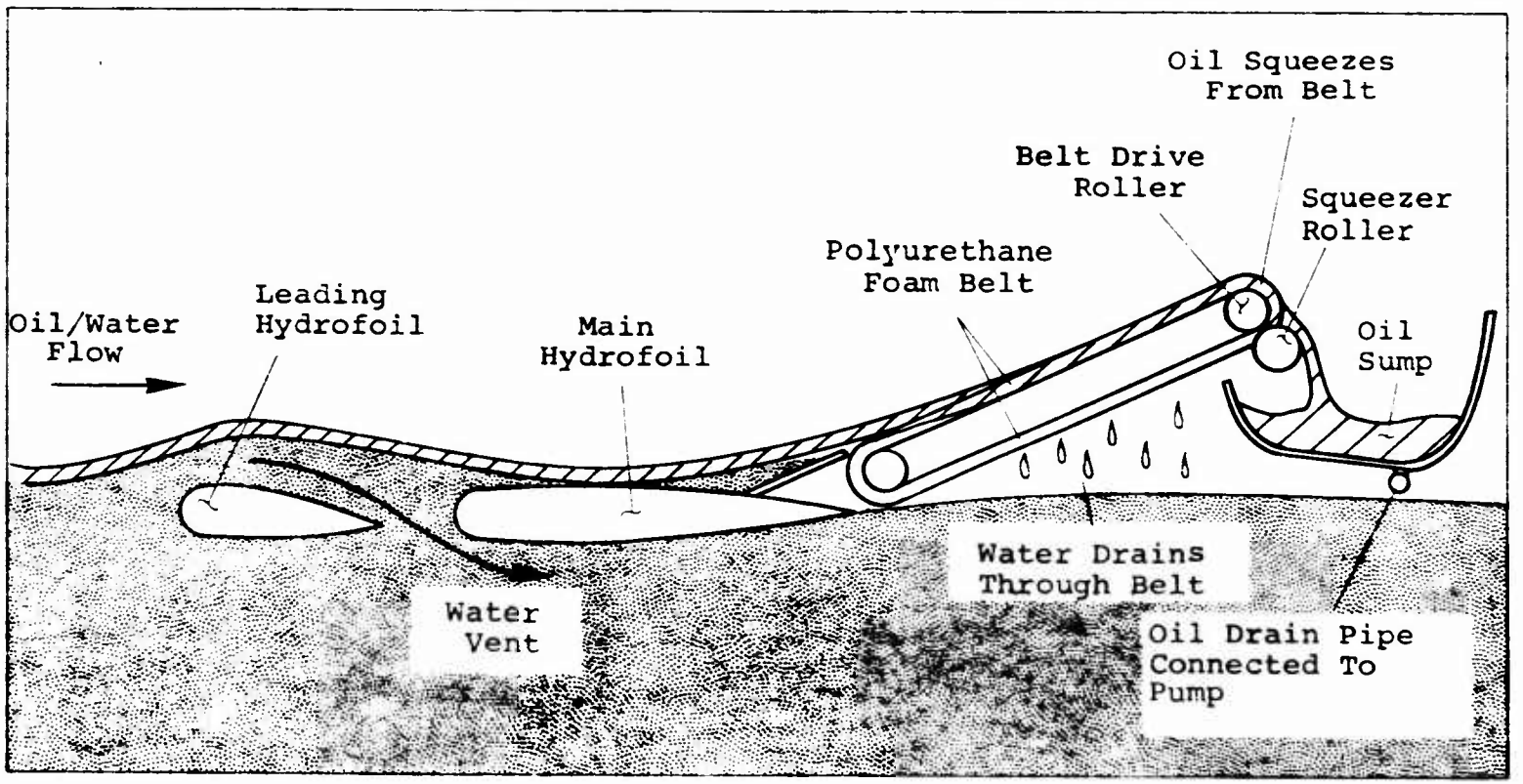

some of the kinetic energy of the flow into potential energy as well as directing the flow tangentially onto the rotating oleophilic and hydrophobic (polyurethane foam) belt material.

1.3 Phase I Program Discussion

The program that was conducted, and which resulted in the evolution of the control/recovery concept from that described in section 1.2.1 to that outlined in section 1.2.2 is the subject of the remaining sections of this report. Sections 2, 3 and 4 describe the three distinct experimental programs conducted during the Phase I contract. In section 2, a summary of the small scale hydrofoil tests conducted in a water flume are described. Section 3 describes the tow tank experiments that were performed to determine concept feasibility. The results of a comprehensive series of oil collection experiments performed in a large flume are discussed in section 4. The preliminary design characteristics for a large scale model are discussed in section 5. Sections 6, 7 and 8 present the conclusions, recommendations and references used in preparing this report, respectively.

SECTION 2

Small Scale Model Hydrofoil Tests

2.1 Introduction

The primary reason for placing a hydrofoil (control device) upstream of the recovery system (oleophilic and hydrophobic belt) is to separate as much as possible of the oil bearing fluid from the non-oil bearing fluid. In this manner, less water would have to be processed downstream by the recovery system. This scheme was first attempted by Wooten[2] with respect to an oil containment boom. One of the main problems associated with the use of the hydrofoil is that it must be operated near the oil/water interface to insure that a small quantity of water is drawn over the top surface of the hydrofoil (Figure 2.1a). Moreover, the hydrofoil cannot be placed too close to the oil/water interface, otherwise waves that are out of phase with respect to the motion of the hydrofoil will momentarily divert all of the fluid (oil and water) beneath the hydrofoil (Figure 2.1b). The only way to solve the latter problem is to design the hydrofoil to operate at a depth such that the very short wavelength waves (high frequency) are smaller in amplitude than the submergence of the hydrofoil, and to design the hydrofoil to follow the longer wavelength waves (low frequency). Moreover, in order to maintain a thin layer of fluid over the hydrofoil, a

---

[2] Wooten, D.C., "Mechanical Control of Oil Spills Utilizing a Streamlined Boom," Proceedings of Joint Conference on Prevention and Control of Oil Spills, March 13-15, 1973, Washington, D.C., pages 383-389 and EPA Report under Contract 68-01-0128, December, 1972.

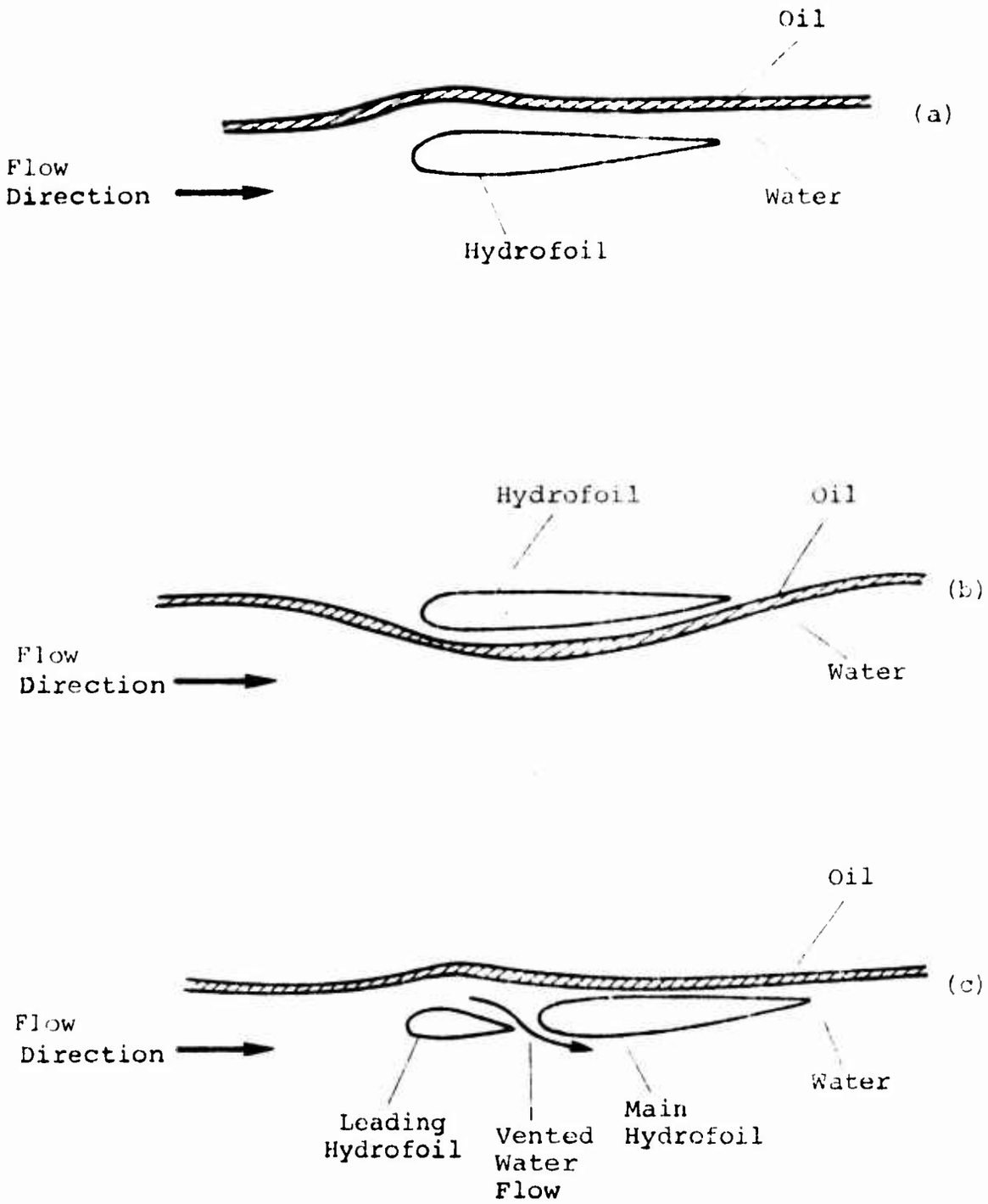

FIGURE 2.1: OPERATION OF A HYDROFOIL IN THE VICINITY OF A FREE SURFACE: (a) SINGLE HYDROFOIL IN NORMAL OPERATION, (b) SINGLE HYDROFOIL WITH LOSS OF FLUID OVER ITS TOP SURFACE AND (c) VENTED HYDROFOIL IN NORMAL OPERATION

vented hydrofoil system has been devised (Figure 2.1c). In this system, the leading hydrofoil acts in much the same manner as the entire hydrofoil shown in Figure 2.1a; however, once the oil/water flow passes over the top surface of the leading foil, much of the water is vented to the underside of the main hydrofoil, resulting in a relatively thin layer of oil and water over the top surface of the hydrofoil. This scheme satisfies the requirement of reducing the quantity of water which must be processed by the recovery device that is placed downstream of the hydrofoil.

Wooten[2] and others[3,4] have discussed some of the flow phenomenon associated with the operation of a single hydrofoil near a free surface. However, there isn't any data known to the author which describes the behavior of the vented hydrofoil in the vicinity of a free surface. Therefore, the first priority in the present program was to investigate the flow phenomenon associated with the latter hydrofoil configuration. In order to accomplish this task efficiently, Science Applications, Inc. subcontracted this task to Ultrasystems, Inc. and requested that Dr. Wooten supervise the study. This approach was the most favorable, since Ultrasystems, Inc. is currently under contract with the U.S. Environmental Protection Agency (EPA) to further investigate other aspects of the behavior of hydrofoils operating near a free surface. Therefore, the results of

---

[3]Parkin, B.R., Perry, B. and Yao-tsu Wu, T., "Pressure Distribution on a Hydrofoil Running Near the Water Surface," Journal of Applied Physics, 1956, Vol.27, No.3, pp.232-240.

[4]Laitone, E.V., "Limiting Pressure on Hydrofoils at Small Submergence Depths," Journal of Applied Physics, 1954, Vol.25, No.5, pp.623-626.

the study described below are those associated with the subcontract agreement.

The objective of this work was to provide information on the hydrodynamic behavior of the vented hydrofoil. Several models were constructed and experiments conducted in an open channel flow facility at approximately one-quarter scale in water - no oil was used. The models were two-dimensional and based on the NACA series of airfoil profiles. Slots were cut at various locations in order to shunt some of the flow passing over the model back underneath, thus reducing the amount of flow to be treated by the recovery system. The raw data consisted of drawings showing the location of the free surface and stagnation streamline relative to the hydrofoil shapes, and photographs utilizing several flow visualization techniques. The experiments revealed that the slots were effective in reducing the amount of flow over the model's rear portions, and in producing a smooth rather than turbulent, bow wave.

The following subsections will first provide an analytical base to determine scaling parameters and place the experiments in perspective; then the experiments and experimental results will be described.

2.2 Hydrodynamics of Hydrofoils Operating Near A Free Surface At Low Speed

SAI's oil control/recovery system requires a hydrofoil operated at low speeds quite near a free surface. One would think that the widespread use of hydrofoils would have required detailed study of all possible operating conditions. However, this is not the case. Although numerous papers,

both analytical and experimental have been written about hydrofoil design and operation for such applications as hydrofoil boats, only a few have even considered the operating conditions important here. One such paper[3] concludes that hydrofoil operation near a free surface is not of practical interest. Indeed, such operation is not of practical interest for the majority of hydrofoil applications where the primary requirement is a high lift/drag ratio. However, there are a few specialized applications where low speed and operation near a free surface are important. One of these is oil collection where the hydrofoil's main purpose is to separate the oil slick and some water from the remaining flow.

In order to determine scaling parameters, and to place the experiments in proper perspective, an analysis was performed by applying the principles of hydraulic flow. The next section outlines the results of this analysis.

2.2.1 Scaling Parameters - The type of hydrofoil operation under study here has been described as low speed and near the free surface. These terms have meaning only in relation to the size of the hydrofoil under consideration. Low speed means the Froude number is small. The Froude number is the square root of the ratio of inertial to gravity forces.

$$F = V_1/\sqrt{gL}$$

where:

F = Froude number

V_1 = Free stream velocity

g = Acceleration of gravity

L = A characteristic length of the hydrofoil, such as the thickness, chord, etc.

The characteristic length used here is the maximum thickness of the hydrofoil, T, and low speed operation means that $F \lesssim 2.0$, say. In this range, gravity forces dominate over the effects of curvature of the streamlines.

Operation near the free surface means that the thickness of the layer of water passing over the model is of the same order of magnitude as the thickness of the hydrofoil itself. Thus, the flow above the hydrofoil is effectively separated from the flow beneath and the two flows behave independently.

Since the flow over the hydrofoil is of major interest and gravity forces dominate, the equations of hydraulic flow may be applied. The important assumptions are:

1. Inertial forces are negligible. This means that the local static pressure is identical to the hydrostatic head of water above any given point.

2. Viscous forces are negligible. This means a large Reynolds number and implies that the velocity across any cross-section is uniform.

3. Surface tension forces are negligible. This means a large Weber number.

4. Vertical component of velocity is negligible. This means that the slope of the model profile as seen by the flow is small.

This analysis identifies another important scaling parameter as: $G_B = gB/V_1^2$ where B is the maximum freeboard, defined as the height of the highest point on the hydrofoil above the undisturbed free surface far upstream. B may be either positive or negative. Technically, G_B is the reciprocal of the Froude number squared where freeboard is the characteristic length.

2.2.2 Flow Map - A flow map is a drawing showing the type of flow produced as a function of the hydrofoil's operating parameters. Figure 2.2 is a typical flow map showing the characteristics of the flow as a function of F and G_B. The uppermost line represents the maximum freeboard for which flow passes over the hydrofoil. Along this line, all of the approaching surface layer's kinetic energy is converted into potential energy to lift the fluid to the hydrofoil's top. Slightly lowering the hydrofoil causes flow to proceed. The region between the two solid lines represents flow with a turbulent recirculating bow wave. The lower solid line is the approximate experimentally observed transition from turbulent to smooth bow wave. Operation at freeboards below this lower solid line produces a smooth bow wave. The dotted lines represent the range in which a hydraulic jump can occur in the flow over the hydrofoil. Above this region flow does not contain enough energy to pass through a hydraulic jump and still flow over the hydrofoil; below this region the flow above the hydrofoil is subcritical and no hydraulic jump is possible. Flow maps like this were determined experimentally for two of the models tested.

2.2.3 Correlations - Another result of the application of the hydraulic flow equations to this problem is a correlation between depths of flow over the hydrofoil at various points and G_B. These depths are expressed in dimensionless form as $G_{11} = gY_1/V_1^2$ and $G_{13} = gY_3/V_1^2$ where:

Y_1 = depth of stagnation streamline beneath free surface far upstream

Y_3 = depth of flow over highest point on hydrofoil.

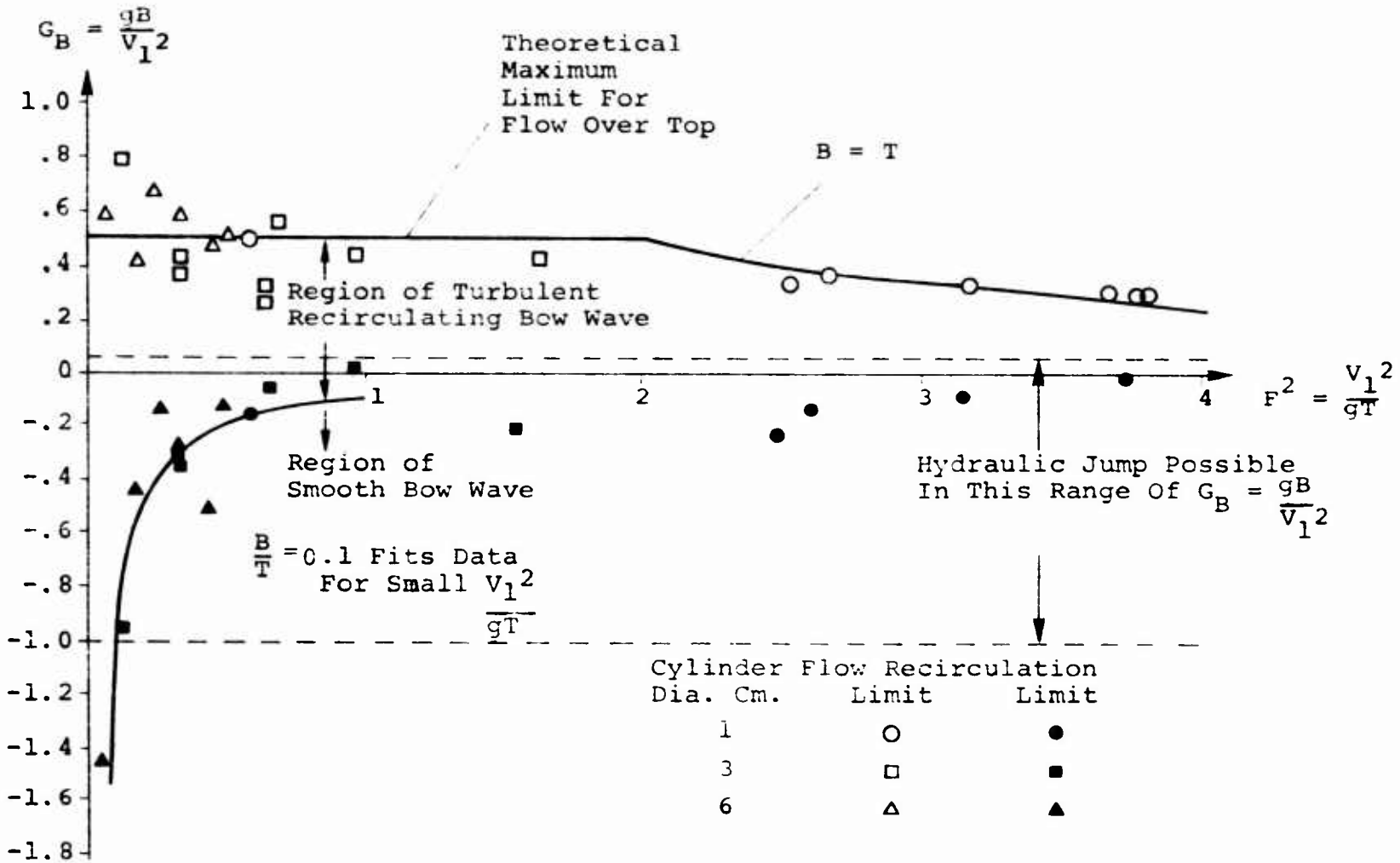

FIGURE 2.2: DIMENSIONLESS FLOW MAP FOR ALL HYDROFOILS; DATA FROM SOME CYLINDRICAL MODELS

Thus, Y_1 is the thickness of material skimmed off by the hydrofoil. Figures 2.3 and 2.4 show the theoretical correlations for both a turbulent hydraulic jump type bow wave, and a smooth bow wave for the scaling parameters Y_3 and Y_1, respectively.

As will be shown later, the experimental data follows these theoretical correlations closely. Deviation between experiment and theory is due to lack of agreement between the assumptions of the hydraulic theory and the actual flow conditions. Some of the more important effects not considered in the theory, but perhaps of importance in the experiments are:

- Viscous effects
- Surface tension effects
- Curvature of the streamlines in the vicinity of the bow
- Three-dimensional effects.

Nevertheless, the good agreement between theory and experiment (to be demonstrated later) indicates that these effects are minor for the small scale hydrofoils that have been observed. Increasing the scale will reduce these effects even further.

2.2.4 Slotted Hydrofoils - The above discussion relates the theory for the solid hydrofoils; slotted hydrofoils add additional complexity. The flow through a slot on a hydrofoil is governed not only by gravitational effects, but also by the pressure distribution near the lower end of the slot. This is in turn a function of the combination of viscous and inertial effects not accounted for in the hydraulic flow theory described above. Consequently, the scaling parameters for slotted hydrofoils are more complex. Nevertheless, if

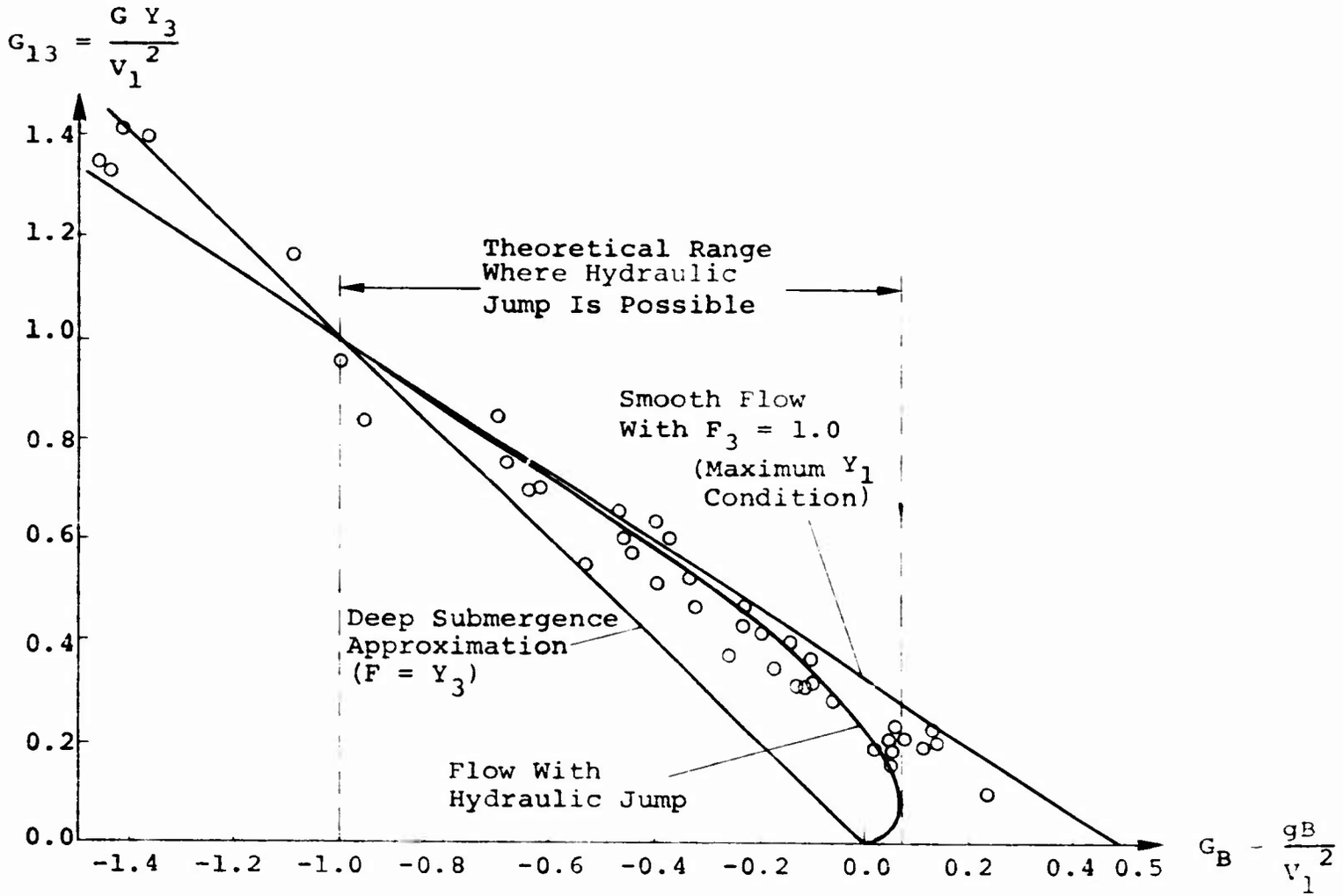

FIGURE 2.3: CORRELATION G_{13} Vs. G_B (AND SOME DATA POINTS)

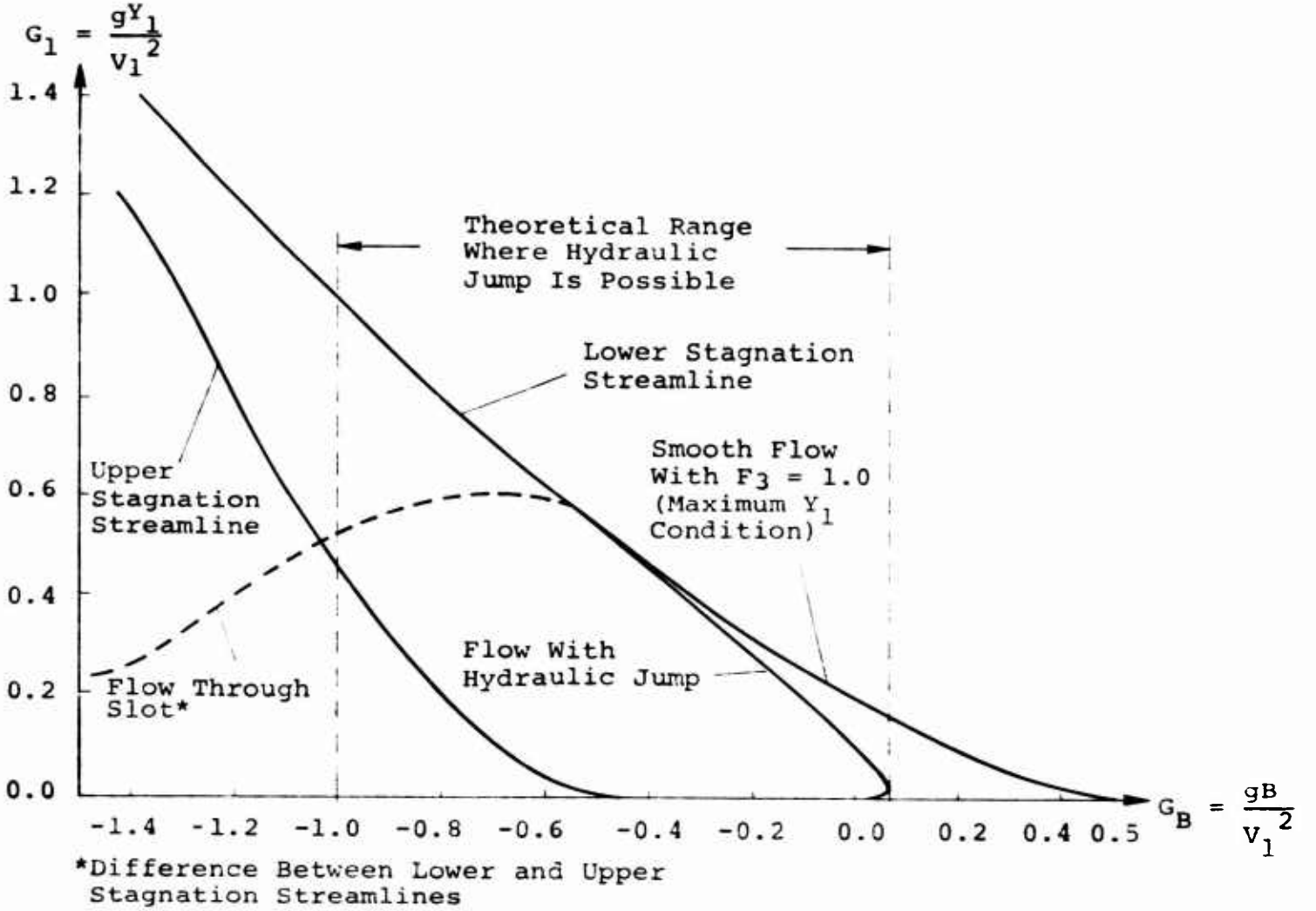

FIGURE 2.4: CORRELATION G_1 Vs. G_B

the velocity is held fixed, the depth of the stagnation streamline for the second portion of the hydrofoil (downstream of the slot) may be expressed in a manner similar to the correlations described above. Figure 2.4 also shows the approximate location of this correlation line for one fixed velocity. The difference in ordinants of the two solid curves is the thickness of the layer, measured far upstream, passing through the slot.

2.3 Experimental Facilities and Testing Equipment

The experimental facilities, measurement techniques and parameters measured during the small scale hydrofoil experimental program are discussed in detail below.

2.3.1 Flow Channel - Experiments were conducted at the California State University at Fullerton (CSUF) in the Civil Engineering Laboratory's open channel flow facility (Figures 2.5 and 2.6). This channel is commonly used to model flow in flumes and rivers and has adjustable slope, flow rate, head gate, and tail gate as shown. The channel was 4.87 m (16 ft.) long and had a cross section 0.30 m (1.0 ft.) wide by 0.45 m (1.5 ft.) deep. The maximum flow rate was 12.5 ℓ/sec (0.47 ft^3/sec). An aluminum restriction (visible in Figure 2.6) reduced the width of the channel to 0.11 m (4.5 in.) and increased the flow velocity substantially. Critical velocity for maximum flow was 1.02 m/sec (3.35 ft/sec). The turbulence level was reduced to a low value by screens and fiber mats inserted in the flow upstream of the model testing area. Velocity profile measurements indicated that the velocity was uniform, within 5 percent, up to within 2.5 cm (1.0 in.) of the solid boundaries of the cross section. Velocity measurements

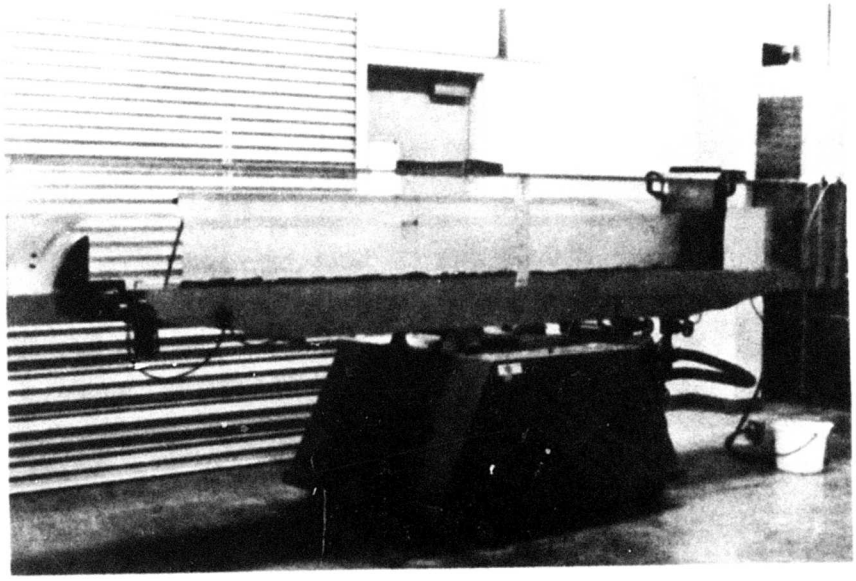

FIGURE 2.5: C.S.U.F. FLOW CHANNEL (Side View)

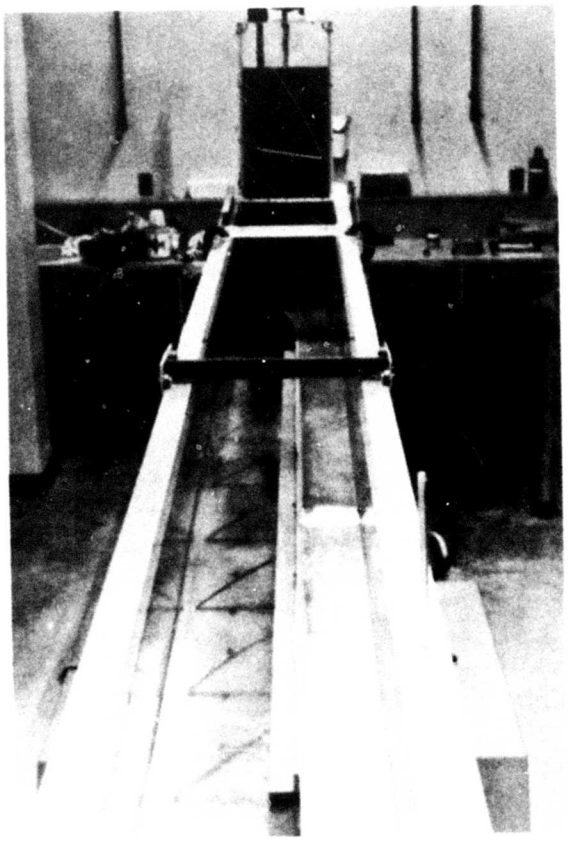

FIGURE 2.6: C.S.U.F. FLOW CHANNEL (Top View)

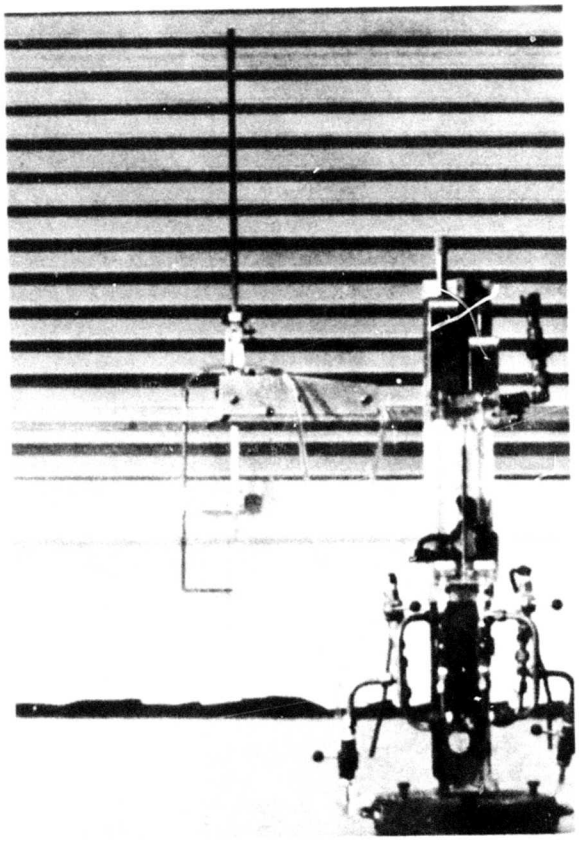

FIGURE 2.7: VELOCITY MEASURING APPARATUS

were obtained with the micromanometer and Pitot Tube shown in Figure 2.7. Figure 2.8 shows velocity profiles for one typical operating condition.

The experiments consisted of qualitative observation of the flow using several methods of flow visualization, and quantitative measurements of the stagnation streamlines and free surface.

2.3.2 Flow Visualization - One very successful flow visualization technique was streak photography of small air bubbles present in the flow. These bubbles were produced by air entrainment and the action of the pump. The bubbles were quite small with a rising velocity much smaller than the water's flow velocity. Consequently, they appeared to follow the streamlines. When the bubbles were illuminated from the side and observed against a black background, their movement could easily be observed. In photographs with exposure times of 1/15 to 1/30 second, the bubbles appeared as streaks, and streamlines were readily discernible. Figures 2.9 and 2.10 demonstrate this technique for a model tested under contract to the EPA.

Another very successful flow visualization technique was dye injection. Here food coloring was injected at about the same linear velocity as the flow upstream of the model. The dye, following the streamlines, gave an excellent indication of flow direction and turbulence level. Figures 2.11 and 2.12 demonstrate this technique.

In order to approximate the movement of an oil slick, small paper chips were deposited upstream of the model and allowed to flow with the current. These paper chips, approximately

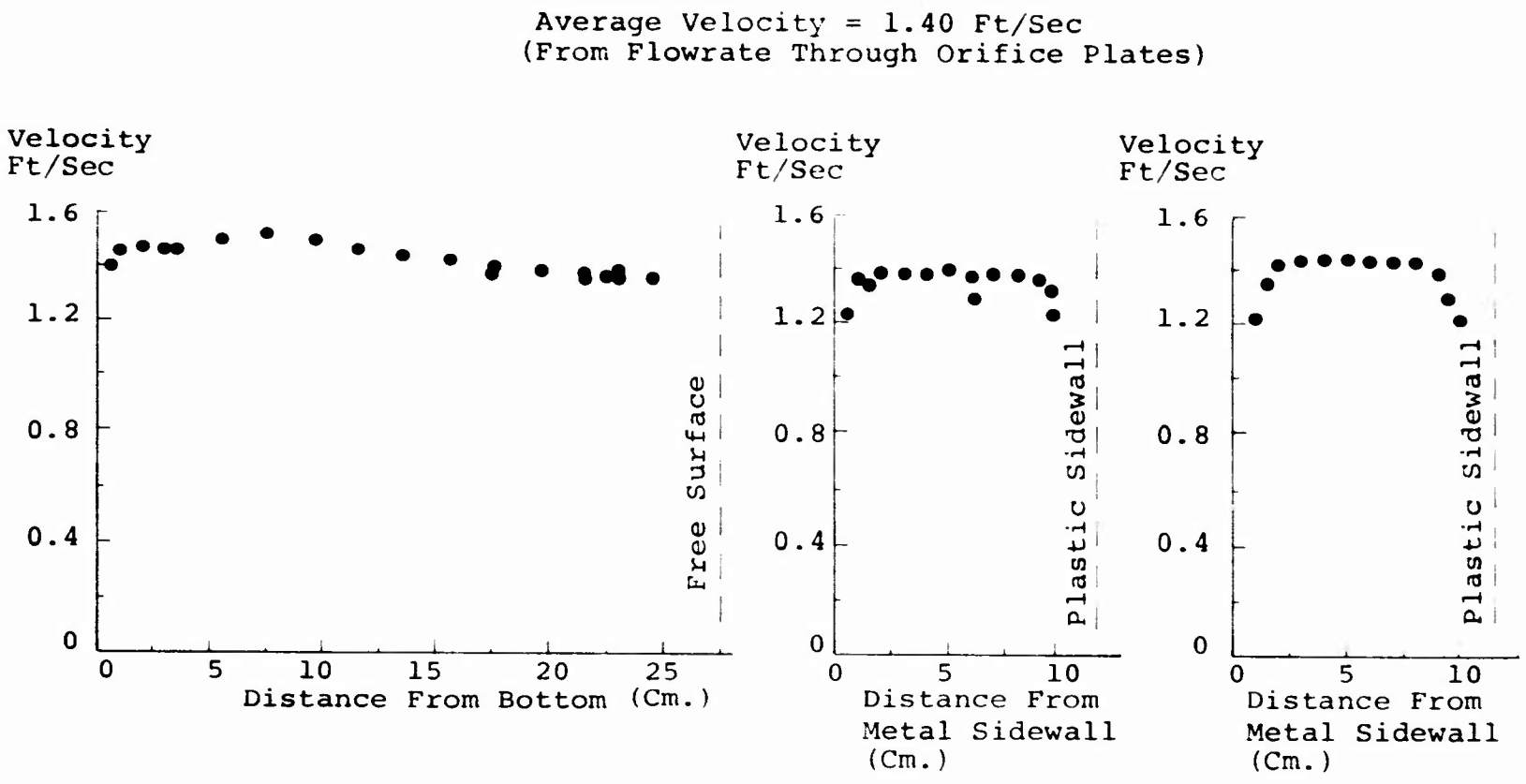

FIGURE 2.8: VELOCITY PROFILES IN THE C.S.U.F. FLOW FACILITY (TYPICAL)

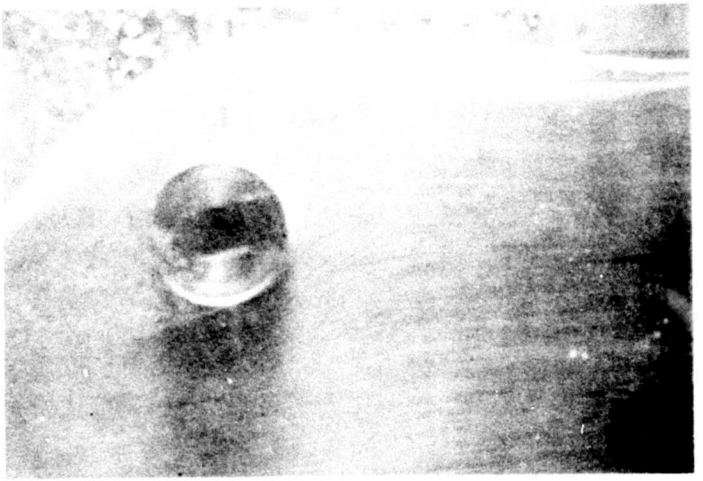

FIGURE 2.9: SEPARATED FLOW OVER REAR PORTION OF 3.0 cm. DIA CYLINDER

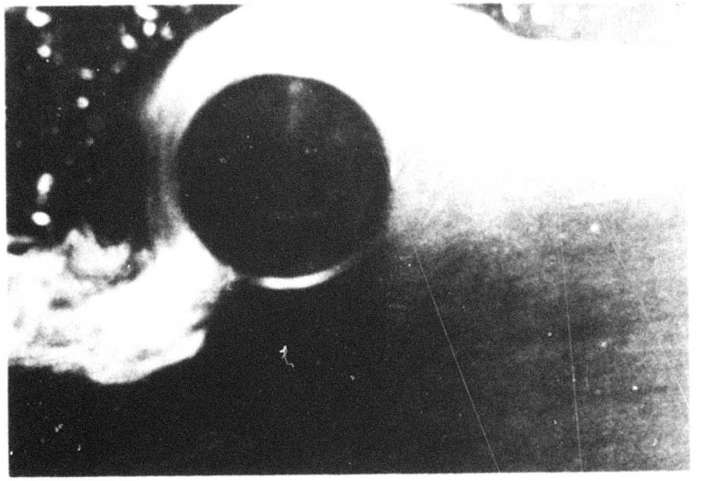

FIGURE 2.10: AIR BUBBLE VISUALIZATION OF TURBULENT FLOW UPSTREAM OF 3.0 cm. DIA CYLINDER AT HIGH POSITIVE FREEBOARD

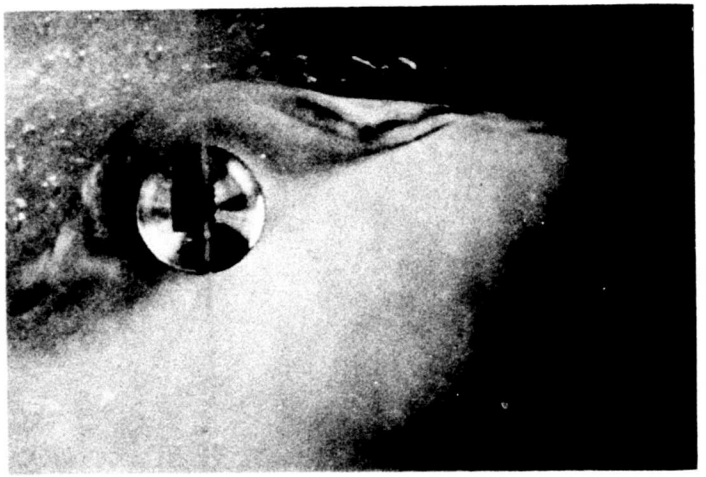

FIGURE 2.11: DIFFUSION OF DYE INJECTION INTO TURBULENT FLOW UPSTREAM OF 3.0 cm. DIA CYLINDER AT HIGH POSITIVE FREEBOARD

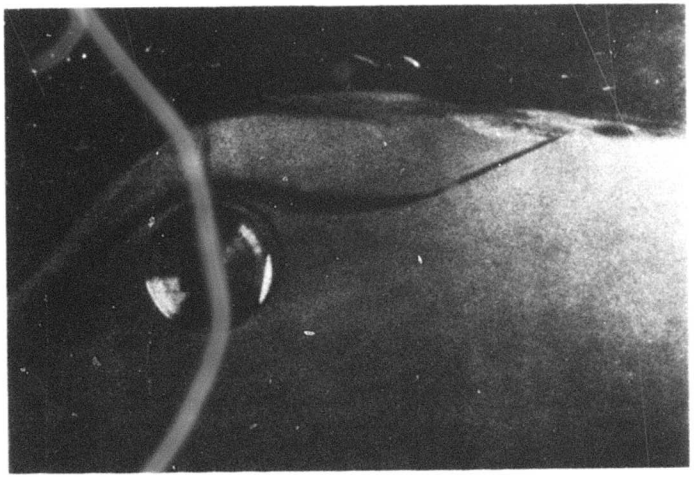

FIGURE 2.12: SMOOTH FLOW OVER THE 3.0 cm. DIA CYLINDER AT NEGATIVE FREEBOARD

2 mm in diameter, floated on the surface until they became soaked with water and sank. This process required about one minute allowing ample time for observation of their floating behavior as they passed over the model.

2.3.3 Quantitative Experiments - For the quantitative experiments the stagnation streamlines were measured by dye injection. The dye injector was mounted on a height gauge and the position of the stagnation streamline was taken as the measured location of the dye injector where approximately half the dye passed over and half under the model. This location was repeatable to within about plus or minus 0.5 mm. The locus of the free surface and model profile were measured with the height gauge directly. These data were then reduced and plotted by a small computer on suitable graph paper. Lines were drawn through the data points by hand to sketch the free surface and stagnation streamlines.

In addition to these systematic measurements, experiments were run to compare model operation with the correlation curves described above, and to determine the transition lines on the flow map. In these experiments only V_1, Y_1, Y_3, and B were measured and the type of bow wave - smooth or turbulent - was observed. The smaller amount of labor required for these experiments allowed many data points to be taken.

2.4 Models

The models tested were standard NACA profile shapes so that the results could be compared with published airfoil data and to provide for easy reference to model shape. All

models were two-dimensional with uniform cross-sections across the model's widths which spanned the channel.

The model size was chosen to properly scale the anticipated operation of SAI's prototype device. Since the prototype was to be three inches in thickness and was expected to operate at a nominal speed of three knots, the Froude number was calculated to be F = 1.8. Since the maximum usable velocity in the CSUF facility was about 80 cm/sec, this corresponded to a model thickness of 2.0 cm or 26 percent of full scale to obtain a Froude number of F = 1.8. While testing at higher velocities was possible, accuracy would have been reduced due to standing waves which appeared as the channel approached critical conditions. Modeling higher speeds could have also been accomplished by reducing the model's size; however, this would also result in reduced experimental accuracy.

2.4.1 NACA Slotted Models - The three models tested were variations of the NACA 0015 and NACA 4415 profiles. The NACA 0015 profile is a non-cambered shape with a maximum thickness of 15 percent of the chord line length. The NACA 4415 profile has the same thickness distribution as the NACA 0015 profile, but with a maximum camber of 4 percent of the chord line at a point 40 percent of the chord from the bow. The coordinates[5] for the NACA 0015 and 4415 airfoils are shown in Tables 2.1 and 2.2 respectively.

---

[5]Abbott, I, von Doenhoff, A. and Stivers, L.S., "Summary of Airfoil Data," NACA Report No. 824, 1945.

TABLE 2.1

NACA 4415 AIRFOIL COORDINATES

(Stations and ordinates given in percent of airfoil chord)

Upper surface		Lower surface	
Axial Station	Ordinate	Axial Station	Ordinate
0	---	0	0
1.25	3.07	1.25	-1.79
2.5	4.17	2.5	-2.48
5.0	5.74	5.0	-3.27
7.5	6.91	7.5	-3.71
10	7.84	10	-3.98
15	9.27	15	-4.18
20	10.25	20	-4.15
25	10.92	25	-3.98
30	11.25	30	-3.75
40	11.25	40	-3.25
50	10.53	50	-2.72
60	9.30	60	-2.14
70	7.63	70	-1.55
80	5.55	80	-1.03
90	3.08	90	- .57
95	1.67	95	- .36
100	(.16)	100	(- .16)
100	---	100	0

TABLE 2.2

NACA 0015 AIRFOIL COORDINATES

(Station and ordinates given in percent of airfoil chord)

Station	Ordinate
0	0
.5	---
1.25	2.367
2.5	3.268
5.0	4.443
7.5	5.250
10	5.853
15	6.682
20	7.172
25	7.427
30	7.502
40	7.254
50	6.617
60	5.704
70	4.580
80	3.279
90	1.810
95	1.008
100	.158

The first two models are shown in Figure 2.13. The models were constructed of acrylic plastic and had slots dividing the profiles into two or three sections. The sections were held in alignment with thin stainless steel rods (not shown) which also provide for adjustment of the slot width. The slots allowed part of the flow passing over the bow to pass through the slots thus reducing the amount passing over the model's rear portion. The slot contours and positions were designed to maximize flow through the slots.

Figure 2.14 shows the ideal velocity distribution on the surface of the NACA 4415 profile operating in an infinite incompressible fluid at zero angle of attack, calculated from potential flow considerations as described in Reference 5. Regions of high velocity are, of course, regions of low pressure and vice versa. Because of the cambered shape, the velocity is higher on one side than the other. Consequently, lift is produced. Any slots tend to equalize the pressure on either side by allowing fluid to pass from one side to the other. This analysis is of maximum accuracy at deep submergence; at shallow submergence it is only approximate because of the free surface.

The location of the slot on the NACA 4415 model was designed to maximize the flow through the slot by locating the upper end in a region of high pressure, and the lower end in a region of low pressure. It was operated inverted - with the cambered side down - so that the low pressure side was on the bottom.

Since the NACA 0015 model was symmetric, the ideal velocity distribution was the same on upper and lower surfaces at zero angle of attack (Figure 2.14b); this reduced the

Full Scale
Chord = 13.3 cm
Thickness = 2.0 cm

NACA 4415 Profile Model With 1 Slot
(Slot Width is Adjustable)

NACA 0015 Profile Model With 2 Slots
(Slot Widths are Adjustable)

FIGURE 2.13: SLOTTED MODELS

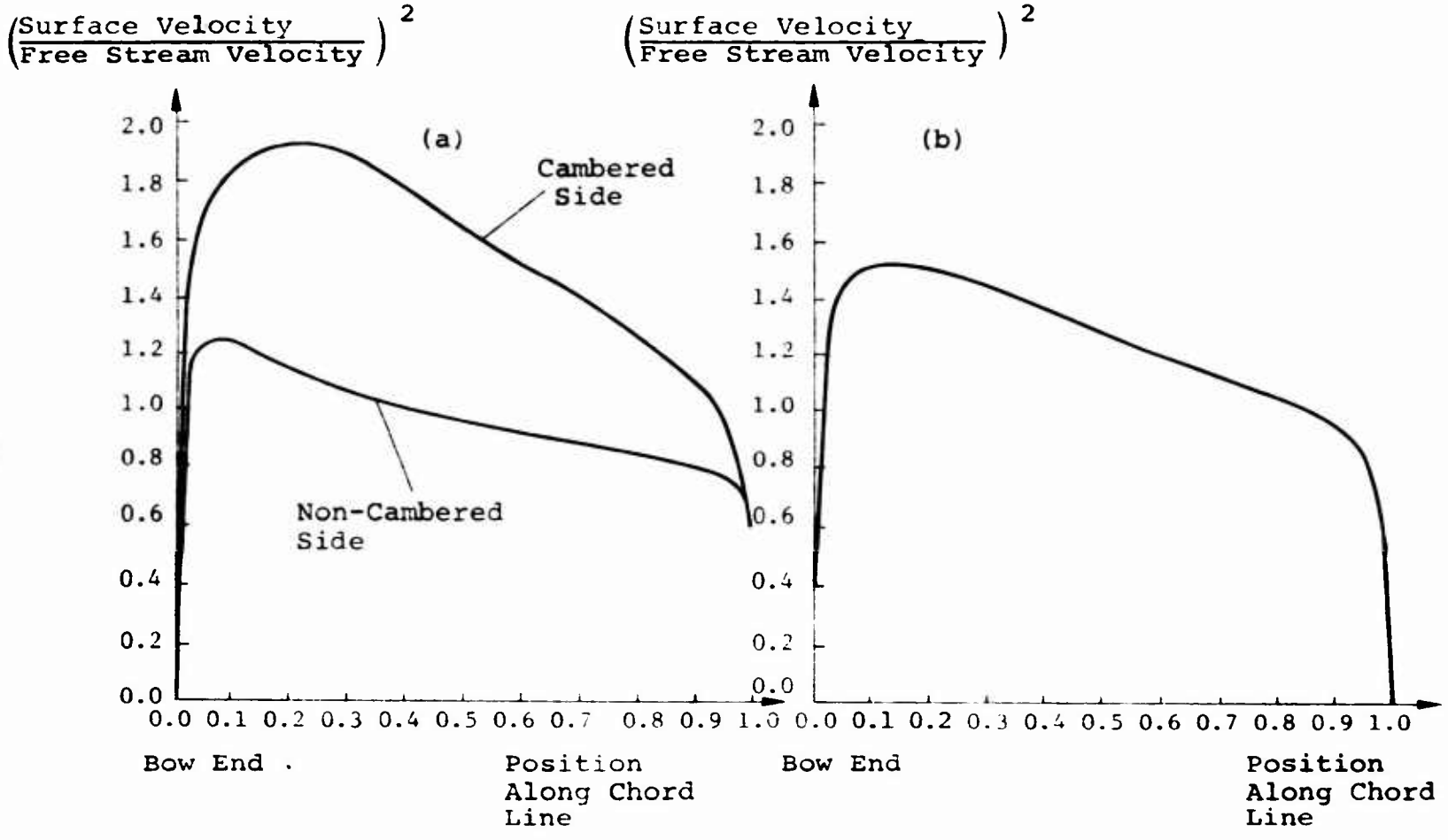

FIGURE 2.14: VELOCITY DISTRIBUTION ON SURFACE OF (a) NACA 4415 PROFILE AND (b) NACA 0015 PROFILE, FROM REFERENCE 5

effectiveness of the slots at deep submergence. Two slots were studied to examine the importance of slot location.

2.4.2 NACA 0015-4415 Model - The third model was an articulated model with a small front element of NACA 0015 profile and a larger rear element of NACA 4415 profile as shown in Figure 2.15. Each section was constructed of three separate parts held in alignment with screws. Thin plastic plates joined the front and rear model parts allowing their positions to be adjusted relative to one another over a wide range as shown in the testing table in Figure 2.15. This model was designed to have the smaller front hydrofoil "condition" the flow as it approached the larger main hydrofoil. The main hydrofoil was the same size as the earlier models, for comparison, and the smaller front hydrofoil was 1/3 as large (thickness = 0.67 cm).

2.5 Experiments and Results

This section describes the scope of tests and outlines the test results. A majority of the data consisted of drawings showing the measured locations of the free surface and stagnation streamlines; however, only the summary of this data is presented here.

2.5.1 Preliminary Tests - Before any special models were constructed, an existing model was modified to allow preliminary testing of the slotted model concept. Figure 2.16 is a full scale drawing of this model showing one approximate operating condition. The model was constructed of three aluminum sections held together with adhesive tape. The bow section was cylindrical, the midsection rectangular with a wide slot, and the tail section triangular in cross section. The model was two dimensional and spanned the channel as did all of the other models tested.

FIGURE 2.15: NACA 0015-4415 MODEL AND TESTING TABLE

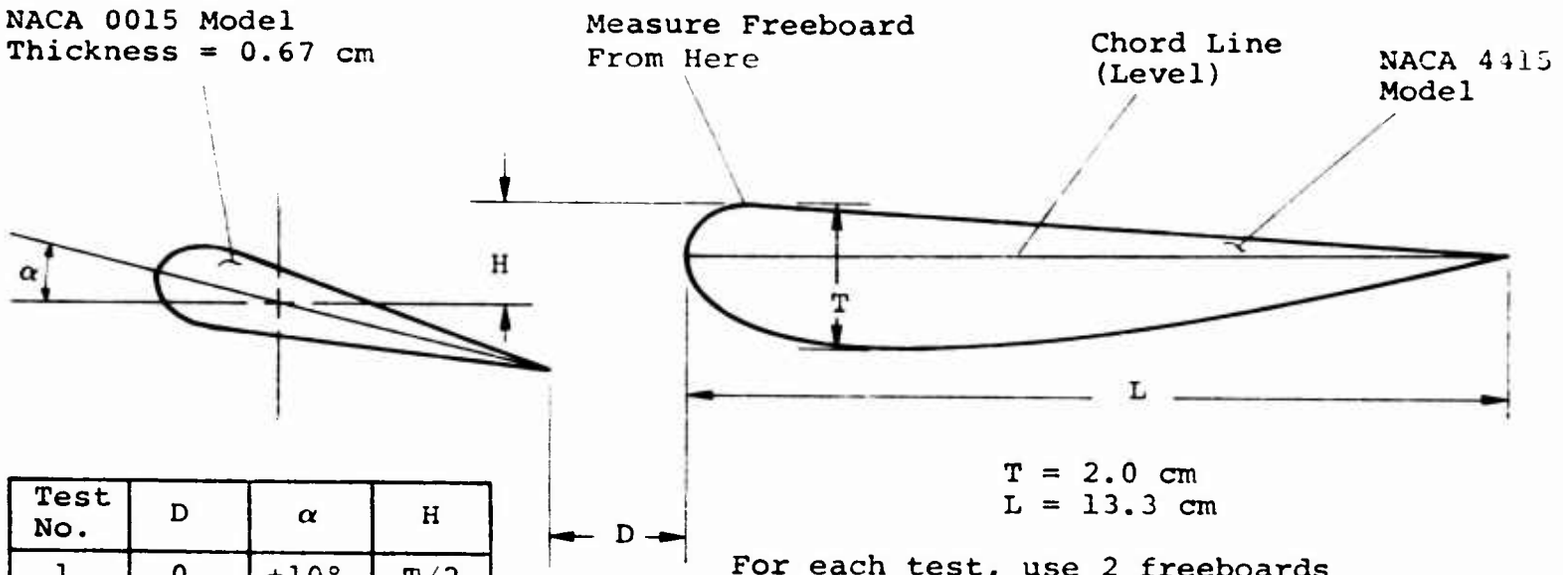

Test No.	D	α	H
1	0	+10°	T/2
2	0	+10°	T
3	L/6	+10°	0
4	L/6	+10°	T
5	L/3	+10°	T/2
6	L/3	0°	T/2
7	L/3	-10°	T/2

T = 2.0 cm
L = 13.3 cm

For each test, use 2 freeboards
1. Freeboard = 0
2. Freeboard so that depth of flow over highest part of NACA 4415 model is 0.5 cm

FIGURE 2.16: PRELIMINARY TESTS ON AVAILABLE SLOTTED MODEL

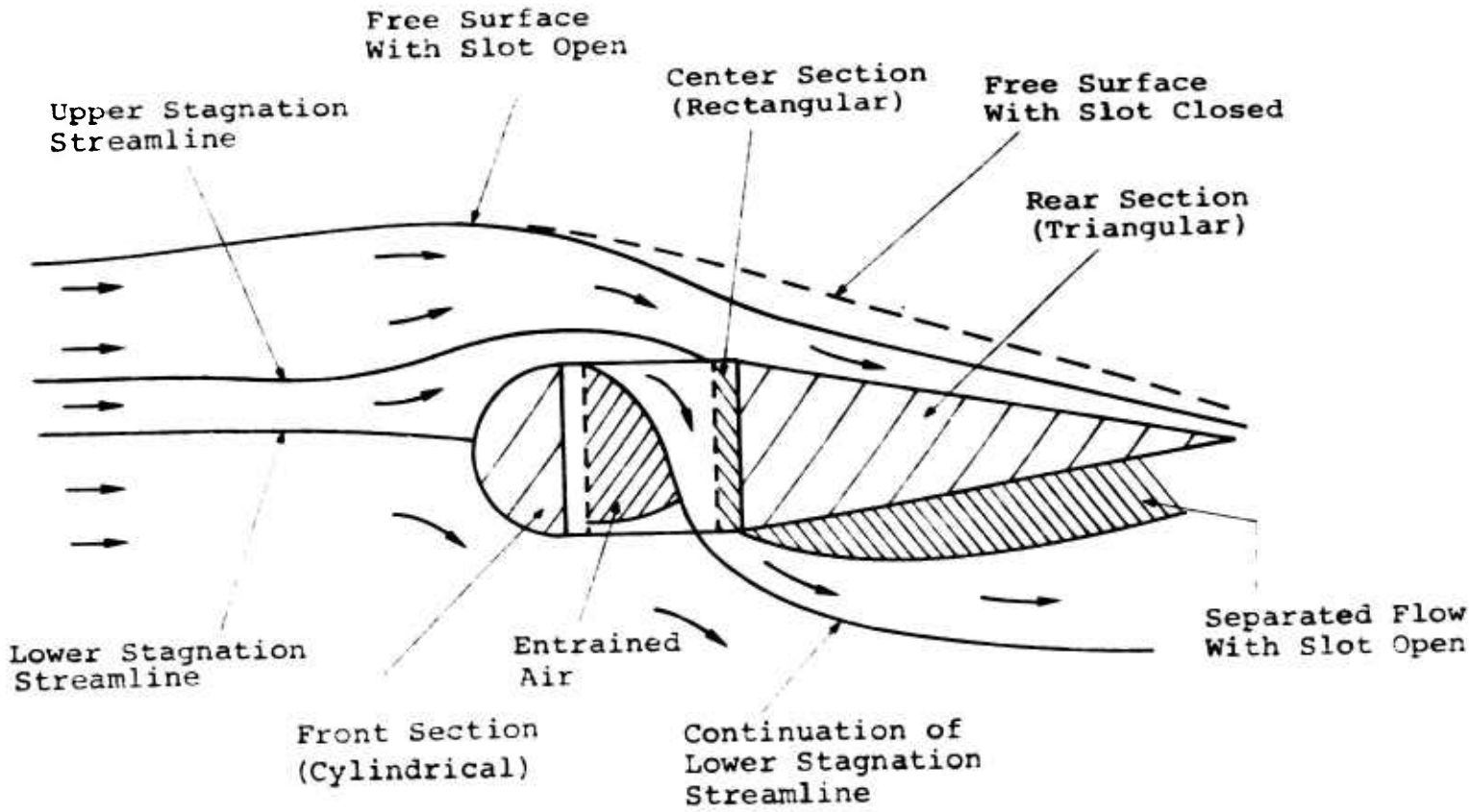

Note: Approximate only
Velocity = 90 cm/sec
(Scales to 5 ft/sec on
3 in. thick hydrofoil)

Brief experiments were run to identify the best operating parameters. As shown in Figure 2.16, there were two stagnation streamlines. The lower one, which ended on the bow, was the dividing line between flow over and flow under the bow. The upper stagnation streamline, which ended at the rear edge of the slot, was the dividing line between flow through the slot from flow over the rear of the model. The drawing shows the observed conditions when the model was near the surface. The sharp slot edges caused ventilation (air entrainment) greatly reducing the effective open area. A separated region on the lower side of the model was also produced. When the slot was closed by tape, the free surface was only slightly changed (as shown), but the separated region was greatly reduced. Thus the flow through the slot appeared responsible for the majority of the flow separation.

As the model was lowered further beneath the free surface, the flow through the slot diminished and the two stagnation streamlines merged. This behavior was expected since the model was symmetric.

These brief tests led to several useful conclusions. First, the slot should be carefully designed to eliminate sharp edges. This would increase the effective slot area and in turn increase flow through the slot. Second, the exit end of the slot should be designed to merge the slot flow with flow passing under the hydrofoil to reduce separation. Third, a cambered profile is desirable to provide an increased pressure difference across the slot thus increasing the flow through it.

2.5.2 NACA 4415 Model - The NACA 4415 model was designed to incorporate these features. This model was first tested briefly to determine favorable operating conditions, and a testing matrix was set up for the detailed tests which followed. Table 2.3, the testing matrix, shows the variety of operating conditions tested. Three slot widths were selected and each slot width was then tested over a range of velocities (Froude numbers) and freeboards. Although most tests were run at zero angle of attack, it was varied on a few tests.

Figure 2.17 shows typical flows observed at slot widths of 1.0 and 3.0 cm, respectively (at zero angle of attack). Both of these experiments were conducted at nearly the same velocity and freeboard, and in both cases two stagnation streamlines were identified. In addition to the stagnation streamline on the bow (the lower stagnation streamline), there was a stagnation streamline for the rear portion of the model (upper stagnation streamline). The lower streamline marks the division of flow over from flow under the bow and the upper stagnation streamline marks the division of flow through the slot from flow over the rear portion of the model. When the slot width was reduced the amount of flow through the slot was also reduced and the upper stagnation streamline approached and, at zero slot opening, merged with the lower stagnation streamline. Figure 2.17 shows that, although the flow rates over the bow were approximately the same for the 1.0 and 3.0 cm slot widths, a larger portion of the flow passed through the slot at the 3.0 cm width. Regions of separated flow were also shown in these drawings. These regions were caused by the small radius of curvature of the slot walls and viscous effects.

TABLE 2.3: TESTING MATRIX FOR NACA 4415 MODEL

Experiment Number (#)	Froude Number (F)	Freeboard cm (B)	Slot Width (w) cm	Angle (α) Degrees
1	1.04	1.24	0	0
2	1.04	- .03	0	0
3	1.04	-0.53	0	0
4	1.03	-1.01	0	0
5	1.50	+ .26	0	0
6	1.48	+ .06	0	0
7	1.49	- .53	0	0
8	1.49	- .99	0	0
9	1.67	1.28	0	0
10	1.67	1.23	0	0
11	1.68	+ .01	0	0
12	1.68	- .43	0	0
13	1.71	-1.03	0	0
14	1.47	- .11	0	-5
15	1.47	- .02	0	+5
16	.43	- .32	1.0	0
17	.81	- .44	1.0	0
18	.81	- .76	1.0	0
19	1.21	-1.04	1.0	0
20	1.20	- .23	1.0	0
21	1.20	- .77	1.0	0
22	1.53	- .32	1.0	0
23	1.53	- .32	1.0	0
24	1.60	1.04	1.0	0
25	1.61	- .43	1.0	0
26	1.58	- .81	1.0	0
27	1.22	- .47	1.0	-3.1
28	1.19	-1.08	1.0	-5.9
29	1.20	-1.23	1.0	+3.1
30	1.19	-1.08	1.0	-5.9
31	.90	- .93	3.0	0
32	.90	-1.40	3.0	0
33	.90	-1.80	3.0	0
34	1.18	- .60	3.0	0
35	1.18	- .93	3.0	0
36	1.18	-1.45	3.0	0
37	1.30	-1.15	3.0	0
38	1.30	-1.75	3.0	0
39	1.30	-2.20	3.0	0
40	1.50	-1.26	3.0	0
41	1.49	-1.91	3.0	0
42	1.49	-2.86	3.0	0

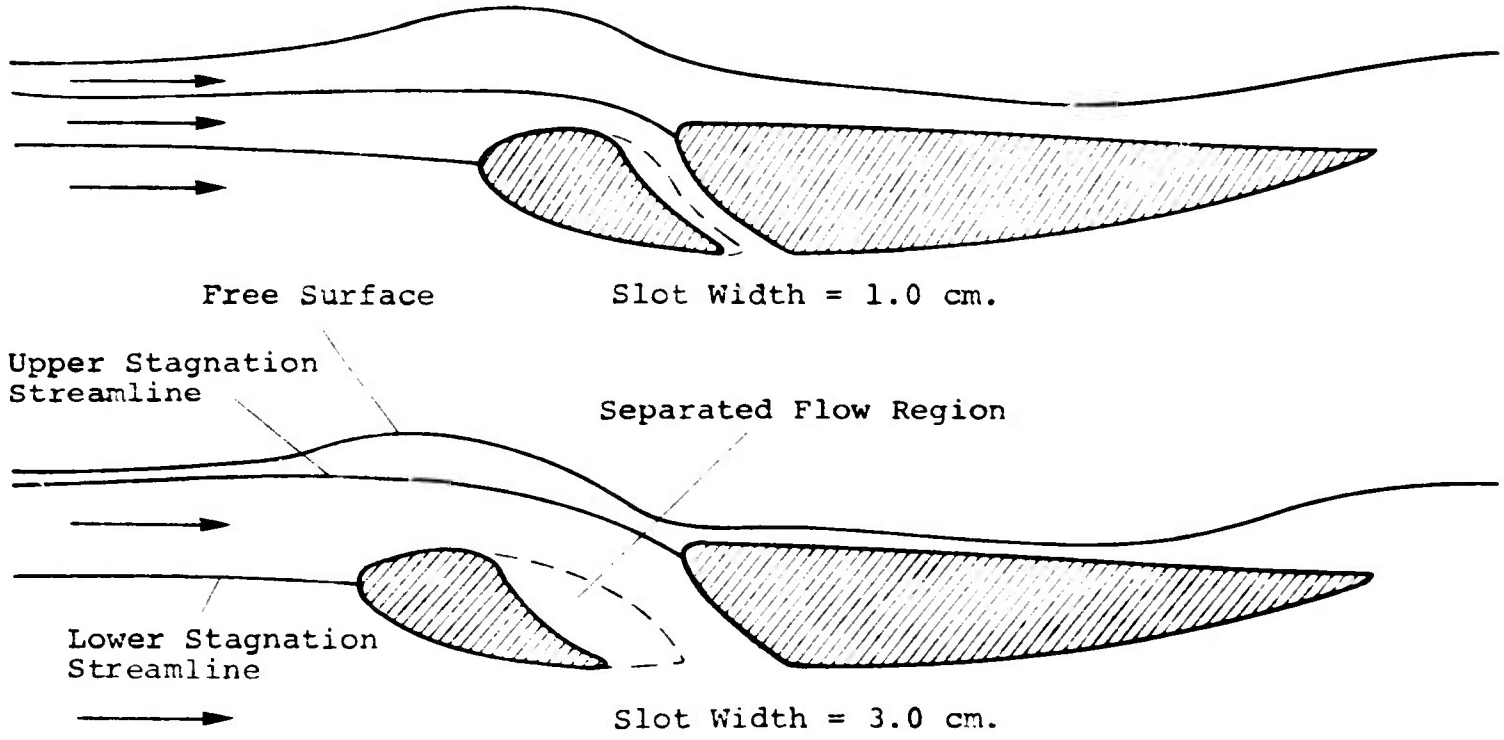

FIGURE 2.17: TYPICAL FLOW FOR NACA 4415 MODEL (SAME VELOCITY, FREEBOARD AND ANGLE OF ATTACK - VARIABLE SLOT WIDTH)

Figures 2.18, 2.19, and 2.20 are photographs showing operation of the NACA 4415 model at slot widths of 1.0 and 3.0 cm. The flow was smooth as opposed to turbulent for each of these photographs. Figure 2.18 and 2.19 are air bubble streak photographs showing the streamlines. A region of separated flow is visible (barely) in Figure 2.19. Figure 2.20 shows the upper stagnation streamline made visible by dye injection. Note the curvature of the streamline in the area above the slot. This curvature is an indication that inertial forces are important.

For a given slot width and angle of attack, a flow map can be drawn to describe the type of flow observed as a function of operating parameters. Flow maps for slot widths of zero and 3.0 cm at zero angle of attack have been superimposed in Figure 2.21. For clarity, the actual data points have been eliminated and only the trends of the data are shown. The transition lines were determined by lowering the model until transition was reached and recording the velocity and freeboard. The exact point of transition was difficult to determine because channel vibration, turbulence, and viscous effects all interacted to make transition gradual rather than abrupt. Consequently, the transition lines shown should be considered approximate.

First consider the lines in Figure 2.21 associated with the 3.0 cm slot width. The dotted line represents constant velocity and along this line, as the freeboard was decreased from a very large value, flow started over the bow (through a hydraulic jump type turbulent bow wave) and through the slot. This transition is the upper line and is identical to that observed with solid models. As the model was lowered further, the flow over the bow increased with all flow

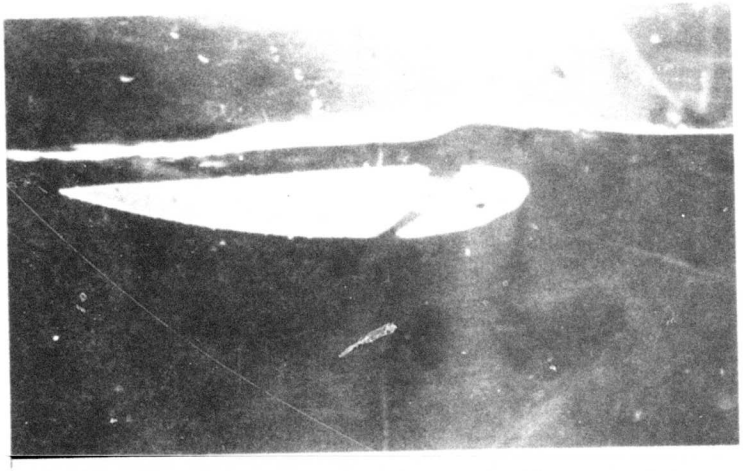

FIGURE 2.18: SLOTTED MODEL
(SLOT WIDTH = 1.0 cm.)
NOTE SMOOTH FLOW

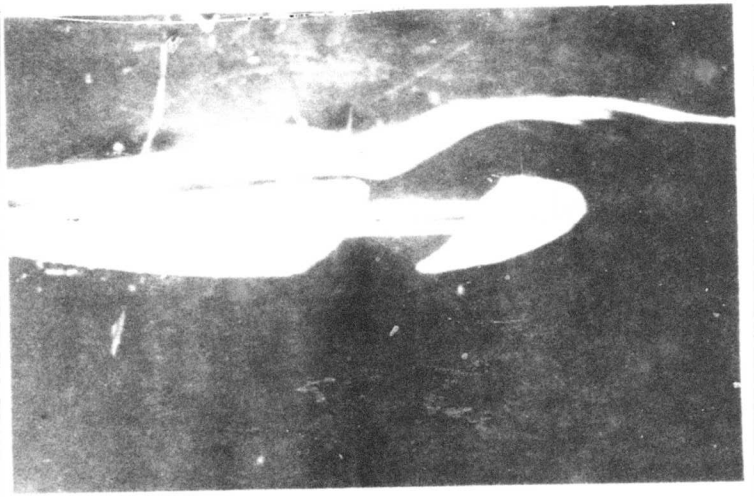

FIGURE 2.19: SLOTTED MODEL
(SLOT WIDTH = 3.0 cm.)
NOTE SEPARATION
INSIDE SLOT

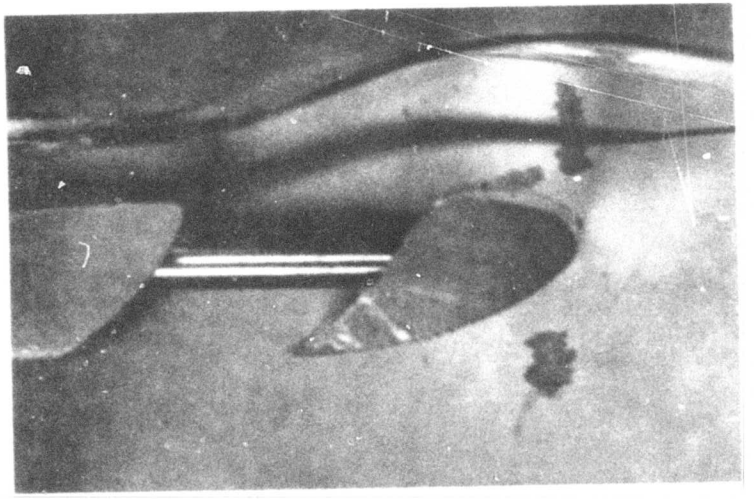

FIGURE 2.20: SLOTTED MODEL
(SLOT WIDTH = 3.0 cm.)
STAGNATION STREAMLINE ON
REAR PORTION VISIBLE WITH
DYE INJECTION

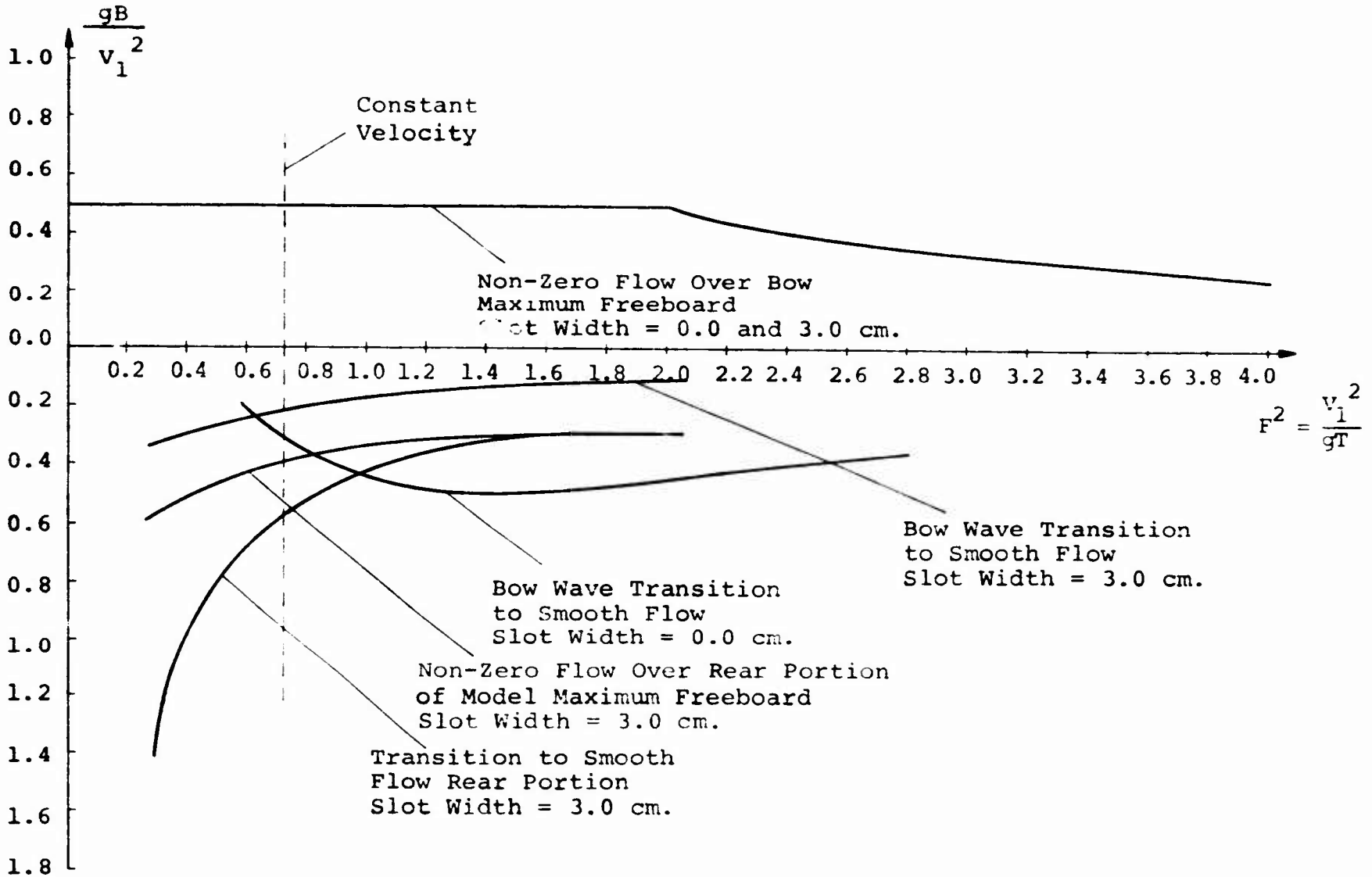

FIGURE 2.21: FLOW MAP FOR NACA 4415 MODEL WITH SLOT WIDTHS = 0.0 AND 3.0 cm AT ZERO ANGLE OF ATTACK (TRENDS OF DATA)

passing through the slot. Then there was transition of the bow wave from turbulent to smooth flow. This transition is the next line where there was still no flow over the model's rear portion. As the model was lowered further, flow started over the rear portion, indicated by the next transition line. At low velocity the flow over the rear portion had a turbulent bow wave. As the model was lowered further there was another transition to smooth flow (the next line). At high velocity, however, the flow was always smooth over the rear portion.

The flow map for the NACA 4415 model with the slot closed was substantially different than with the slot open. For a 0.0 cm slot width, there was no flow through the slot and hence only one transition line. The opening of the slot caused transition to occur at higher freeboard, and has great impact on the design of a full scale system. For a given velocity, an open slot will allow the hydrofoil system (control device) to operate much closer to the surface and still maintain smooth flow over the bow. This results in a reduction of the amount of flow passing over the bow and simplifies the design of the control device. For example, at a $F^2 = 1.6$, opening the slot to a width of 3.0 cm results in a reduction of the flow rate over the hydrofoil by about 54 percent. If the flow over the rear portion of the hydrofoil is also required to be smooth, the reduction is still about 28 percent. These reductions are significant.

Under some conditions stagnant or reverse flow occurred on the rear portion of the model as shown in Figure 2.22. This was only observed near transition to smooth flow over the rear portion of the model. As the model was lowered further,

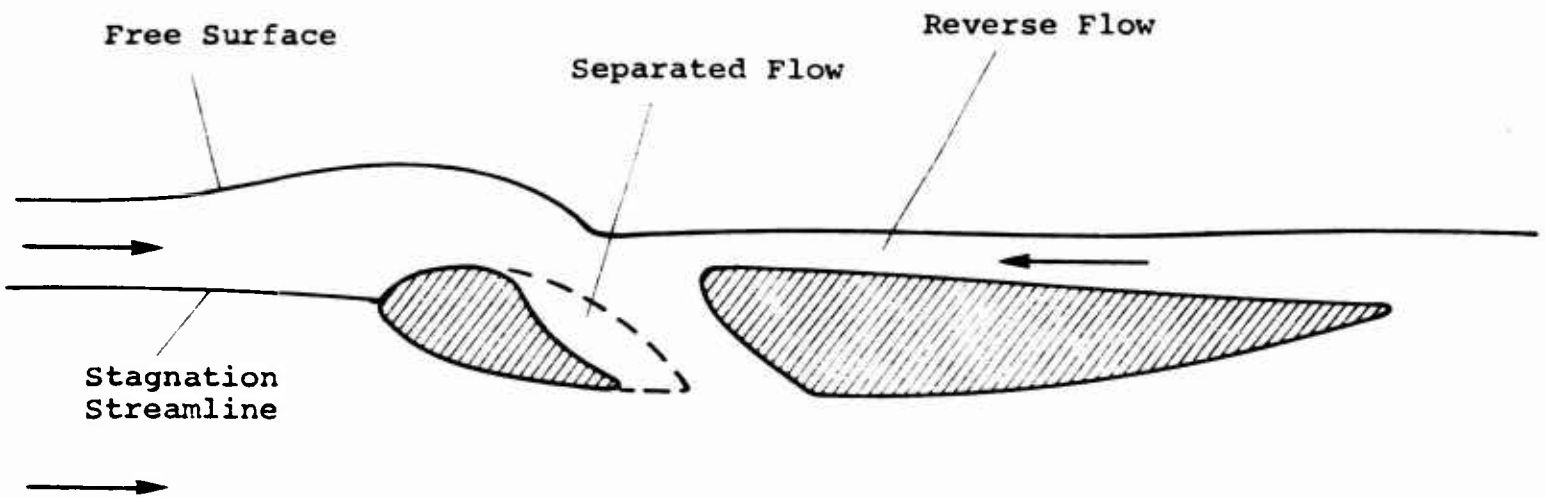

FIGURE 2.22: REVERSE FLOW ON NACA 4415 MODEL WITH SLOT WIDTH = 3.0 cm

flow proceeded in the normal direction. For stagnant or reverse flow over the rear portion there was of course no upper stagnation streamline.

Although the phenomenological theory developed for solid bodies has no provision for slot effects, the data for the front portion of the model can still be expressed on the same coordinates. Figure 2.23 shows the data for the experiments on the NACA 4415 and NACA 0015 slotted models. It can be seen that both the depth of the stagnation streamline data and the depth of the flow over the model data, followed the correlation lines closely.

The phenomenological theory is only valid where there is no significant curvature of the streamlines, the flow is essentially parallel to the undisturbed free surface, and the other conditions listed in Section 2.2 are met. These conditions are not met in the vicinity of the slot, and consequently the theory cannot be applied directly. Figure 2.24 shows the trends of the data with zero angle of attack and 1.0 cm and 3.0 cm slot widths. The coordinates of these graphs are similar to the correlation relating depth of stagnation streamline to freeboard except that the depth of the stagnation streamline has been generalized to include both stagnation streamlines and the net flow through the slot. As the model was lowered (moving from right to left) the flow rate through the slot increased from zero and reached a maximum near the point where the flow started over the rear portion of the model. As the model was lowered further, the flow rate over rear portion increased, but the flow through the slot remained relatively unchanged. At large negative freeboards, the free surface was unimportant and the model behaved as though it were immersed in an

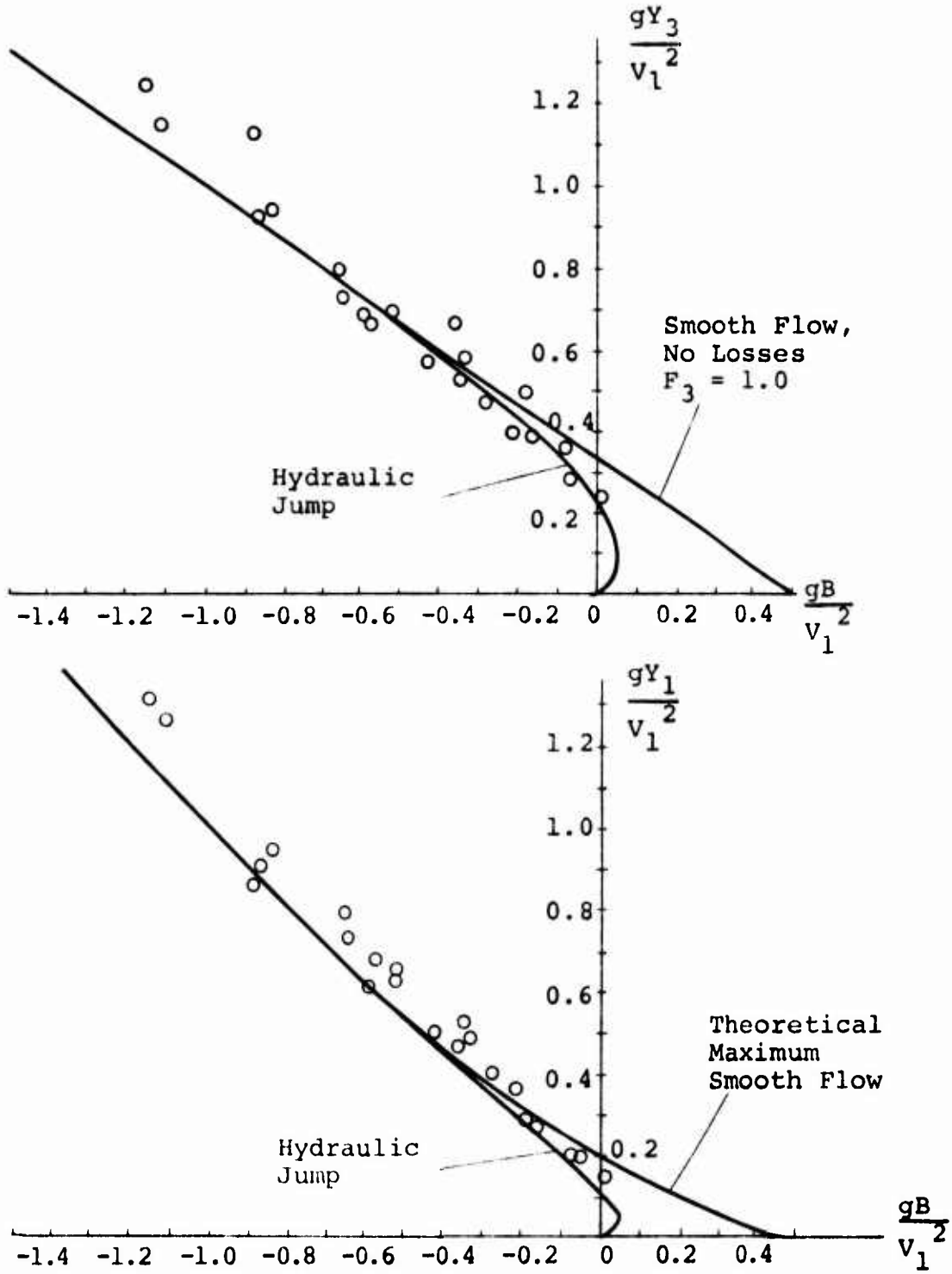

FIGURE 2.23: CORRELATIONS FOR BOWS OF SLOTTED MODELS: NACA 4415 and NACA 0015 PROFILES

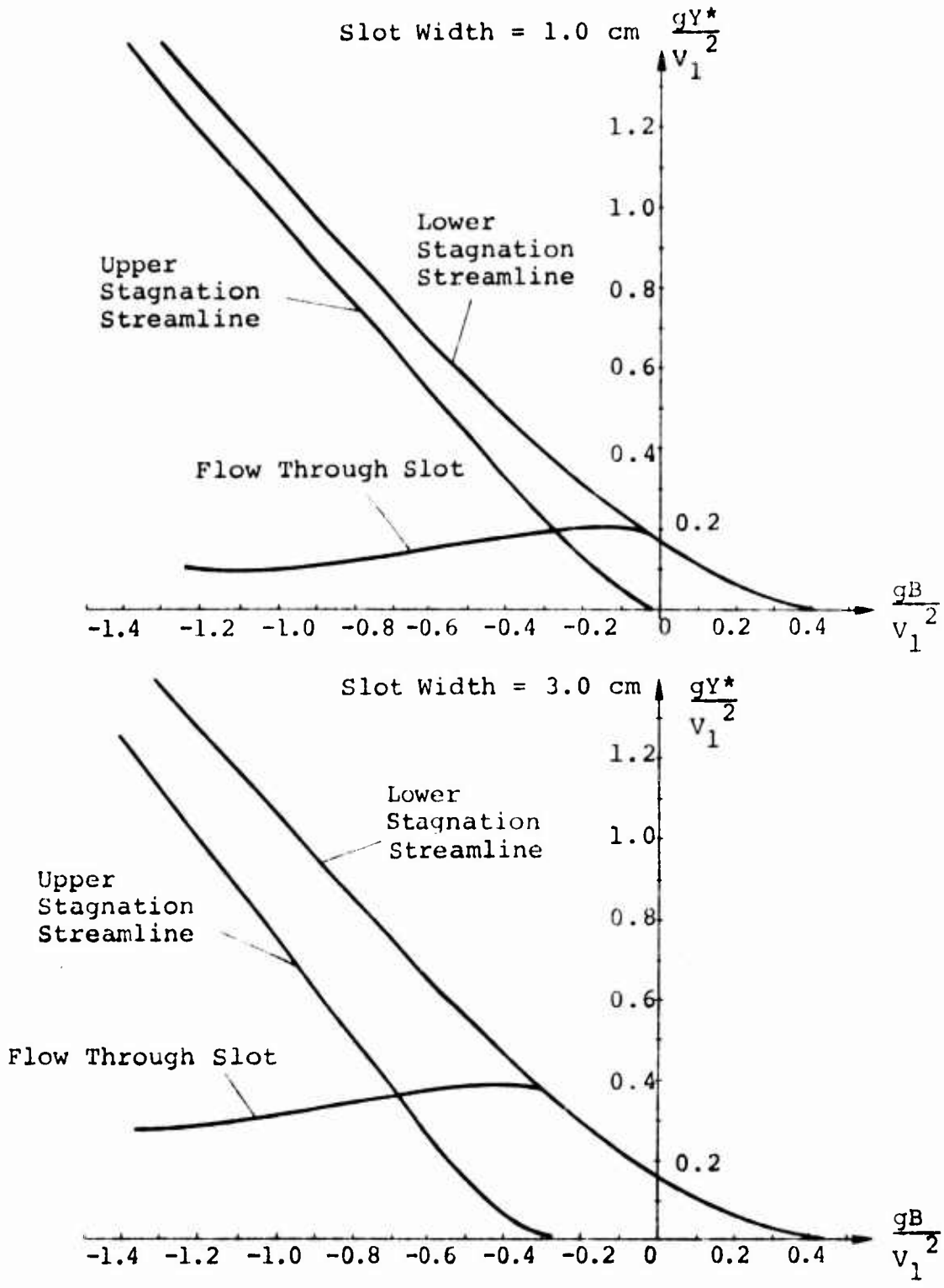

FIGURE 2.24: STAGNATION STREAMLINE DATA TRENDS FOR NACA 4415 PROFILE

infinite medium. Since the model was cambered, the flow rate through the slot should reach a non-zero asymptote. With a symmetric model, however, the pressure difference from top to bottom is reduced resulting in less flow through the slot at deep submergence. Nevertheless some slot flow at deep submergence will probably take place due to secondary flow effects.

2.5.3 NACA 0015 Model

The NACA 0015 model was built in an attempt to reduce the separation observed on the earlier models and to test the effects of slot position on a non-cambered profile.

As with the NACA 4415, the NACA 0015 model was tested briefly to determine favorable operating conditions and a testing matrix was set up for the systematic tests which followed. This matrix, Table 2.4, included experiments over a range of Froude numbers, freeboards, and relative widths of the two slots. Since the effect of slot width was determined for the NACA 4415 profile, the combined widths of the front and rear slots of the NACA 0015 profile was set to 3.0 cm and the relative widths of the two slots were varied as shown in Table 2.4.

The center section of this model was designed with a well-rounded bow and sharp trailing edge. In order to determine the effect of a sharp leading edge, this section was reversed for three tests. The Froude numbers and freeboards for these three tests were the same as those used on some of the tests with the center section in its normal position for comparison.

TABLE 2.4: TESTING MATRIX FOR NACA 0015 MODEL

Experiment Number (#)	Froude Number (F)	Freeboard cm (B)	Slot Widths Front	Slot Widths Rear	Angle (α)
Center Section Normal					
43	1.66	-1.26	3.0	0	0
44	1.69	-2.69	3.0	0	0
45	1.67	-4.55	3.0	0	0
46	.89	-1.09	1.5	1.5	0
47	1.13	-1.29	1.5	1.5	0
48	1.36	-1.08	1.5	1.5	0
49	1.36	-1.08	1.5	1.5	0
50	1.67	-1.22	1.5	1.5	0
51	1.68	-2.59	1.5	1.5	0
52	1.67	-4.28	1.5	1.5	0
53	1.61	-1.19	0	3.0	0
54	1.66	-2.69	0	3.0	0
55	1.68	-4.14	0	3.0	0
Center Section Reversed					
56	.91	-1.03	1.5	1.5	0
57	1.16	-1.32	1.5	1.5	0
58	1.59	-1.47	1.5	1.5	0

Since there were three model sections there were three stagnation streamlines - one for each portion of the model. Figures 2.25, 2.26 and 2.27 are photographs showing the location of these stagnation streamlines (made visible by dye injection) for a series of experiments. The velocity, freeboard and combined width of the slots were held constant, and the model's center portion was moved to vary the individual slot widths. These conditions are similar to those of experiments 43, 50, and 53. The free surface diagrams for these experiments have been reproduced in Figure 2.28. For all, the Froude number varied by less than 4 percent and the freeboard was constant within 0.07 cm. Since the total width of the slots remained fixed, the variation in these experiments consisted of different positions of the center portion of the model. When this portion was pushed forward the front slot was closed and the rear slot was 3.0 cm wide, etc.

In all three tests the flow rates over the rear portion of the model were approximately the same. It appears that this flow rate was independent of the position of the model's middle portion. This trend was born out by tests at other values of freeboard as well. The position of the model's middle portion did affect other aspects of the flow, however. In the forward position there was a hydraulic jump type bow wave; as the middle portion of the body was moved rearward there was a transition to smooth flow. Thus the location of the transition to smooth flow for the bow wave was a function of slot location. This shows that the slot can be used to provide smooth flow at greater values of freeboard than without the slot and allows thinner layers (and hence less water) to be skimmed off the surface.

Lower Stagnation Streamline (on Bow)

Upper Stagnation Streamline (on Rear Section)

FIGURE 2.25: STAGNATION STREAMLINES ON NACA 0015 MODEL:
FRONT SLOT CLOSED, REAR SLOT WIDTH = 3.0 Cm.

Lowest Stagnation Streamline (on Bow)

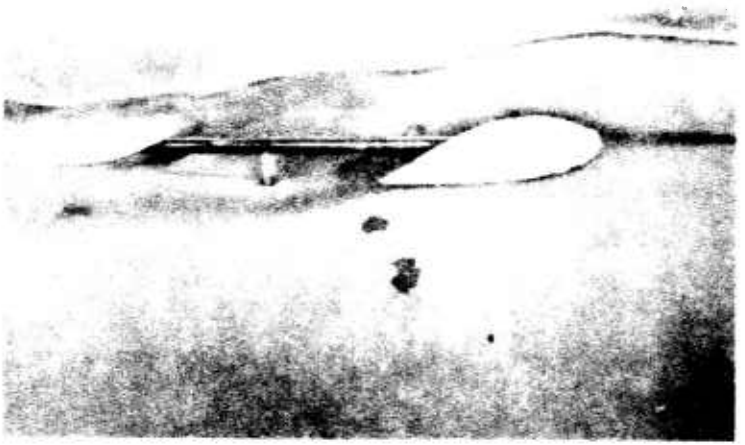

Middle Stagnation Streamline (on Center Section)

Upper Stagnation Streamline (on Rear Section

FIGURE 2.26: STAGNATION STREAMLINES ON NACA 0015 MODEL: BOTH SLOT WIDTHS = 1.5 Cm.

Lower Stagnation Streamline (on Bow)

Upper Stagnation Streamline (on Rear Section)

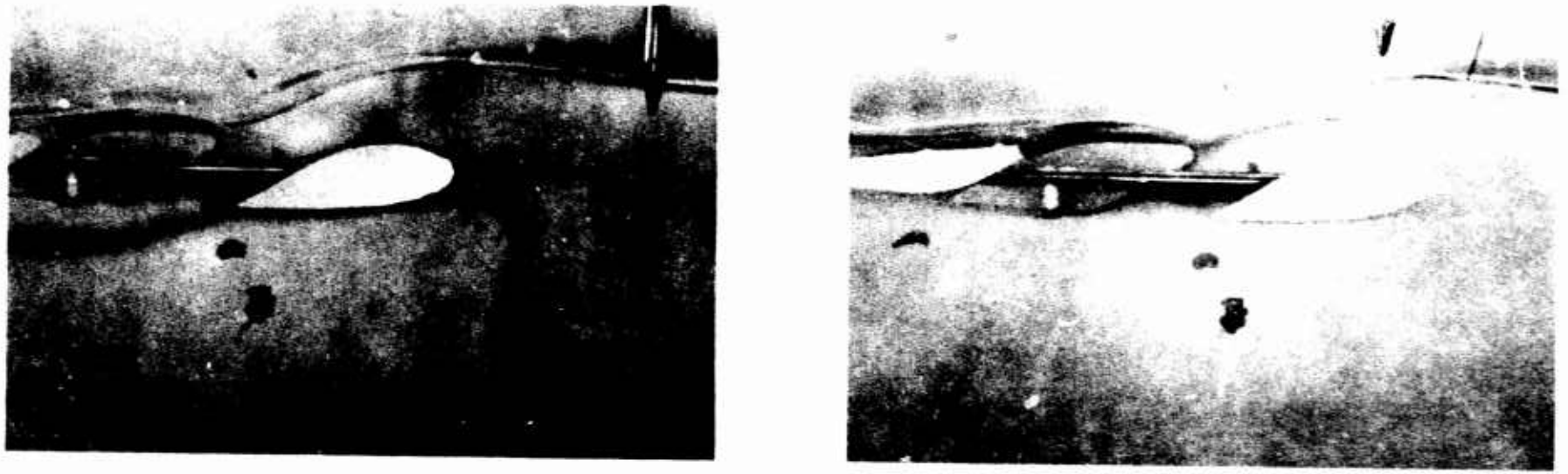

FIGURE 2.27: STAGNATION STREAMLINES ON NACA 0015 MODEL:
FRONT SLOT WIDTH = 3.0 Cm, REAR SLOT CLOSED

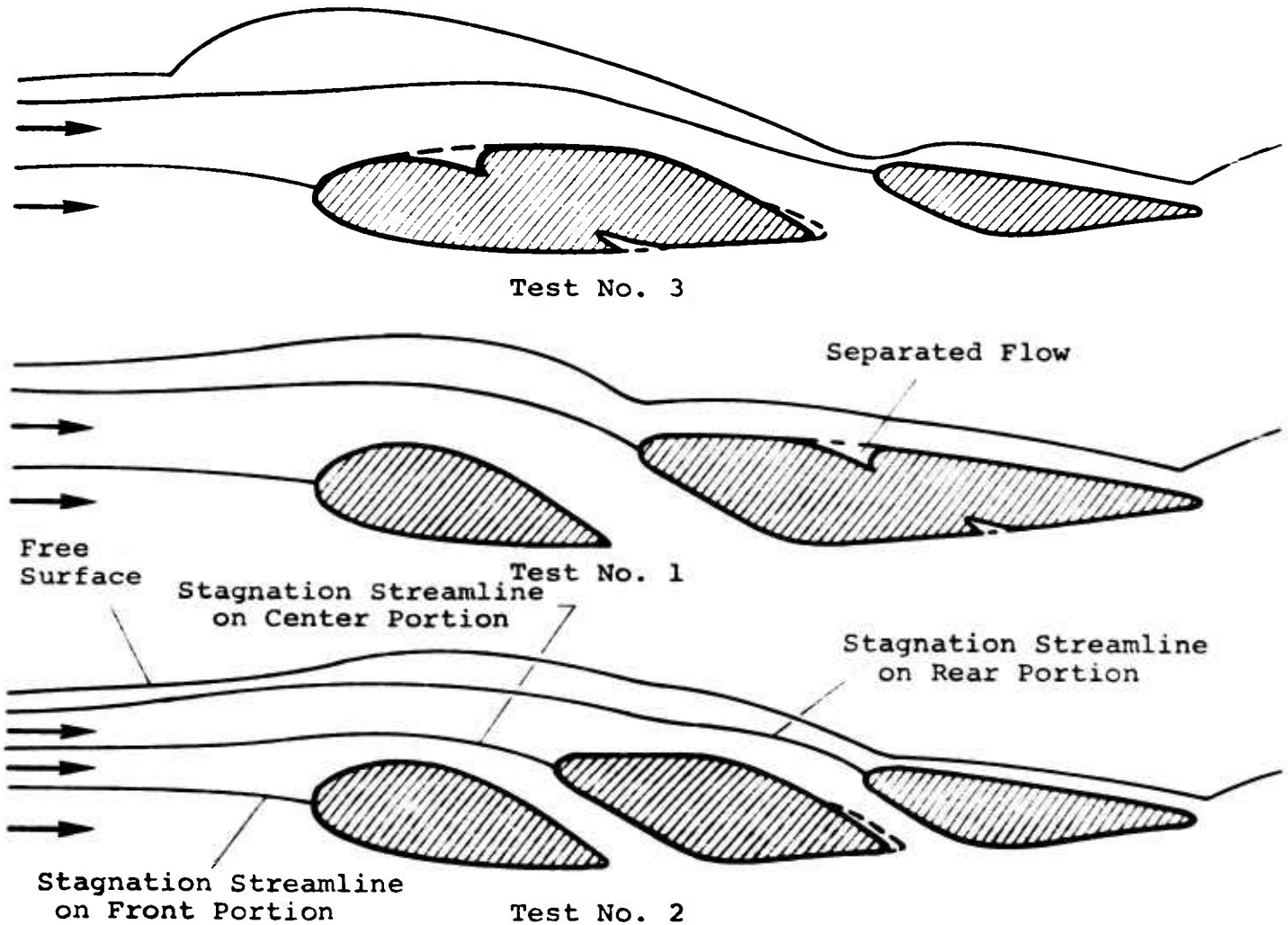

FIGURE 2.28: RESULTS OF EXPERIMENT NUMBERS 43, 50 AND 53 oN NACA 0015 MODEL

The separation of the flow within the front slot noted on the NACA 4415 model was greatly reduced here as a result of more careful slot contour design. A small piece of tape was placed on the upper surface of the model's front portion to determine the effect of surface roughness. The result was a further reduction in size of the separated flow region. This implies that the separation occurs as a result of a boundary layer phenomenon. Roughening the surface churned up the flow increasing the fluid momentum near the surface and thus separation was reduced.

Under some operating conditions no flow passed through the second slot even though it was submerged. By the time flow reached the second slot, it had passed over much of the model surface and a substantial boundary layer had developed. In addition the symmetric design of the model provided little pressure differential across the slot. These effects combined to reduce flow in the second slot.

The flow map for the NACA 0015 model with each slot width at 1.5 cm appears in Figure 2.29. This flow map is more complex than the others presented previously because this model had three separate sections and consequently three lines of maximum freeboard, and three transition lines. Although the flow map is complicated, the behavior of the model was as expected. At very high freeboards no flow passed over any of the model's sections. As the model was lowered, flow started first over the front section with a turbulent bow wave. As freeboard was lowered further, there was a transition to a smooth bow wave. Lowering the freeboard also started flow over the other model sections. As with the NACA 4415 model flow map, the transition lines on this drawing are approximate due to difficulty in observing the exact points of transition experimentally.

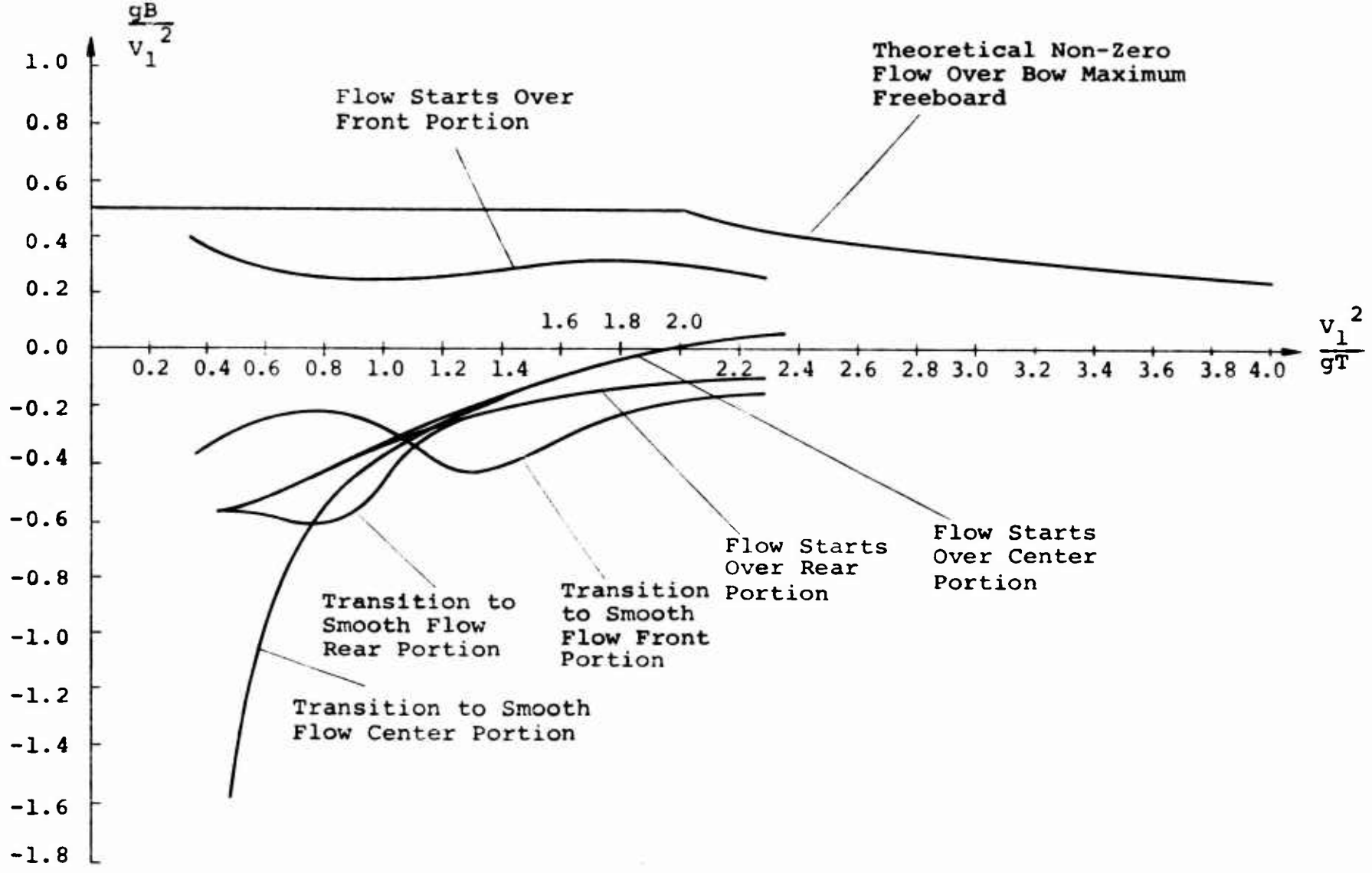

FIGURE 2.29: FLOW MAP FOR NACA MODEL WITH EACH SLOT SET AT 1.5 cm WIDE (TRENDS OF DATA)

The correlation of NACA 0015 data with the phenomenological theory appears in Figures 2.30 and 2.31 and, as expected, the depth of flow over the front section, Y_3, followed the correlation closely. The depth of the stagnation streamlines on the center and rear model sections however, were influenced by inertial effects and thus the data do not fit the correlation lines. Since there are three separate portions there are three stagnation streamlines and the depth of each stagnation streamline may be plotted on the same coordinates as the bow wave correlation lines. Figure 2.31 shows that the depth of the stagnation streamlines on the second and third portions are functions of velocity (this may be taken as a dependence on Froude number based on model thickness, $V_1/\sqrt{gT}$.

This dependence on velocity was not understood when experiments were run on the NACA 4415 model. Consequently, the scatter in the data was attributed to experimental error rather than any systematic inertial effects. Consequently, the correlation data for the upper stagnation streamline on the NACA 4415 model should be considered as an average of all velocities tested.

Experiments were also run on the NACA 0015 double-slot model with center section reversed. The purpose of these tests was to determine the effect of a sharp leading edge for the second (or third) portion of a hydrofoil. Tests were run at values of freeboard, velocity, and slot width similar to some of the tests on the NACA 0015 model in its normal configuration.

It was expected that the sharp leading edge would act like a knife to cut off a layer of water with little disturbance

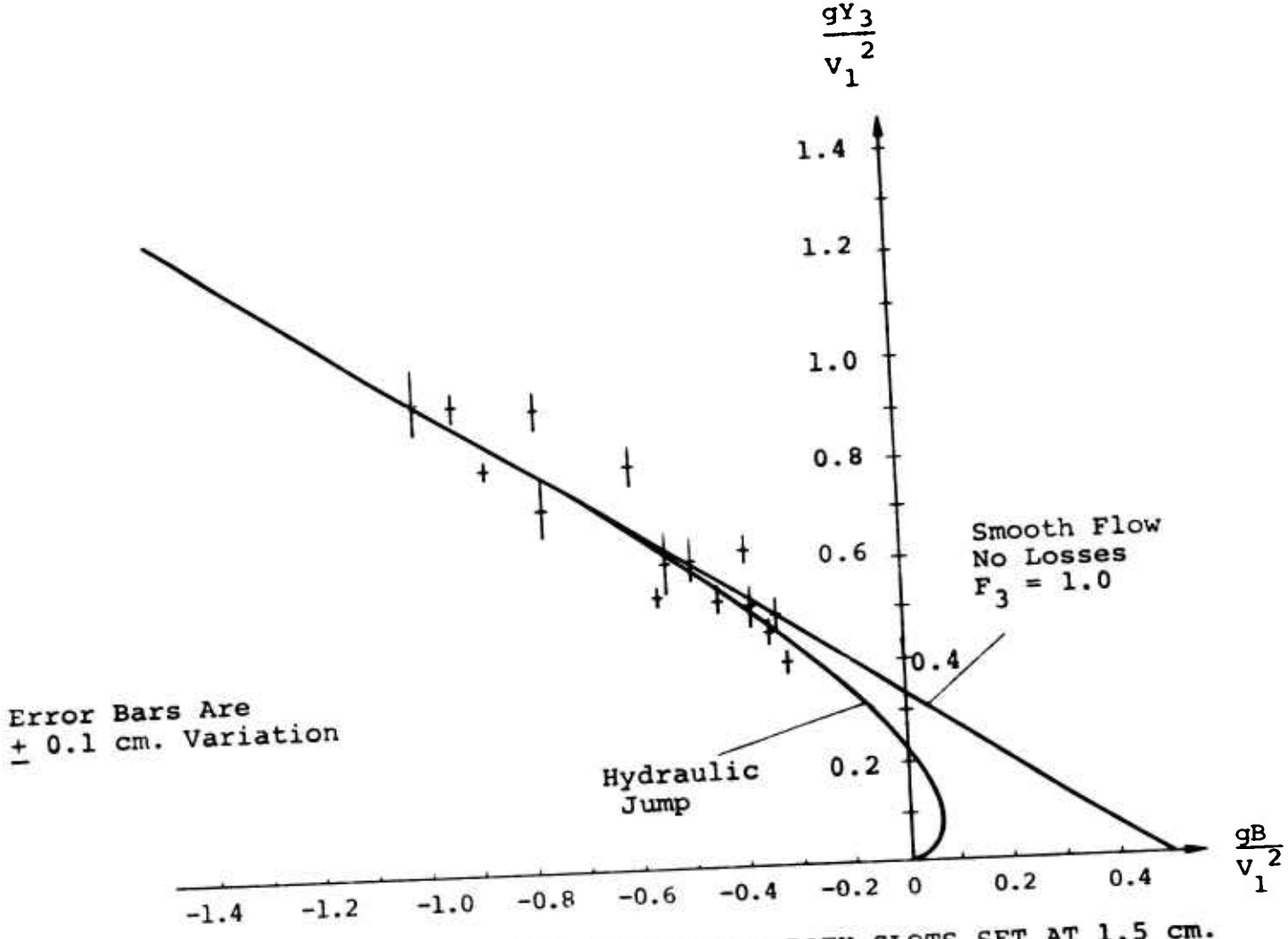

FIGURE 2.30: NACA 0015 MODEL WITH BOTH SLOTS SET AT 1.5 cm.
CORRELATION OF DATA WITH THEORY (FRONT PORTION)

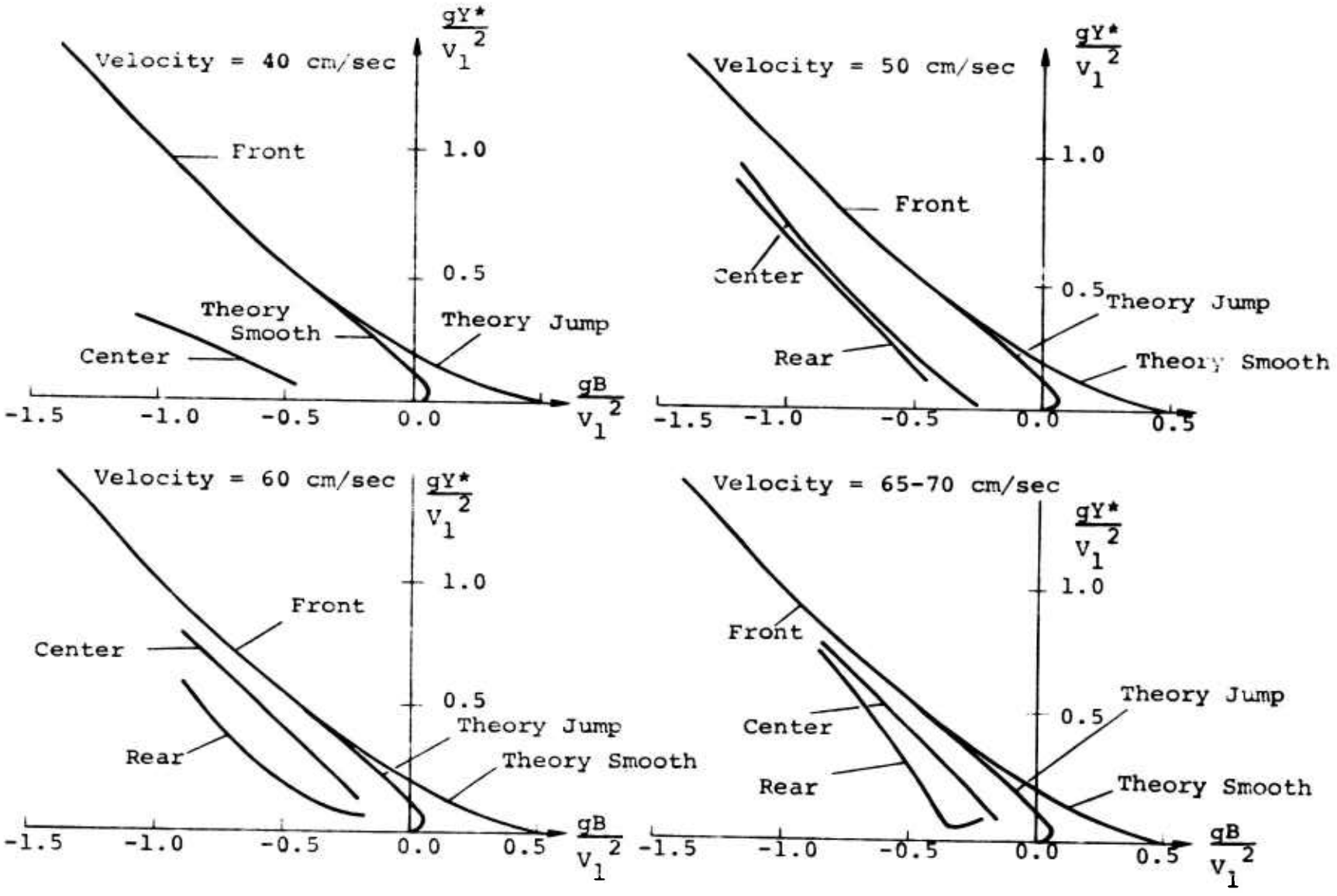

FIGURE 2.31: NACA 0015 MODEL WITH EACH SLOT WIDTH = 1.5 cm. CORRELATION OF DEPTHS OF STAGNATION STREAMLINES WITH THEORY AT VARIOUS VELOCITIES (TRENDS OF DATA)

to the surface. The free surface drawings bear this out. The location of the stagnation streamlines were essentially unchanged upstream of the sharp leading edge. Downstream, however, the flow through the second slot was greatly affected as was the flow behind the model.

2.5.4 NACA 0015-4415 Model

Although the previous two models were based on standard NACA profiles, operation at large slot widths altered the overall shape substantially. A better design technique would be to consider the front and rear portions of the model as individual hydrofoils and perhaps choose standard profiles for each. A new model was constructed using this technique with a small front section of NACA 0015 profile, and a larger rear section of NACA 4415 profile (Figure 2.32). The slot was the space between the two profiles, and it could be changed by orienting the two model sections in various configurations.

A series of tests were performed at several orientations of the front and rear sections with constant velocity (in order to compare results). For each orientation, data were taken at two values of freeboard: zero, and the value such that the depth of flow over the model's rear portion was about 0.5 cm. The testing matrix appears in Table 2.5. The data consisted of drawings of the free surfaces and stagnation streamlines, and photographs. These tests were designed to give an overview of this model's operation rather than a detailed systematic determination of flow maps and correlation lines.

TABLE 2.5: TESTING MATRIX FOR NACA 0015 - 4415 MODEL

Experiment Number (#)	Froude Number (F)	Freeboard cm (B)	Test Number* (#)
59	1.44	-0.16	1
60	1.48	+ .57	2
61	1.43	+ .07	2
62	1.45	+ .06	3
63	1.43	- .13	3
64	1.40	+ .03	4
65	1.37	- .37	4
66	1.48	+ .06	5
67	1.43	- .46	5
68	1.44	+ .72	6
69	1.38	+ .04	6
70	1.47	+ .53	7
71	1.43	- .04	7

*Test numbers refer to orientations of front and rear section described in Figure 2.15.

Figures 2.33 through 2.39 show typical operation of this model at various orientations of the front section relative to the rear section. In several photographs it appears that there are two free surfaces - an effect of the means of support. Each model section was divided into three parts separated and held in alignment by thin transparent plastic plates, and the side channels, thus formed, contained flow in the boundary layers on the channel walls; consequently, the side channels had a lower effective velocity than the main channel and the flow behaved differently. Measurements of the stagnation streamlines and free surfaces were taken in the center of the channel so the additional free surfaces appearing in the photographs can be disregarded.

In these experiments, the flow over the rear section of the model was always turbulent (hydraulic jump type bow wave), and the raising of the transition-to-smooth-flow-line on the flow map, as in the other slotted models, was not observed. However, the intensity and location of the bow wave were functions of orientation. Varying the orientation had other substantial effects also. When the front portion was far upstream and at zero angle of attack, it had little effect and the flow over the rear portion was quite similar to that observed over the single NACA 4415 model with the slot closed (Figures 2.34, 2.35, and 2.37). However, as the front portion was rotated or moved rearward, the flow downstream was affected (Figures 2.33, 2.36, 2.38, and 2.39). The depth of flow over the rear portion varied from 0.0 to 0.8 cm resulting in substantially different free surface conditions. In addition, the location of the stagnation streamline changed considerably. In all cases, however, the flow downstream from the model was essentially the same--the various orientations only changed the local

FIGURE 2.32: NACA 0015-4415 MODEL

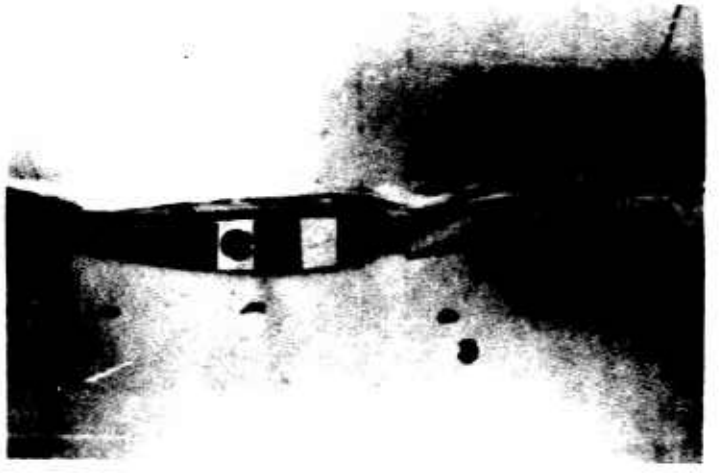

FIGURE 2.33: NACA 0015-4415 MODEL: PORTIONS CLOSE TOGETHER - DYE INJECTION REVEALS UPPER STAGNATION STREAMLINE

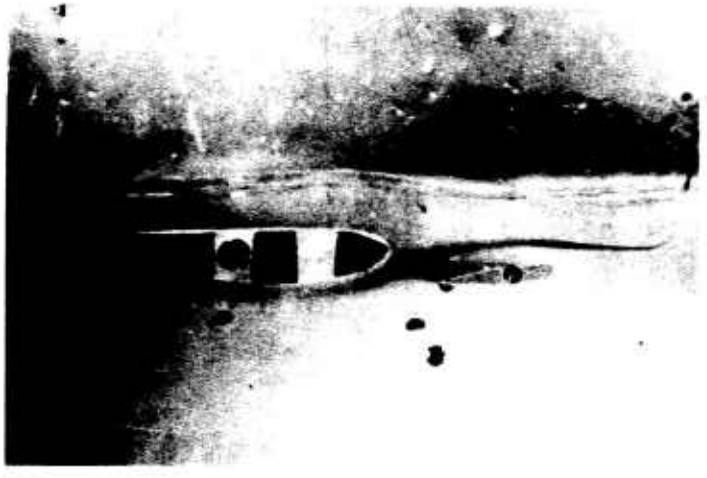

FIGURE 2.34: NACA 0015-4415 MODEL: FRONT PORTION AT NEAR ZERO ANGLE OF ATTACK-NOTE SMALL DISTURBANCE TO FLOW-DYE REVEALS FLOW THROUGH SLOT

FIGURE 2.35: NACA 0015-4415 MODEL: PORTIONS FAR APART-DYE INJECTION REVEALS LOWER STAGNATION STREAMLINE

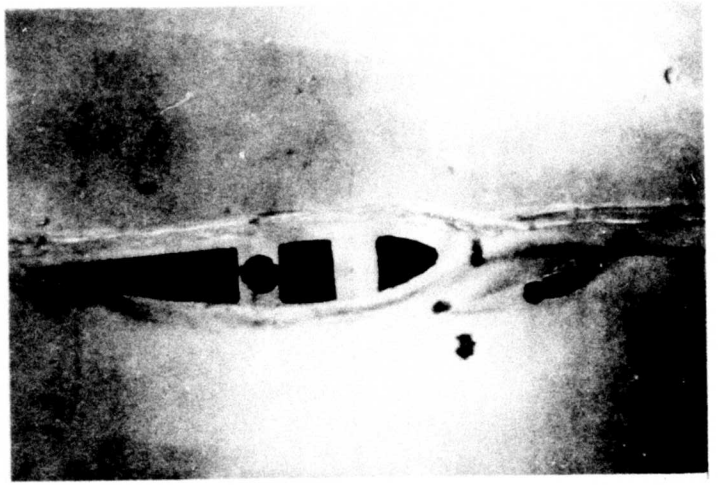

FIGURE 2.36: NACA 0015-4415 MODEL: SECTIONS CLOSE TOGETHER - FRONT SECTION LOWER THAN IN FIGURE 2.33

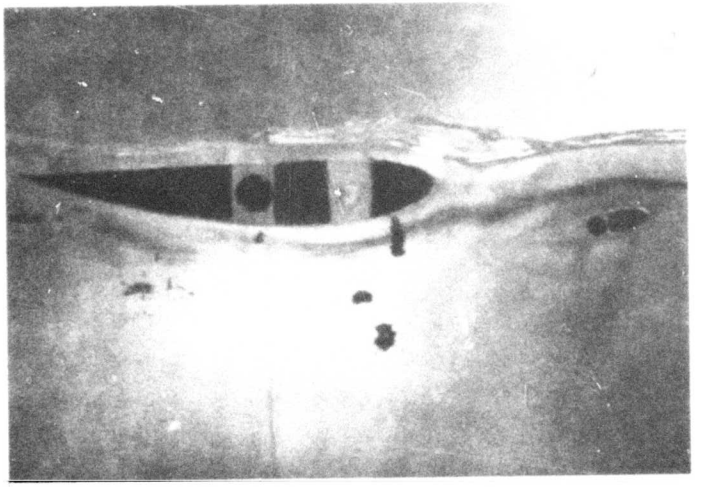

FIGURE 2.37: NACA 0015-4415 MODEL: SECTIONS FAR APART - DYE INJECTION REVEALS FLOW THROUGH SLOT

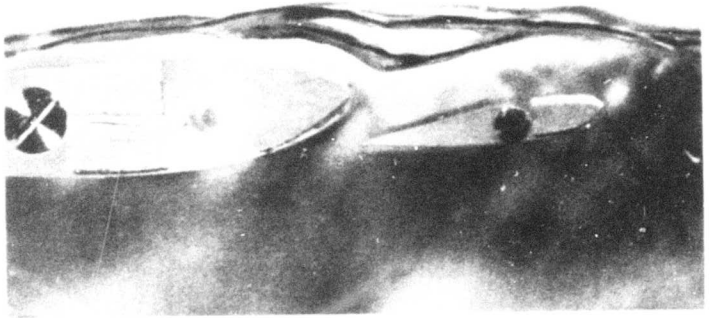

FIGURE 2.38: NACA 0015-4415 MODEL: CLOSEUP SHOWING TWO FREE SURFACES IN UNDISTURBED MODE

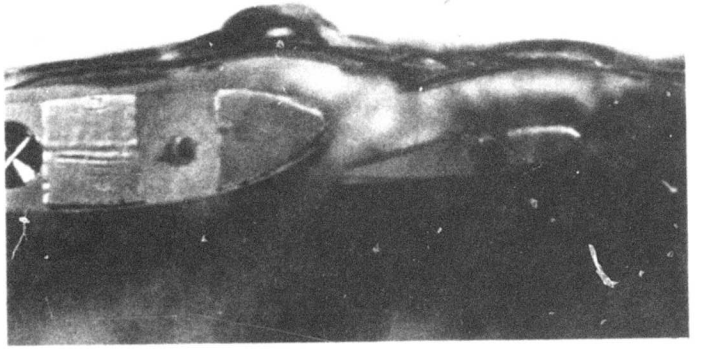

FIGURE 2.39: NACA 0015-4415 MODEL - NOTE SURFACE FLUCTUATIONS

flow conditions. This was a reasonable result considering that the freeboard, velocity, and size of the model did not change.

In summary, tests on this model have indicated that its performance was inferior to the other slotted models. Although the model's construction allowed the slot shape to be varied over a wide range, the elimination of a turbulent bow wave at high freeboards (noticed on the other slotted models) could not be effected. None of the orientations tested proved significantly superior to the others and consequently no systematic tests were performed to determine flow maps or correlation lines.

2.6 Conclusions

The following general conclusions apply to the operation of the slotted hydrofoil:

1. The important scaling parameters are: $F = V_1/\sqrt{gT}$ and $G_B = gB/V_1^2$
2. Operation at high positive freeboard produces a turbulent bow wave and a small amount of flow over the hydrofoil.
3. Operation at lower freeboards causes a transition to a smooth bow wave and increases the flow rate over the hydrofoil.
4. The point of transition from turbulent to smooth bow wave is determined by model shape and the scaling parameters.
5. Slots in the profile can bypass some flow from the upper side to the lower side of the hydrofoil, thus reducing the amount passing over the model's rear portion.
6. The flow through a slot increases with slot width.
7. Slot position does not appear to be of major importance in determining total flow through it; however, slot geometry is a significant parameter.
8. Operation with an open slot, in some cases, allows a smooth bow wave to form at higher freeboards where, with the slot closed, a turbulent bow wave would normally result.

SECTION 3

Tow Tank Experimental Program

3.1 Introduction

The general philosophy behind the development of the SAI Services Fast Current Oil Response System has been to experiment with models that are full scale. In this manner, the problems associated with scaling a device over an order of magnitude are eliminated from the outset. In order to achieve this objective during the Phase I program, the type of model and its size were matched to the available test facilities. The test facility ultimately chosen for the bulk of the concept feasibility work was the U.S. Environmental Protection Agency 30.5 m long tow tank located in Edison, New Jersey. The main reasons for choosing this facility were that it had a reasonable velocity range, was capable of generating waves and was able to accomodate a realistically sized model. Once the question of the test facility was resolved, a very flexible control/recovery device was designed and fabricated. The control/recovery device was designed to allow for a multitude of changes to be made without reconstructing major components of the system. Thus, the model had provisions for moving the hydrofoil, polyurethane foam belt, air jet and flotation pontoons over a wide range of positions. This flexibility in design proved to be quite useful during the course of the experimental program. The experiments performed in the tow tank were primarily aimed at determining the configuration of the control/recovery device which performed most efficiently. Therefore, a systematic variation of the many parameters involved in this experiment was undertaken until a final

design was established. However, this design was not determined until very late in the program, and therefore a minimum of experience with its operating characteristics was obtained prior to the initiation of the final demonstration program at the University of Michigan.

3.2 Description of Test Facility

The major portion of the control/recovery system development was performed in the U.S. Environmental Protection Agency tow tank. This tank is 30.5 m long, 3.65 m wide and 0.75 m deep. The test carriage (Figure 3.1) is capable of towing models at speeds up to 4.05 knots and in waves not exceeding 30.0 cm in height. Figure 3.2 is a photograph of the wave generator which is located in the far end of the tank. This device consists of two triangular wedges which can be lowered at various frequencies, in or out of phase, into the water to produce waves. Figure 3.3 is a photograph of the near end of the tank (from which the carriage initiates the towing sequence) and shows the wave absorbing beach and the A-frame used to remove the beach from the tank. The beach consists of two sections of 25-2.5 cm x 2.5 cm x 3.65 m wood slats supported at the ends and in the middle by 4-7.5 cm x 7.5 cm x 1.8 m aluminum angles. In between the 38.0 cm space separating the two sections are placed six wire mesh cages containing rubberized horse hair. The wave generator and beach have combined to produce reasonable non-reflecting waves of up to 30.0 cm in height. The towing carriage (Figure 3.4) is a 3.65 m wide and 1.83 m long rectangular aluminum frame with a plywood deck, and is supported by 4-38.0 cm diameter bicycle tires. The towing carriage is attached to a moving cable system (located on either side of the tank) by friction clamps and is driven with a variable speed electric motor.

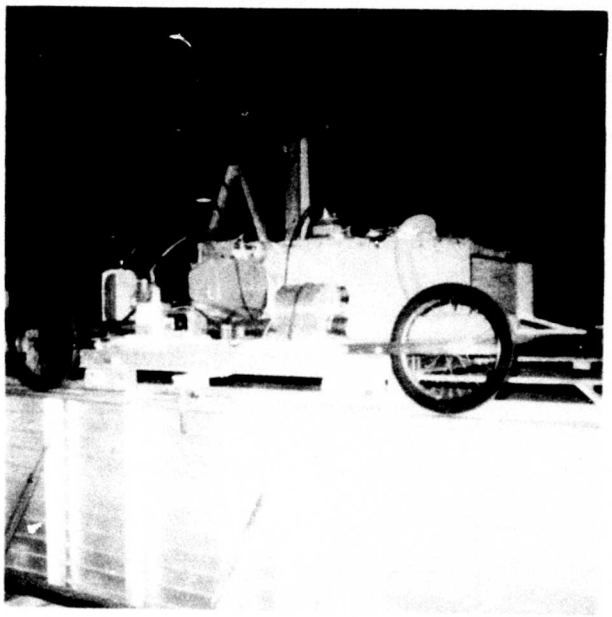

FIGURE 3.1: EPA TOW TANK TEST CARRIAGE

FIGURE 3.2: EPA TOW TANK WAVE GENERATOR

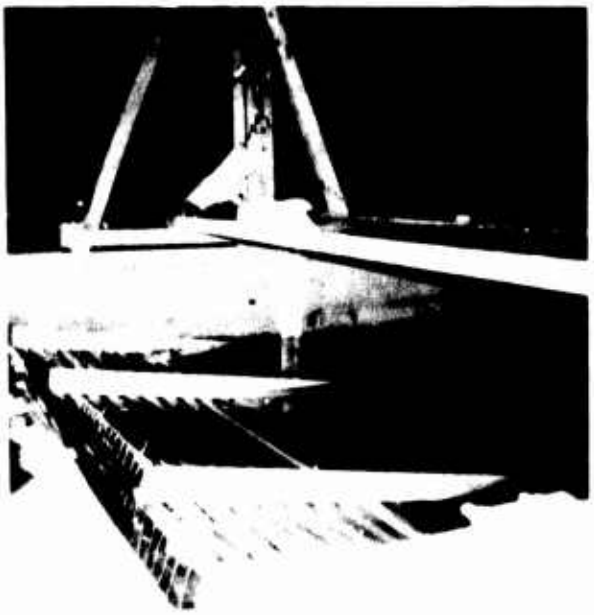

FIGURE 3.3: EPA TOW TANK WAVE ABSORBING BEACH

FIGURE 3.4: EPA TOW TANK TEST CARRIAGE DECK SHOWING AIR BLOWER UNIT AND RELATED EQUIPMENT

For the present series of tests, several additional pieces of equipment were added to the carriage. Figure 3.4 is a photograph of the carriage deck showing the Paxton CB-80-H air blower and related equipment. The performance curves for the air blower are shown in Figures 3.5 and 3.6 for the discharge pressure versus air flow and for discharge pressure versus motor RPM, respectively. Figure 3.7 is a photograph of the front end of the carriage and shows the towing arms attached to the control/recovery device as well as the oil distributor. The oil distributor consists of a 6.0 cm. long and 10.5 cm. diameter aluminum tube, closed at either end, with a series of 11 holes placed 2.5 cm on centers in a straight line. The tube is filled with oil and turned downward (with the holes facing the water surface) during an oil test sequence. The oil flow rate is determined by the size and number of holes and by the height and viscosity of fluid in the tube. The hole diameters can be varied by taping aluminum inserts over the existing holes. Very few oil tests were conducted in the test program, and for these 0.35 cm diameter holes were used which resulted in an oil delivery rate of 8.9 gms/sec of 500 cs oil.

3.3 Control/Recovery Model Description

Schematic drawings showing the various components of the SAI control/recovery system appear in section 1 of this report. Photographs of this model during the various stages of development are shown here and discussed in detail. Figure 3.8 is a photograph of the NACA 4415 hydrofoil section during the preliminary stages of construction. This hydrofoil had a chord length of 51.0 cm and a maximum thickness of 7.6 cm and a total width of 0.61 m. An

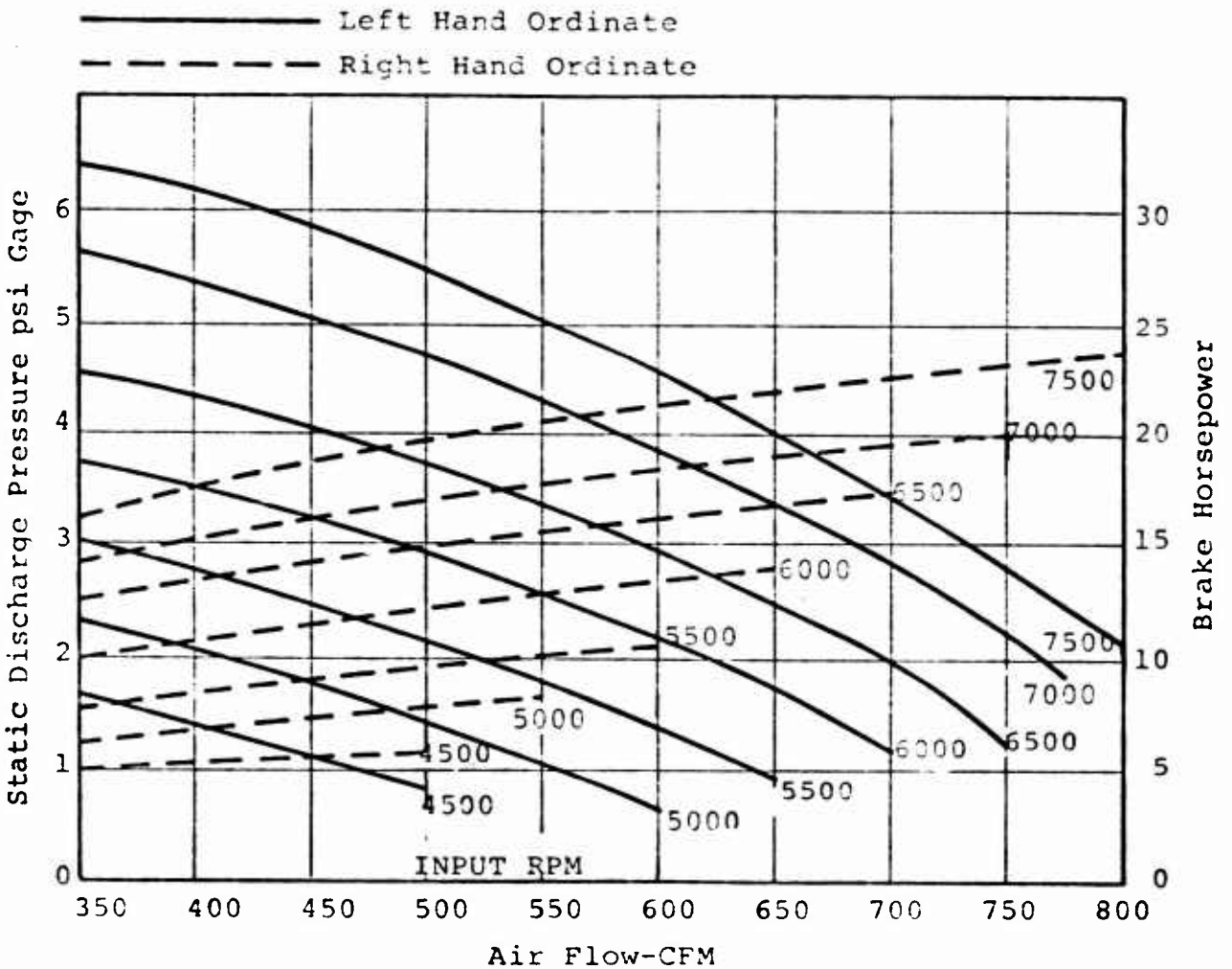

FIGURE 3.5: PERFORMANCE CURVE FOR PAXTON CB-80-H AIR BLOWER: STATIC DISCHARGE PRESSURE (psi gage) VERSUS AIR FLOW (CFM)

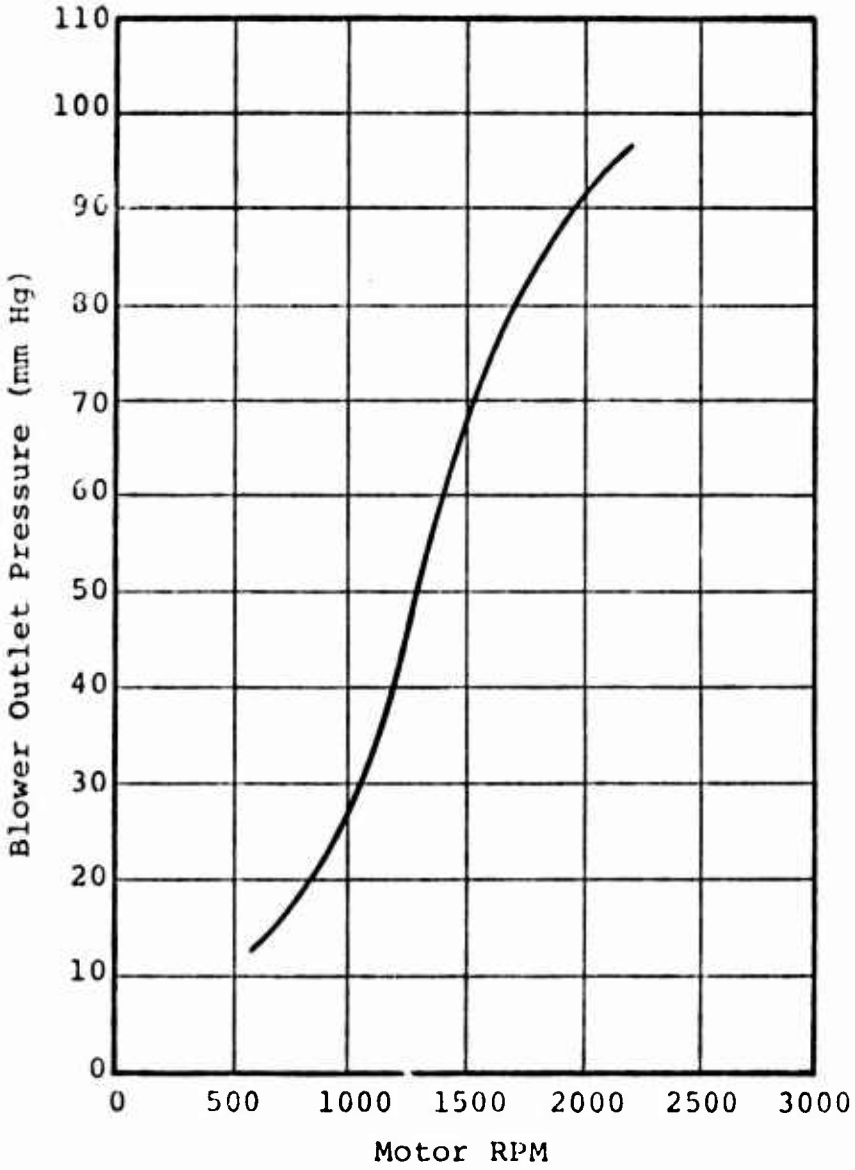

FIGURE 3.6: PAXTON CB-80-H AIR BLOWER CALIBRATION CURVE: MOTOR REVOLUTIONS PER MINUTE (RPM) VERSUS BLOWER OUTLET PRESSURE (mm Hg)

FIGURE 3.7: CONTROL/RECOVERY SYSTEM TOWING ARMS AND OIL DISTRIBUTION SYSTEM MOUNTED ON TOWING CARRIAGE

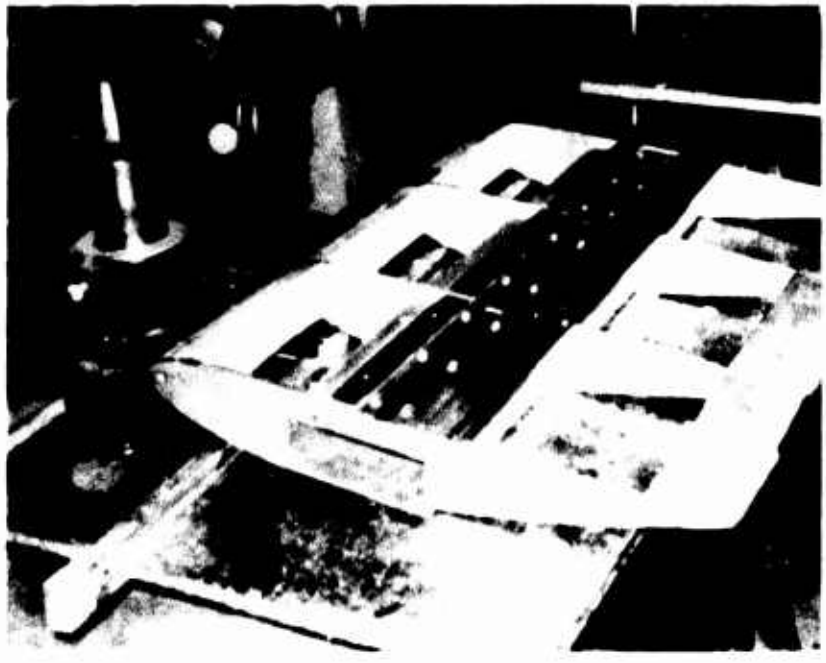

FIGURE 3.8: PHOTOGRAPH OF NACA 4415 HYDROFOIL SECTION DURING PRELIMINARY STAGES OF CONSTRUCTION

aluminum extrusion was placed through the hydrofoil at the midchord to serve as a plenum chamber for the hydrofoil air jet. This plenum chamber had a cross section which measured 12.6 cm x 5.6 cm. A slot was cut along the entire 0.61 m width of the extrusion to serve as the outlet for the air jet. Various plexiglass nozzle inserts were designed to fit into this slot so that the angle and width of the hydrofoil jet could easily be changed. In Figure 3.9 the hydrofoil is shown nearly completed. Polystyrene blocks were used to fill in the empty spaces between the ribs of the hydrofoil and a 0.058 cm aluminum skin was pop riveted onto the 0.63 cm aluminum ribs. The hydrofoil is shown installed on the main frame of the control/recovery device in Figure 3.10. The main frame of this system was constructed of 0.63 cm plexiglass and measured 1.2. m in length and 0.76 m in height. The hydrofoil was adjustable in the vertical direction and in angle of attack by bolting it to plexiglass side plates which covered the bolt hole and clearance slots. Various mounting brackets are also shown in Figure 3.10 which were used to mount the vertically and horizontally adjustable flotation pontoons. Figure 3.11 is another view of the main frame which more clearly shows the adjustable mounting brackets for the rotating belt of polyurethane foam and the air jet apparatus used to blow over the top surface of the hydrofoil. The air jet plenum chamber was constructed from 10.0 cm diameter copper tubing and had two 7.6 cm diameter air inlets. Wire mesh screen was placed inside of the plenum chamber to provide for a uniform exit velocity condition. The air jet also had an adjustable exit slot width (between 0.0 and 0.94 cm) and was capable of being rotated through an angle of 180° and moved both vertically and horizontally. Figure 3.12 shows

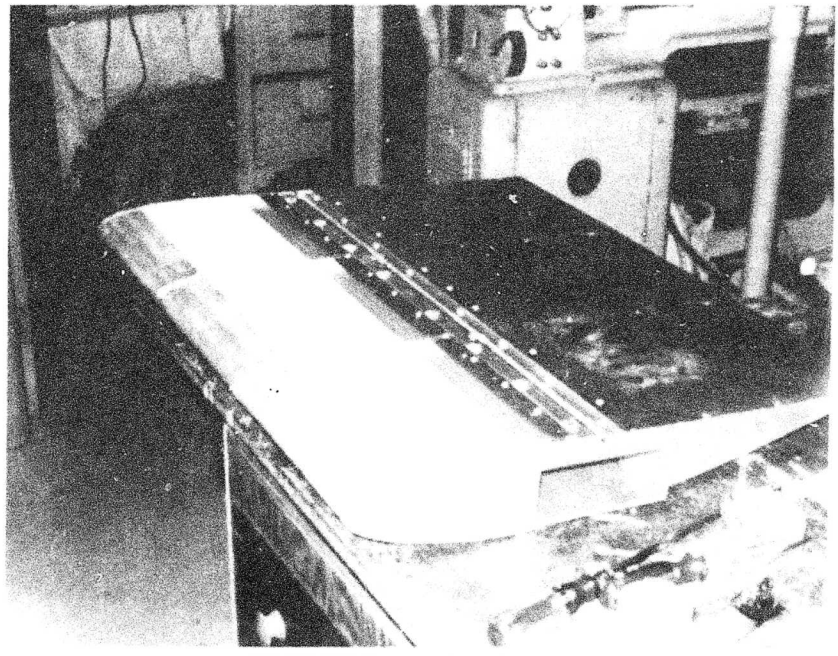

FIGURE 3.9: PHOTOGRAPH OF NACA 4415 HYDROFOIL SECTION NEAR COMPLETION

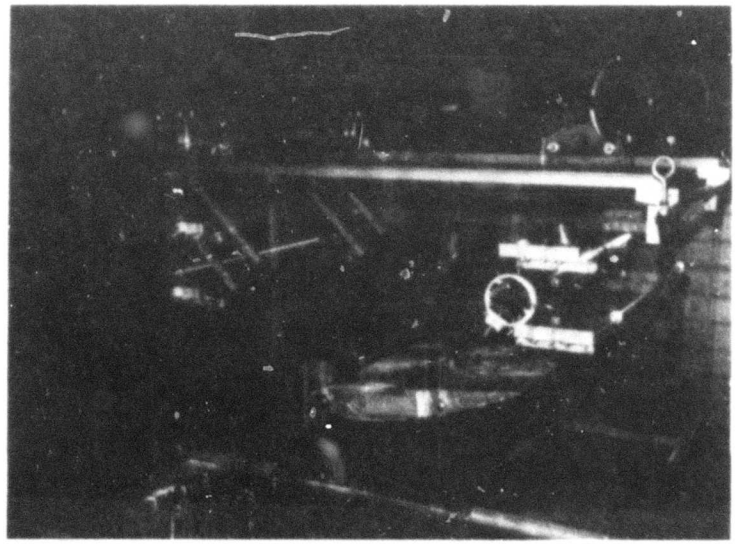

FIGURE 3.10: PHOTOGRAPH OF COMPLETED NACA 4415 HYDROFOIL SECTION INSTALLED ON MAIN FRAME OF CONTROL/RECOVERY DEVICE

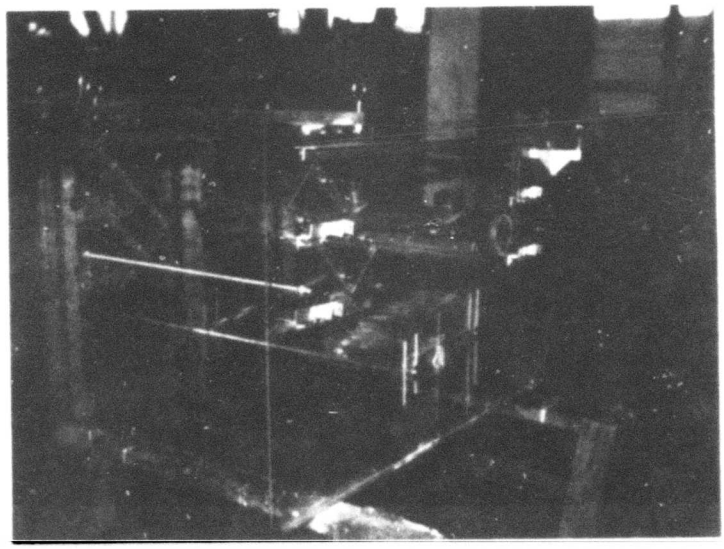

FIGURE 3.11: PHOTOGRAPH OF THE MAIN FRAME OF THE CONTROL/RECOVERY DEVICE SHOWING FOAM BELT MOUNTING BRACKETS AND AIR JET MANIFOLD

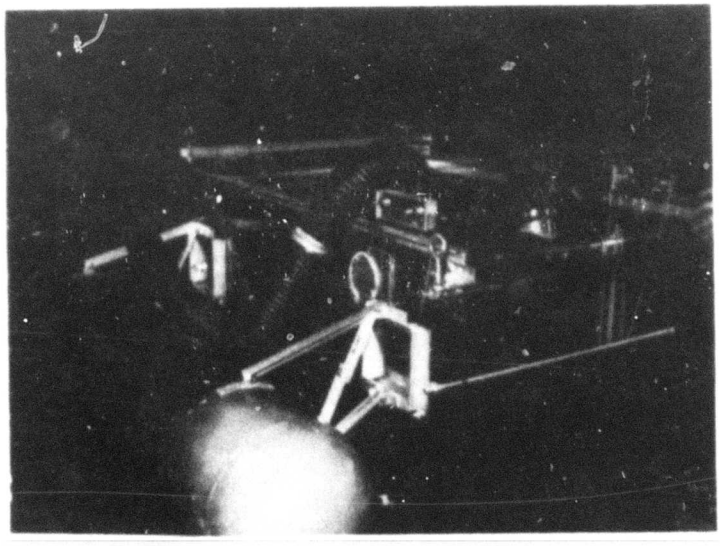

FIGURE 3.12: PHOTOGRAPH SHOWING THE FLOTATION PONTOONS MOUNTED ON THE MAIN FRAME OF THE CONTROL/ RECOVERY DEVICE

the flotation pontoons connected to the main frame of the control/recovery device, as well as the two 7.6 cm diameter flexaust tubes used to supply air to the air jet plenum chamber. The flotation pontoons were constructed of 1.21 m lengths of 25.0 cm diameter polyvinyl-chloride (PVC) pipe with balsa wood nose and rear inserts. The interior of the pontoons were filled with a foaming material to prevent water from entering and changing its buoyancy characteristics. Figure 3.13 is a side view of the front portion of the control/recovery device showing the aluminum extensions to the main frame which were used to prevent water from being pushed by the flotation pontoons into the interior of the system. Figure 3.14 is a front view of the interior to the control/recovery system and shows the leading hydrofoil (which forms the vented slot) installed into the system. The leading hydrofoil is of the same design (NACA 4415) as the main hydrofoil but is only 20.3 cm in length. This hydrofoil section slides along the chord line of the main hydrofoil on two side rails and has an adjustable vented slot from 0.0 to 45.0 cm in length. Figure 3.15 is a rear side view of the control/recovery device mounted on the towing carriage with the air jet in operation. A fine water spray can be seen covering the entire rear exit plane of the system.

During the course of the test program (discussed in section 3.5) the air jet was eliminated from consideration. The final system then resembled that shown schematically in Figure 1.2. The actual hardware appearing in that drawing is shown in Figure 3.16. The 10.0 cm long 30° angle ramp has a 2.5 cm separation from the 30° angle polyurethane foam belt. The belt is shown in Figure 3.17; it is a 2.5 cm thick 10 ppi polyurethane foam belt which has a wrapped around

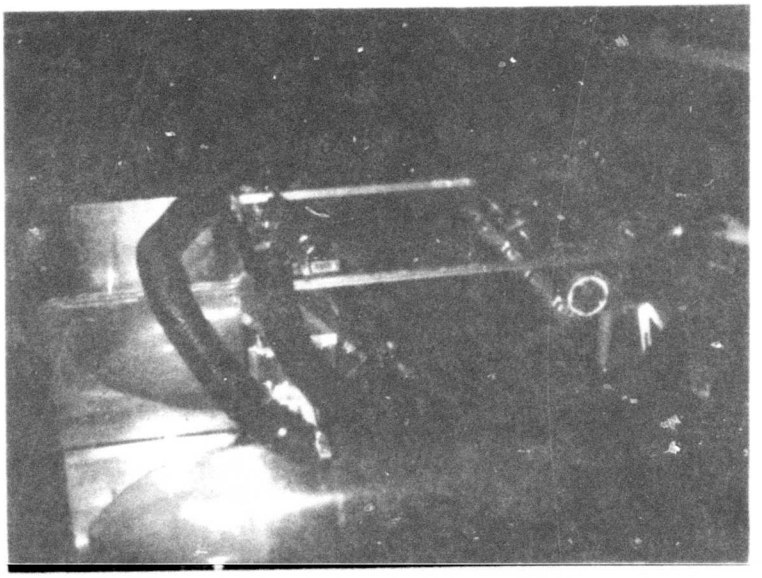

FIGURE 3.13: PHOTOGRAPH SHOWING THE SIDE VIEW OF THE MAIN FRAME OF THE CONTROL/ RECOVERY DEVICE

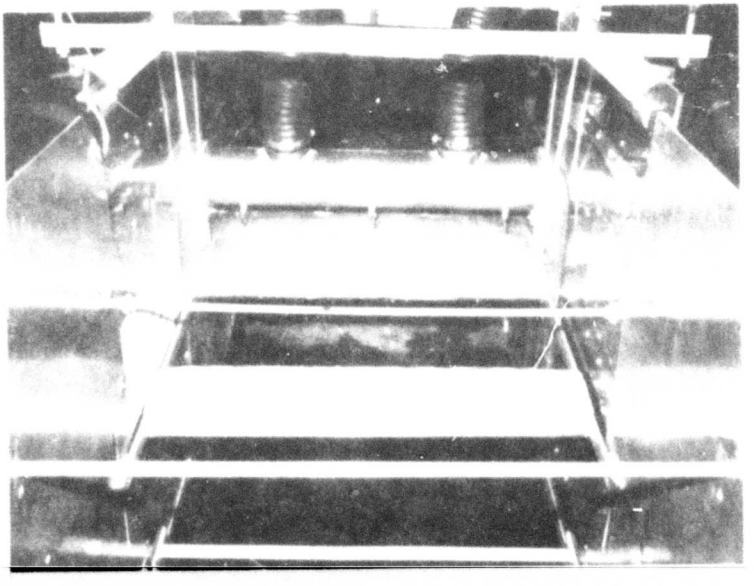

FIGURE 3.14: PHOTOGRAPH OF THE FRONT VIEW OF THE CONTROL/ RECOVERY DEVICE

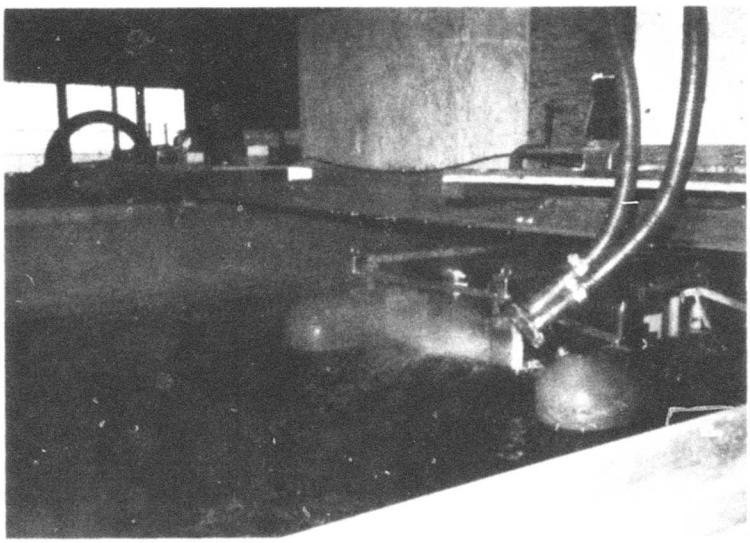

FIGURE 3.15: PHOTOGRAPH OF THE REAR OF THE CONTROL/RECOVERY DEVICE IN OPERATION

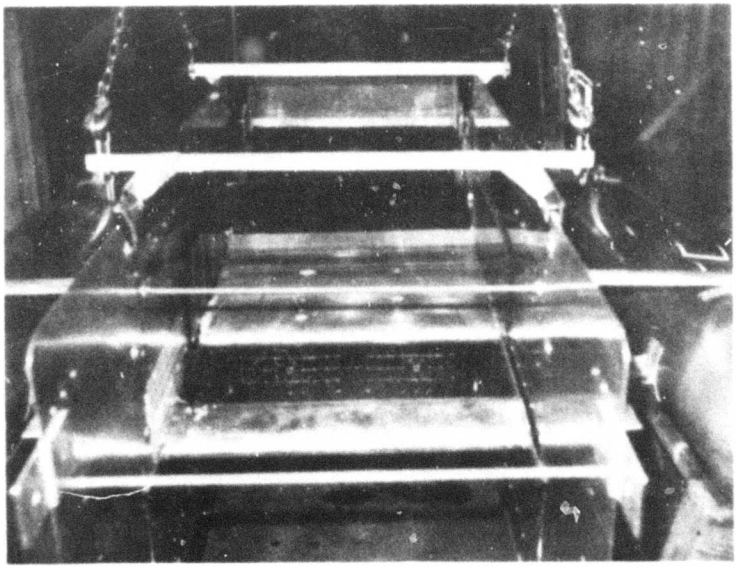

FIGURE 3.16: PHOTOGRAPH OF THE FRONT VIEW OF THE FINAL CONTROL/ RECOVERY SYSTEM HARDWARE

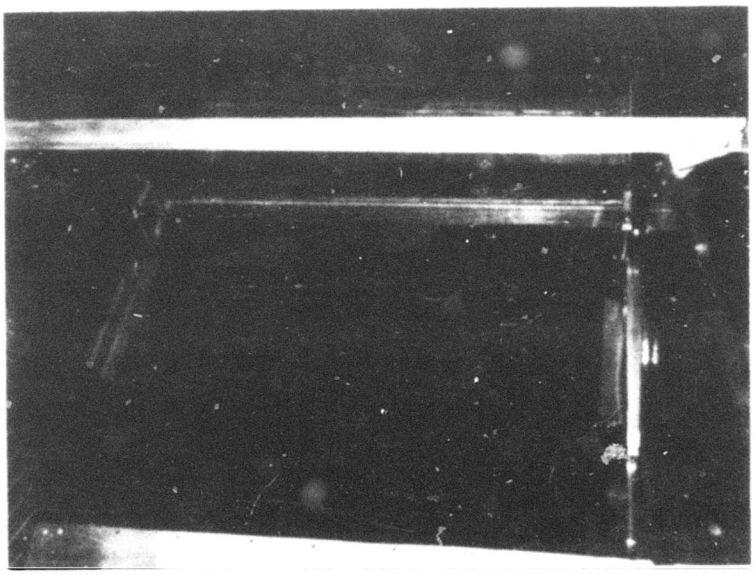

FIGURE 3.17: PHOTOGRAPH OF THE POLYURETHANE FOAM BELT INSTALLED ON THE FINAL CONTROL/RECOVERY SYSTEM MODEL

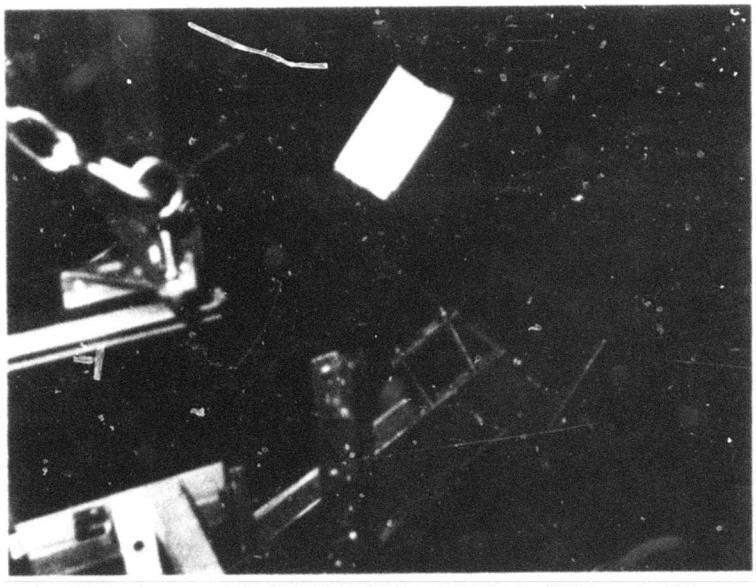

FIGURE 3.18: PHOTOGRAPH OF THE BELT TENSIONING DEVICE, OIL COLLECTION SUMP AND SPLASH PLATE FOR THE FINAL CONTROL/RECOVERY MODEL

length of 85.0 cm. The belt was driven initially by a Zeromax variable speed electric motor which provided a belt surface speed of 15.0 cm/sec. At a later date it was decided that faster belt speeds would be required and therefore a hydraulically driven motor was used which was capable of moving the belt at speeds up to 1.8 m/sec. The belt was wrapped around two rollers; the drive roller at the top and a guide roller located at the bottom of the belt. The drive roller was knurled to provide a no-slip condition on the belt. Below the drive roller a perforated oil squeezing roller was kept under spring tension to remove the collected fluid from the belt. The spring tension device is shown in Figure 3.18 along with the fluid collection sump and splash plate. Figure 3.19 shows the drain pipe leading from the sump to a 15 GPM diaphragm pump located on the deck of the towing carriage.

The control/recovery system described in the latter part of this section (Figures 3.16 through 3.19) was the final design for the phase I program. This model was subsequently tested at the University of Michigan (discussed in section 4).

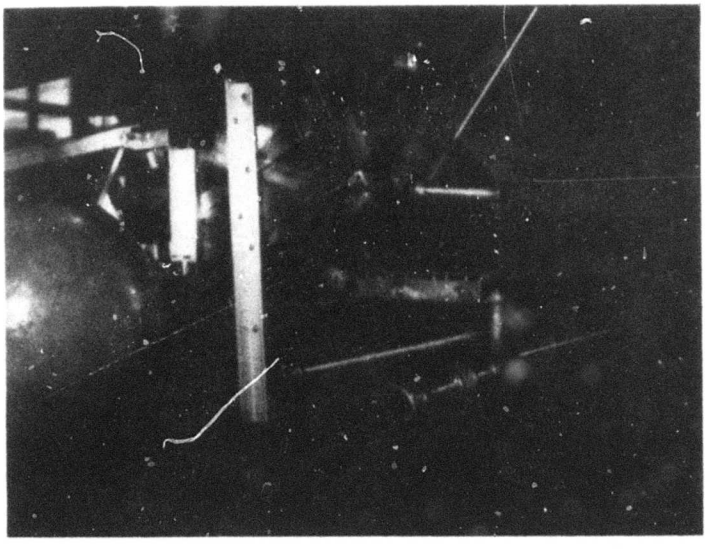

FIGURE 3.19: PHOTOGRAPH OF THE SUMP AND ITS DRAIN PIPE FOR THE FINAL CONTROL/ RECOVERY MODEL

3.4 Tow Tank Instrumentation

The primary instrumentation for the tow tank test program was visual. Approximately 75% of the tests conducted were recorded on a Sony 5.08 cm tape, video recoder. Moreover, during the test program a number of Polaroid photographs showing the different stages of development of the control/recovery system were taken (these photographs appeared primarily in section 3.3). The remainder of the instrumentation consisted of nozzle exit and plenum chamber pressure measurements which were performed with Pitot tubes and pressure taps, respectively, and recorded with a single U tube water manometer. Measurements of the water depth over the top surface of the vented hydrofoil system were also made. These measurements were taken by placing a grid system on one sidewall of the control/recovery system's outer frame. This grid system was subsequently photographed with the video tape system and the measurements recorded. This technique lacked good accuracy for two reasons: (1) the height of the fluid near the wall was always higher than in the center of the hydrofoil (because of the boundary layer in the corners) and (2) measurements taken from the 30.0 cm video screen were very difficult to read accurately.

More sophisticated measurements would have been extremely difficult to obtain in the tow tank environment. The most significant measurement relating to the phase I program is the quantity of oil and water recovered by the system. These measurements were obtained during the University of Michigan test series (see section 4), but not during the tow tank model development program.

3.5 Description of Tow Tank Test Program and Results

This portion of the report has been divided into four subsections. In the first part, a brief description of the air jet nozzle calibration is presented. The second part contains a detailed discussion of the water spray tests performed in conjunction with the single (main) hydrofoil. In the third part, a detailed presentation is made of the water flow tests with the vented hydrofoil system. The last subsection presents the oil/water tests conducted with the final control/recovery system design.

3.5.1 Air Jet Nozzle Calibration - Prior to initiating the water spray tests, the nozzle manifold and exit pressure distribution were monitored over the range of expected pressures to be used in the test sequences. The nozzle manifold had three pressure ports located along its length as shown in Figure 3.20a. The results of the calibration tests are reported in Tables 3.1 and 3.2 for two nozzle exit openings and for several air blower motor RPM settings. These results indicate that the manifold (plenum chamber) pressure is reasonably uniform. However, note should be made of the data reported in the first three entries of Table 3.1. The very low pressure data indicates the existence of a non-uniform pressure distribution in the manifold; however, these low pressures were not easily read from the manometer with great accuracy. Therefore, these readings can generally be disregarded.

Measurements were also taken of the pressure distribution across the nozzle exit plane as shown in Figure 3.20b. These data are reported in Tables 3.3 and 3.4 for two different nozzle openings and a few air blower motor RPM settings.

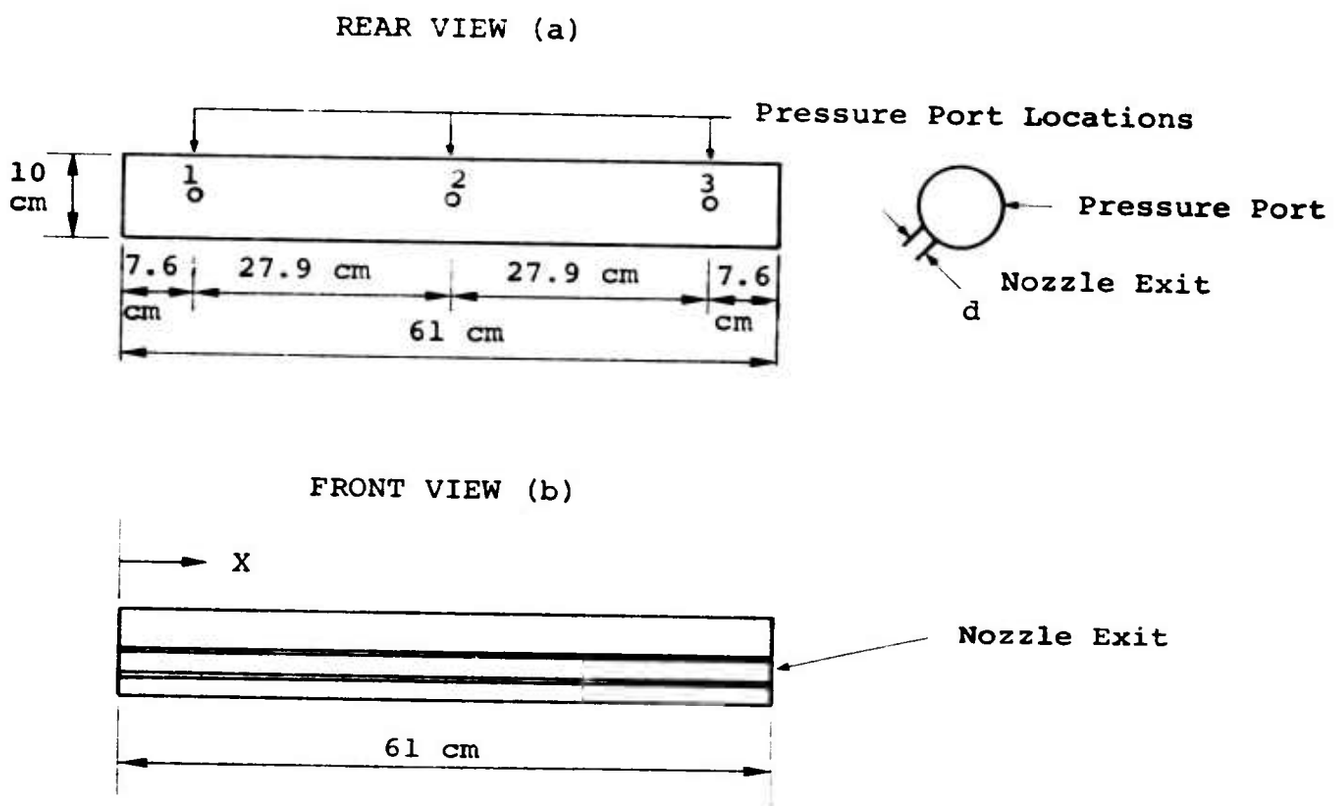

FIGURE 3.20: MANIFOLD AIR JET (a) REAR VIEW AND (b) FRONT VIEW

TABLE 3.1: MANIFOLD PRESSURE CALIBRATION
NOZZLE EXIT OPENING: 0.56 cm

Motor RPM	Tube No. and Pressure in mm Hg		
	1	2	3
500	6	3	6
700	9	6	11
900	17	8	18
1,000	20	21	22
1,200	33	35	35

TABLE 3.2: MANIFOLD PRESSURE CALIBRATION
NOZZLE EXIT OPENING: 0.48 cm

Motor RPM	Tube No. and Pressure in mm Hg		
	1	2	3
500	10	12	12
700	20	22	25
900	38	43	43
1,000	55	54	55
1,200	88	87	88

TABLE 3.3: NOZZLE EXIT PLANE PRESSURE MEASUREMENTS
NOZZLE EXIT OPENING: 0.56 cm

Motor RPM	Distance from Left Hand Side of Manifold in cm and Pressure in mm Hg												
	2.5	5.1	10.1	15.2	20.2	25.3	30.4	35.5	40.6	45.7	50.8	55.9	58.4
700	4	11	10	10	10	10	10	1.0	6	9	10	7	1
1,000	-	22	20	20	20	21	20	21	12	17	22	11	-

TABLE 3.4: NOZZLE EXIT PLANE PRESSURE MEASUREMENTS
NOZZLE EXIT OPENING: 0.32 cm

Motor RPM	Distance from Left Hand Side of Manifold in cm and pressure in mm Hg												
	2.5	5.1	10.1	15.2	20.2	25.3	30.4	35.5	40.6	45.7	50.8	55.9	58.4
700	.5	14	12	11	10	10	10	10	11	11	16	4	1
1,000	-	-	-	-	-	-	-	-	-	-	-	-	-

The Pitot tube used for these measurements was hand held and therefore, in some cases, erroneous readings may have resulted. However, the data generally indicates that the pressure was reasonably uniform across the exit plane of the nozzle. A few data points indicate a low pressure, which is believed to be caused by the wake of some fasteners located at the points of measurement. Moreover, at either end of the nozzle there exists a boundary layer which would explain the low pressure readings obtained there.

3.5.2 Water Spray Tests - The control/recovery system alluded to in Figure 1.1 and which consists of the hydrofoil, air jet and polyurethane foam belt was the first configuration to be tested in the tow tank. Four basic combinations of the hydrofoil, air jet and polyurethane foam belt were tested to determine the feasibility of using an air jet to separate the surface layer of oil and some water. These four configurations are shown in Figure 3.21; however, the addition of the vented hydrofoil to the system did not appear to be of importance for these tests and was not included in order to maintain simplicity in design.

The parameters and the range over which they were varied for configurations A through D of Figure 3.21 are shown in Table 3.5. A qualitative discussion of the test results for each of the four configurations would be more informative than a detailed narrative of each test, since measurements of the droplet size and distribution were not made and the only data obtained were video tapes of each sequence.

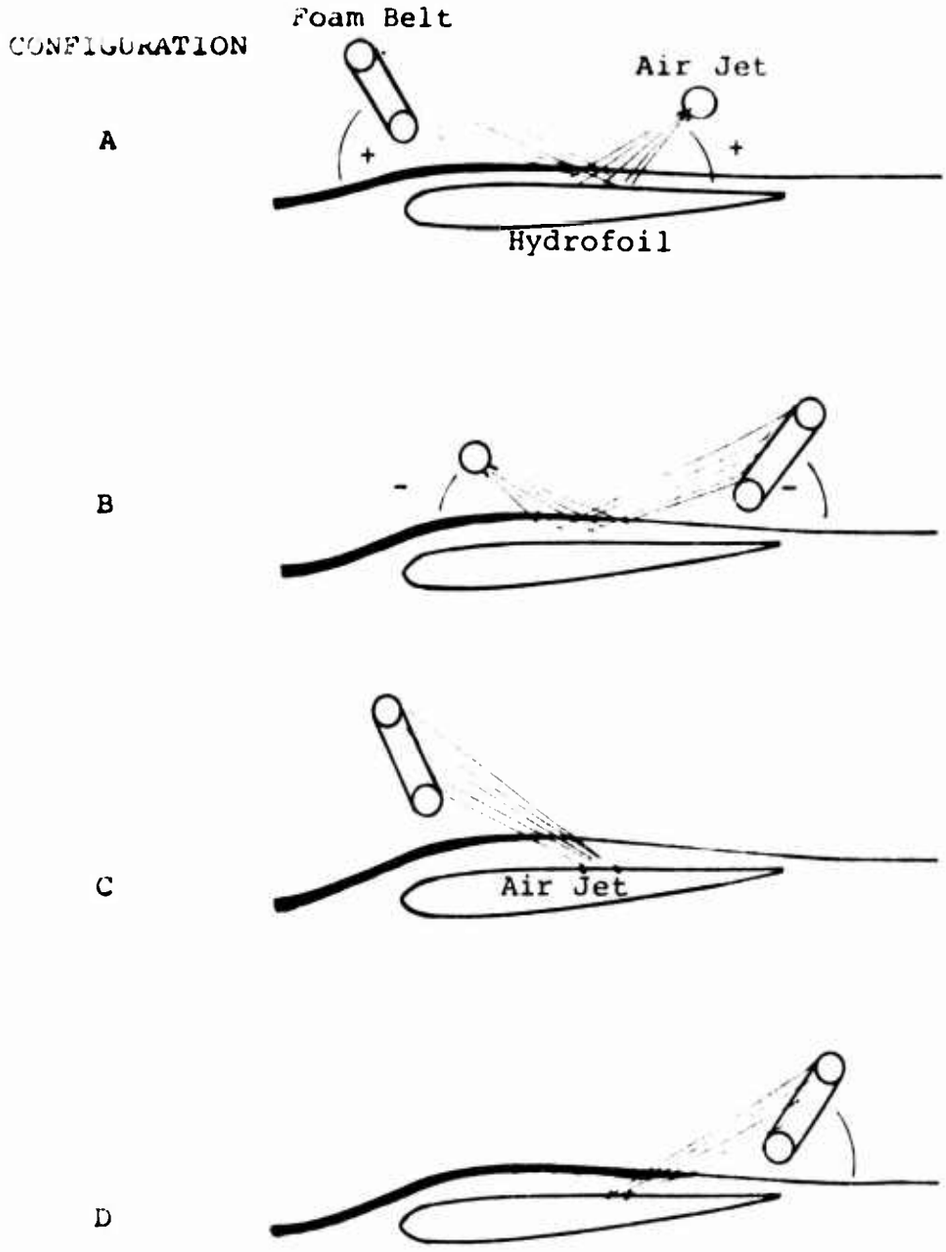

FIGURE 3.21: SINGLE HYDROFOIL/AIR JET CONFIGURATIONS A, B, C AND D

TABLE 3.5: TEST PARAMETERS AND THEIR RANGE FOR CONFIGURATIONS A, B, C AND D OF FIGURE 3.21

Parameter	Configuration				Range
	A	B	C	D	
Wave Condition	yes	yes	yes	yes	Calm
Hydrofoil Velocity	yes	yes	yes	yes	0 to 3 knots
Air Jet Velocity	yes	yes	yes	yes	61 to 122 m/sec
Hydrofoil Depth	yes	yes	yes	yes	0 to 5.1 cm
Hydrofoil Angle	yes	yes	yes	yes	-5° to +5°
Air Jet Angle	+	-	+	-	-30° to +30°
Air Jet Height Above Hydrofoil Surface	yes	yes	NA	NA	2.5 to 7.5 cm
Air Jet Exit Thickness	yes	yes	yes	yes	0.32 to 0.64 cm
Air Jet Impingement Point on Hydrofoil	yes	yes	NA	NA	.25 to .75 of chord length
Foam Belt Angle	+	-	+	-	45°

(a) Configuration A

The parameters that had the most significant impact on the qualitative features of the resulting water spray were hydrofoil velocity and the air jet angle with respect to the hydrofoil surface. The video tapes indicated that as the hydrofoil increased in velocity from 0.0 m/sec for a spray angle greater than 30°, the spray fan resembled that shown in Figure 3.22a as long as the air jet velocity was sufficiently high to create a spray. Thus, for increasing hydrofoil velocity, the spray fan is rotated clockwise, thus making it difficult to intercept its trajectory with a fixed belt position. For air jet angles of 30° and less (Figure 3.22b), the resulting spray is much finer throughout the entire volume of the device and loses its character of resembling a spray fan - it looks more like a cloud, also making it difficult to intercept with a fixed position belt.

(b) Configuration B

The parameter that had the most impact on the qualitative features of the spray was the hydrofoil velocity. The air jet angle with respect to the hydrofoil surface did not impact the spray characteristics primarily because the resulting air flow from the jet spread along the hydrofoil's surface in much the same manner regardless of jet angle. The spray characteristics for the present case resemble those shown in Figure 3.22a, but in reverse (see Figure 3.23). However, much of the spray was at a very low angle and appeared to be a result of blowing off the wave at the rear of the hydrofoil. The air jet, although it generated some spray, appeared to accelerate the water over the rear surface of the hydrofoil and did not produce a significant amount of spray. Any spray

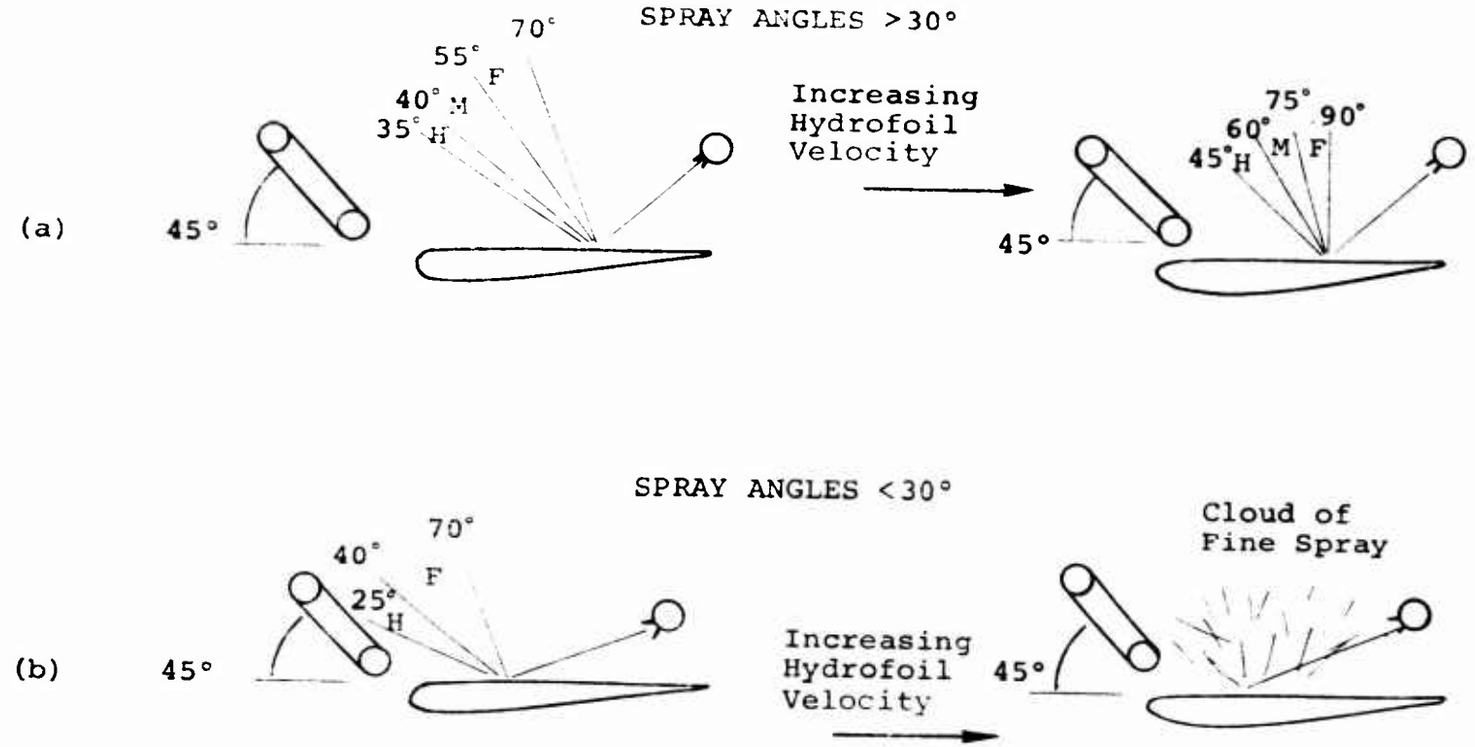

NOTE: F: Fine Spray
M: Medium Spray
H: Heavy Spray

FIGURE 3.22: WATER SPRAY CHARACTERISTICS FOR INCREASING HYDROFOIL VELOCITY: (a) CONFIGURATION A, JET ANGLE >30° AND (b) CONFIGURATION A, JET ANGLE <30°

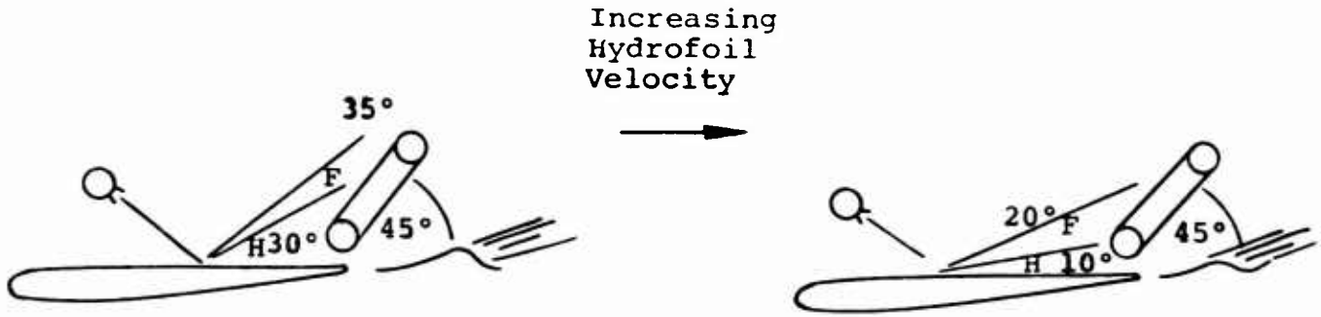

NOTE: F: Fine Spray
H: Heavy Spray

FIGURE 3.23: WATER SPRAY CHARACTERISTICS FOR INCREASING HYDROFOIL VELOCITY AT ALL JET ANGLES FOR CONFIGURATION B

that was generated would be difficult to deposit on the foam belt, since the latter would have to be placed at the water surface. This latter condition would seriously disrupt the flow over the hydrofoil and result in a significant amount of high velocity water flowing through the belt.

(c) Configuration C and D

The results of the spray tests for configurations C and D have been combined because they were generally similar to each other. The most important parameters in this series of tests were hydrofoil velocity and air jet velocity (momentum of the air jet to be more specific). For hydrofoil velocities near 0.0 m/sec a generally larger droplet spray was formed than in the previous cases. However, as the hydrofoil increased in velocity, very little if any water spray was developed - just a large disturbed bubbly region in the vicinity of the air jet's exit plane. As the jet velocity was increased further, this disturbed region over the top surface of the hydrofoil became unstable; that is, changed its dimensions both vertically and laterally in a random manner. At times some water spray developed; however, the droplet size was large and very short range - in most cases the droplets did not reach the foam belt but were confined to the region of the air jet's exit plane. The main reason for this behavior is that a very large air jet momentum is required to penetrate through and alter the direction of the water flow. Even if the quantity of air and velocity could be supplied with a reasonable sized air blower, the ultimate trajectory of the water spray would be unstable because it is very sensitive to the hydrofoil's velocity. Therefore, for these reasons the configuration of the jet penetrating through the water surface has been eliminated from consideration.

It can generally be concluded then, that the use of an air jet to separate the surface layer of oil and some water from the hydrofoil and direct it onto a polyurethane foam belt is not a viable control/recovery system. Thus, the control/recovery system shown in Figure 1.2 appeared to be the only other alternative at this point in the program. The remaining sections, 3.5.3 and 3.5.4, describe the development of that system.

3.5.3 Vented Hydrofoil Experiments - A series of tests were conducted in the tow tank facility with the vented hydrofoil system described in section 3.3. The primary objective of this work was to determine the behavior of the vented hydrofoil model in calm, wavy and choppy water conditions. The five variables in these experiments were; (1) depth of hydrofoil submergence (h) below the surface of the water prior to the initiation of a test, (2) separation distance (d) between the hydrofoils measured at the chord line, (3) the hydrofoil velocity (V), (4) the hydrofoil angle of attack (α) with respect to the water surface prior to a test and (5) the water conditions, represented as calm, wavy and choppy. Seventy-seven individual tests were performed in order to cover a sufficient number of combinations of these variables. The primary quantity that was measured throughout the test program was the depth of water at specific points, along the hydrofoil's surface. These measurements were obtained from the video tapes in the manner described in section 3.4., and the measurement points are represented in Figure 3.24 which is a schematic of the vented hydrofoil system. Table 3.6 is a compilation of the data obtained during the test program. The numbering system for these tests begins with 4, since the first three tests conducted were of an exploratory nature and no data

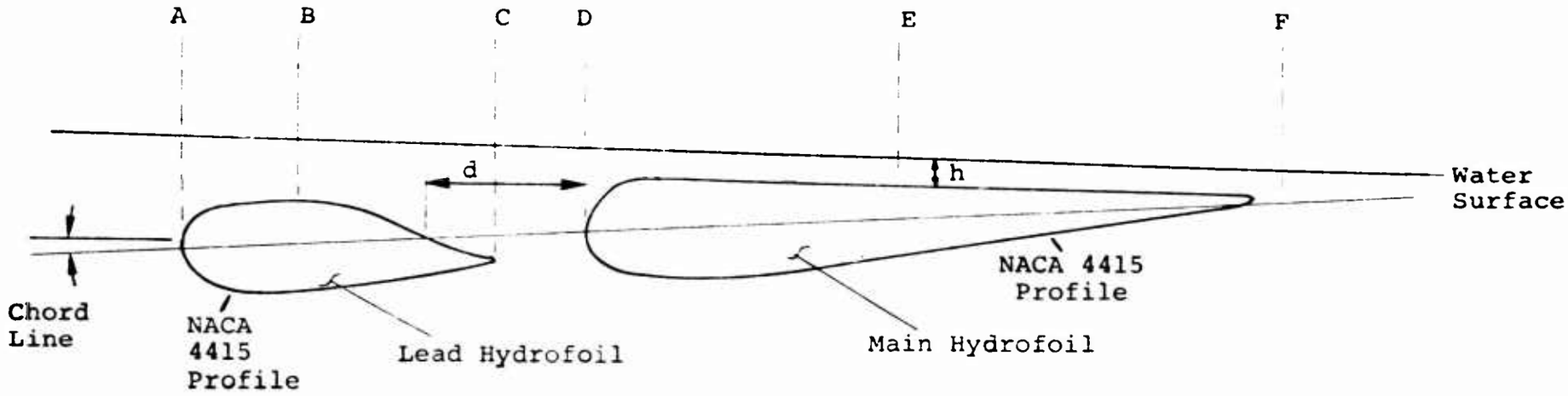

	Point	Description	Distance From Leading Edge of Lead Hydrofoil in cm.
Lead Hydrofoil	A	Leading Edge	0.0
	B	1/2 Chord	7.5
	C	Trailing Edge	23.0
Main Hydrofoil	D	Leading Edge	d + 15.0
	E	1/2 Chord	d + 40.0
	F	Trailing Edge	d + 65.0

FIGURE 3.24: SCHEMATIC OF VENTED HYDROFOIL MODEL SHOWING THE LOCATION OF THE MEASUREMENT POINTS

TABLE 3.6: SUMMARY OF VENTED HYDROFOIL TOW TANK TEST DATA (WITHOUT RAMP)

Tape # / Footage	Test #	h (cm)	d (cm)	V (m/sec)	α	A (cm)	B (cm)	C (cm)	D (cm)	E (cm)	F (cm)	Wave Amp (cm)	Wave Length (meters)
1/11.0	4	2.5	1.3	0.9	-4°	8.6	8.6	8.6	9.1	6.6	6.1	Calm	Water
1/12.0	5	2.5	2.5	0.9	-4°	8.6	8.6	8.6	7.6	6.1	6.1		
1/13.5	6	2.5	3.8	0.9	-4°	6.6	7.1	7.1	3.6	6.1	6.1		
1/14.7	7	2.5	5.1	0.9	-4°	6.6	7.1	7.1	3.6	4.6	5.1		
1/16.2	8	2.5	6.4	0.9	-4°	6.1	7.1	5.1	3.0	3.6	3.6		
1/17.1	9	2.5	7.6	0.9	-4°	6.1	7.1	5.1	2.0	2.5	3.0		
1/18.2	10	2.5	8.9	0.9	-4°	6.1	7.1	5.1	2.0	2.5	3.0		
1/20.0	11	2.5	10.2	0.9	-4°	6.1	7.1	5.1	2.0	2.5	3.6		
1/20.8	12	2.5	11.4	0.9	-4°	6.1	7.1	5.1	2.5	5.1	5.1		
1/21.8	13	5.1	1.3	0.9	-4°	8.9	8.9	8.9	8.9	7.6	6.4		
1/22.7	14	5.1	2.5	0.9	-4°	8.9	8.9	8.9	8.9	7.6	6.4		
2/0.0	15	5.1	3.8	0.9	-4°	10.7	10.7	10.7	11.7	10.2	9.1		
2/1.1	16	5.1	5.1	0.9	-4°	11.2	10.7	10.2	11.2	10.2	9.1		
2/1.9	17	5.1	6.4	0.9	-4°	11.2	10.7	10.2	10.7	10.2	9.1		
2/2.7	18	5.1	7.6	0.9	-4°	10.7	10.7	10.2	10.2	9.7	8.6		
2/3.5	19	5.1	8.9	0.9	-4°	10.7	10.2	10.2	9.7	9.7	-		
2/4.4	20	-	-	-	-	-	-	-	-	-	-		
2/5.2	21	5.1	8.9	1.6	-4°	15.2	15.2	15.2	15.2	14.2	15.2		
2/6.1	22	5.1	10.2	0.9	-4°	10.2	10.2	7.6	11.7	11.7	11.2		

TABLE 3.6

(Continued)

Tape # / Footage	Test #	h (cm)	d (cm)	V (m/sec)	α	A (cm)	B (cm)	C (cm)	D (cm)	E (cm)	F (cm)	Wave Amp (cm)	Wave Length (meters)
2/6.8	23	5.1	10.2	1.6	-4°	15.2	15.2	13.2	13.7	12.7	13.7	Calm	Water
2/7.6	24	5.1	12.7	0.9	-4°	12.7	12.7	7.1	10.2	9.7	8.1		
2/8.6	25	5.1	12.7	1.6	-4°	14.7	14.2	12.7	12.2	10.7	12.2		
2/9.2	26	5.1	15.2	0.9	-4°	10.2	10.2	7.6	10.2	9.7	8.6		
2/9.9	27	5.1	15.2	1.6	-4°	14.7	14.2	11.2	11.7	10.2	11.2		
2/10.5	28	5.1	22.9	1.6	-4°	14.2	12.7	10.2	8.1	7.6	9.1		
2/11.1	29	1.3	2.5	0.9	-4°	6.6	6.6	7.1	7.6	6.6	5.1		
2/11.9	30	1.3	1.6	1.6	-4°	13.7	13.7	13.7	15.2	16.5	15.2		
2/12.6	31	1.3	5.1	0.9	-4°	6.6	7.1	5.1	3.0	4.1	3.6		
2/13.3	32	1.3	5.1	1.6	-4°	11.2	11.2	11.2	12.7	12.2	12.7		
2/14.1	33	6.4	0.9	0.9	-4°	6.1	6.6	4.6	1.5	5.1	3.0		
2/14.8	34	1.3	6.4	1.6	-4°	11.2	11.2	11.2	11.7	10.7	11.2		
2/15.4	35	1.3	7.6	0.9	-4°	6.1	6.1	3.6	1.0	2.0	3.0		
2/16.2	36	1.3	7.6	1.6	-4°	10.7	10.7	10.7	10.7	10.2	9.7		
2/16.8	37	1.3	8.9	0.9	-4°	5.6	6.1	3.6	0.5	2.0	3.0		
2/17.6	38	1.3	8.9	1.6	-4°	10.7	11.2	9.7	9.7	9.1	9.7		
2/18.2	39	1.3	10.2	0.9	-4°	6.6	6.6	3.6	3.6	4.6	4.1		
2/18.8	40	1.3	10.2	1.6	-4°	10.2	10.7	9.7	9.7	9.1	8.6		
2/19.5	41	1.3	12.7	1.6	-4°	9.7	9.7	8.1	6.6	6.6	7.6		

TABLE 3.6
(Continued)

Tape # / Footage	Test #	h(cm)	d(cm)	V(m/sec)	α	A(cm)	B(cm)	C(cm)	D(cm)	E(cm)	F(cm)	Wave Amp (cm)	Wave Length (meters)
2/20.1	42	1.3	15.2	1.6	-4°	10.7	10.2	7.6	9.1	8.1	9.1	Calm	Water
2/20.8	43	1.3	22.9	1.6	-4°	10.2	8.1	5.1	4.1	3.0	4.6		
2/21.4	44	1.3	30.5	1.6	-4°	10.7	7.6	3.0	4.1	1.5	1.5		
2/22.0	45	2.5	2.5	1.6	-4°	19.8	19.8	19.8	19.8	19.8	19.8		
2/22.8	46	2.5	10.2	1.6	-4°	12.2	12.7	12.2	10.2	10.2	10.2		
3/0.0	47	2.5	22.9	1.6	-4°	9.7	5.1	5.1	5.1	3.8	5.1		
3/0.5	48	2.5	26.7	1.6	-4°	10.2	8.1	3.0	4.1	3.6	3.6		
3/1.1	49	2.5	30.5	1.6	-4°	10.2	7.1	3.6	3.6	3.0	3.6		
3/1.6	50	2.5	35.6	1.6	-4°	10.2	7.1	4.6	3.6	3.0	3.6		
3/2.1	51	2.5	12.7	1.6	-4°	11.2	11.2	10.2	9.1	8.6	9.1		
3/2.5	52	2.5	15.2	1.6	0°	8.1	8.1	7.1	4.1	3.6	3.6		
3/3.0	53	2.5	30.5	1.6	0°	-	-	-	-	-	-		
3/3.5	54	2.5	22.9	1.6	0°	10.7	9.7	5.1	2.0	1.0	-		
3/4.0	55	2.5	22.9	0.9	0°	7.6	5.1	2.5	1.5	2.5	3.0		
3/4.7	56	2.5	7.6	0.9	0°	-	-	-	-	-	-		
3/5.8	57	2.5	2.5	0.9	0°	6.6	7.6	6.6	2.5	2.5	2.0	Smooth Waves	
3/6.6	58	2.5	2.5	0.9	0°	6.1	7.6	6.1	3.0	2.5	2.5	6.4	4.6
3/7.5	59	2.5	22.9	1.6	0°	-	-	-	-	-	-	6.4	4.6
3/8.3	60	2.5	12.7	1.6	0°	10.2	10.2	5.1	4.1	3.0	2.5	6.4	4.6

TABLE 3.6
(Continued)

Tape # / Footage	Test #	h(cm)	d(cm)	V(m/sec)	α	A(cm)	B(cm)	C(cm)	D(cm)	E(cm)	F(cm)	Wave Amp (cm)	Wave Length (meters)
												Smooth Waves	
3/8.9	61	2.5	7.6	1.6	0°	11.2	10.2	10.2	10.2	7.6	7.6	6.4	4.6
3/9.8	62	2.5	12.7	1.6	0°	7.6-12.7	7.6-15.2	5.1-10.2	2.5-5.1	2.5-5.1	2.5-6.1	15.2	4.6
3/10.7	63	2.5	3.8	0.9	0°	-	-	2.5-10.2	2.5-3.8	1.3-2.5	1.3-2.5	15.2	4.6
3/11.5	64	2.5	22.9	0.9	-4°	-	-	2.5-10.2	2.5	2.5	2.5	15.2	4.6
3/12.2	65	1.3	15.2	1.6	-4°	10.2	10.2	7.6	5.1	5.1	4.1	15.2	4.6
3/12.8	66	1.3	8.9	0.9	-4°	8.9	8.9	7.6	5.1	5.1	5.1	15.2	4.6
3/13.8	67	1.3	8.9	0.9	-4°	6.4	8.9	5.1	5.1	5.1	4.1	7.6	4.6
3/14.7	68	1.3	15.2	1.6	-4°	8.9	11.4	5.1	3.8	3.8	2.5	7.6	4.6
3/15.3	69	1.3	15.2	1.6	-4°	10.2	10.2	5.1	3.8	3.8	3.8	Choppy Water 2.5-15.2	0.3-2.4
3/16.1	70	1.3	15.2	1.6	-4°	10.2	10.2	6.4	3.8	3.8	3.8	2.5-15.2	0.3-2.4
3/16.9	71	1.3	6.4	0.9	-4°	6.4	6.4	6.4	3.8	3.8	3.8	2.5-15.2	0.3-2.4
3/18.0	72	1.3	22.9	1.6	-4°	10.2	10.2	5.1	3.8	3.8	2.5	2.5-15.2	0.3-2.4
3/18.7	73	2.5	20.3	1.6	-4°	8.9	10.2	5.1	3.8	2.5	2.5	2.5-15.2	0.3-2.4

TABLE 3.6
(Continued)

Tape # / Footage	Test #	h(cm)	d(cm)	V(m/sec)	α	A(cm)	B(cm)	C(cm)	D(cm)	E(cm)	F(cm)	Wave Amp (cm)	Wave Length (meters)
												Choppy	Water
3/19.4	74	2.5	20.3	1.6	-4°	-	-	-	-	-	-	30.5	0.3-2.4
3/20.5	75	2.5	20.3	1.6	-4°	-	-	-	-	-	-	22.9	1.8
3/21.7	76	2.5	20.3	1.6	-4°	8.9	10.2	5.1	2.5	2.5	2.5	8.9	3.7
4/0.0	77	1.3	22.9	1.6	-4°	7.1	6.6	2.5	2.5	1.3	2.0	-	-
												Calm	Water
4/0.9	78	1.3	22.9	1.6	-4°	7.1	6.6	2.5	2.5	1.3	2.0	↕	↕
4/1.4	79	1.3	22.9	1.6	-4°	7.1	6.6	2.5	2.5	1.3	2.0		
4/1.9	80	1.3	15.2	1.6	-4°	-	-	-	5.1	4.1	5.1		

were recorded. A numbering system for the location of the test sequence (in feet) from the beginning of a specified video tape number appears in the first column of Table 3.6. The data reported in Table 3.6 has been reduced to free surface diagrams of the flow over the vented hydrofoil's surface, and appear in Figures 3.25 through 3.33.

The free surface data of Figures 3.25 through 3.33 could not be compared directly with the small scale hydrofoil data presented in section 2. The reason for this is that the freeboard and stagnation streamline locations were not directly measurable in the tow tank tests. These latter quantities are the primary parameters for hydrodynamically scaling the hydrofoils. However, the data reported in Figure 3.33 for the water submergence depth on the main hydrofoil at the mid-chord versus the vented slot opening, and some qualitative observations concerning the character of the bow wave and the flow conditions over the rear of the main hydrofoil are sufficient for choosing some representative operating points for the vented hydrofoil system.

During the tow tank experimental program, two hydrofoil velocities were used, 0.9 and 1.6 m/sec. These velocities in turn represent Froude numbers ($F = V/\sqrt{gT}$) of 1.18 and 1.96 respectively. If estimates of the freeboard are made for some representative tests, in addition to observations of the bow wave and flow over the rear of the main hydrofoil, the data generally agree with the type of flow characterized in Figure 2.2. Thus, at the lower $F = 1.18$, a turbulent bow wave was always present, and the flow over the rear of the main hydrofoil generally had a hydraulic jump and some noticeable turbulence associated with it. However, at the higher $F = 1.96$, the bow wave was smooth and no hydraulic

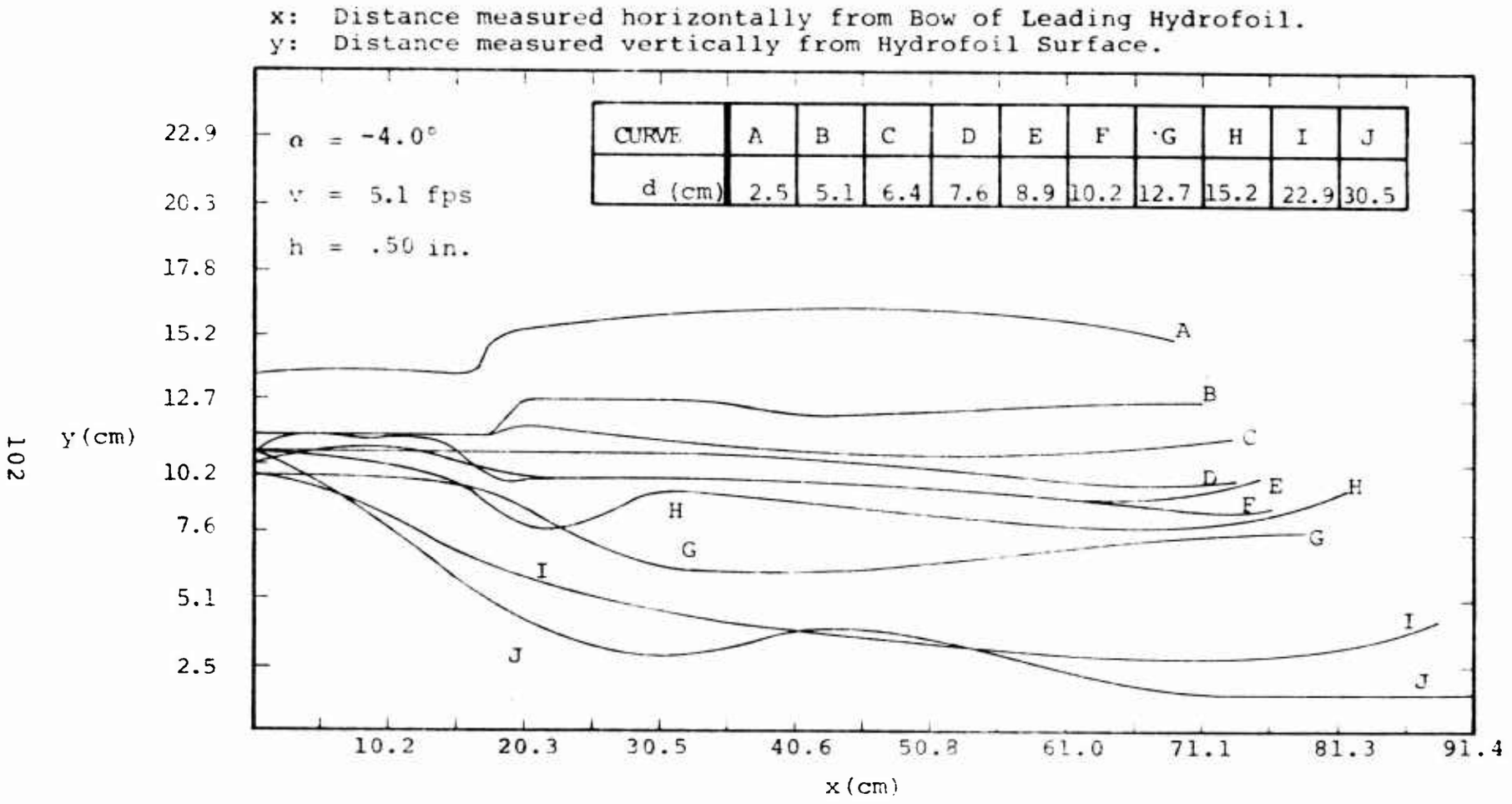

FIGURE 3.25: FREE SURFACE DIAGRAM: $\alpha = -4.0°$
$v = 5.1$ fps; and $h = 0.50$ in.

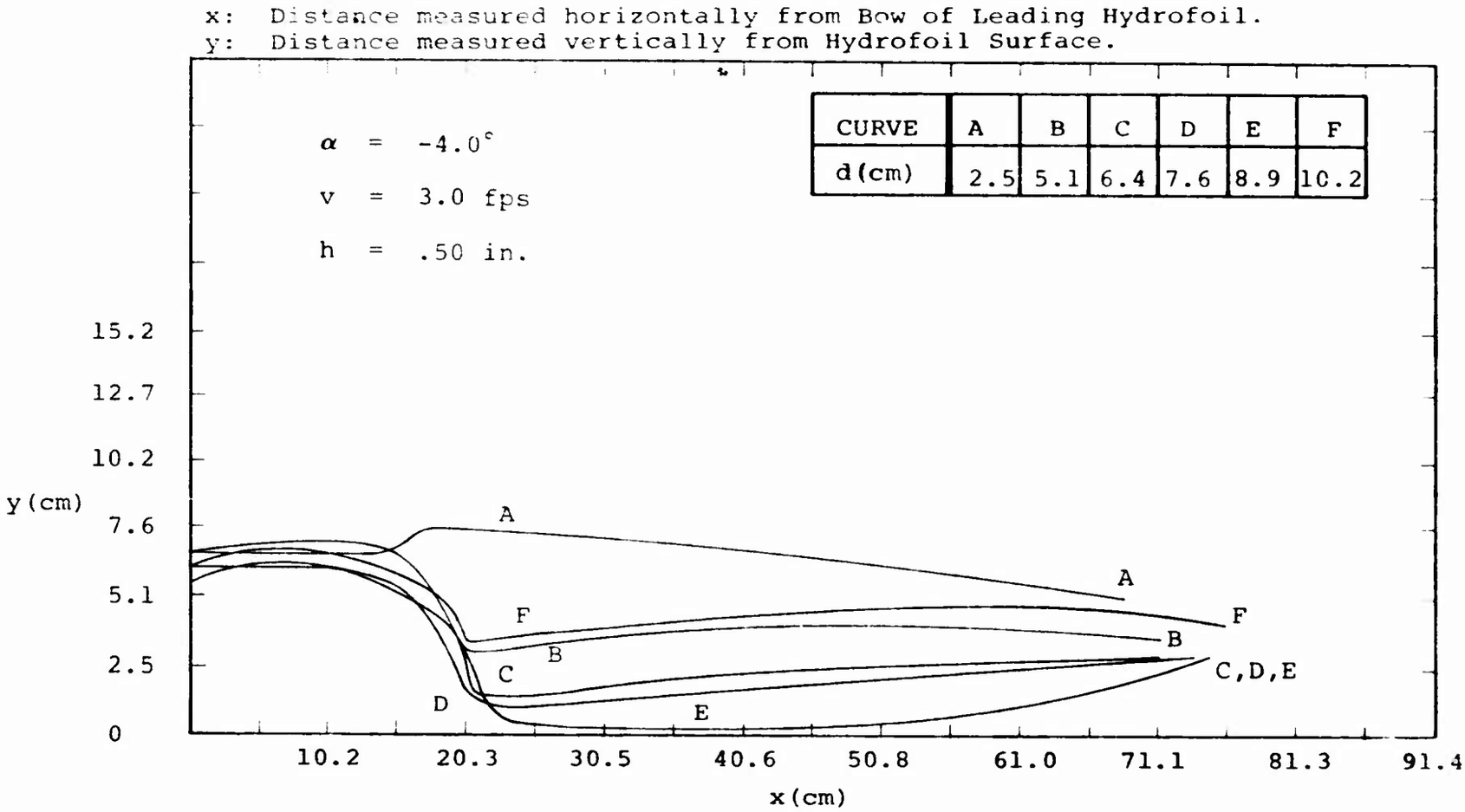

FIGURE 3.26: FREE SURFACE DIAGRAM: $\alpha = -4.0°$; v = 3.0 fps and h =0.50 in.

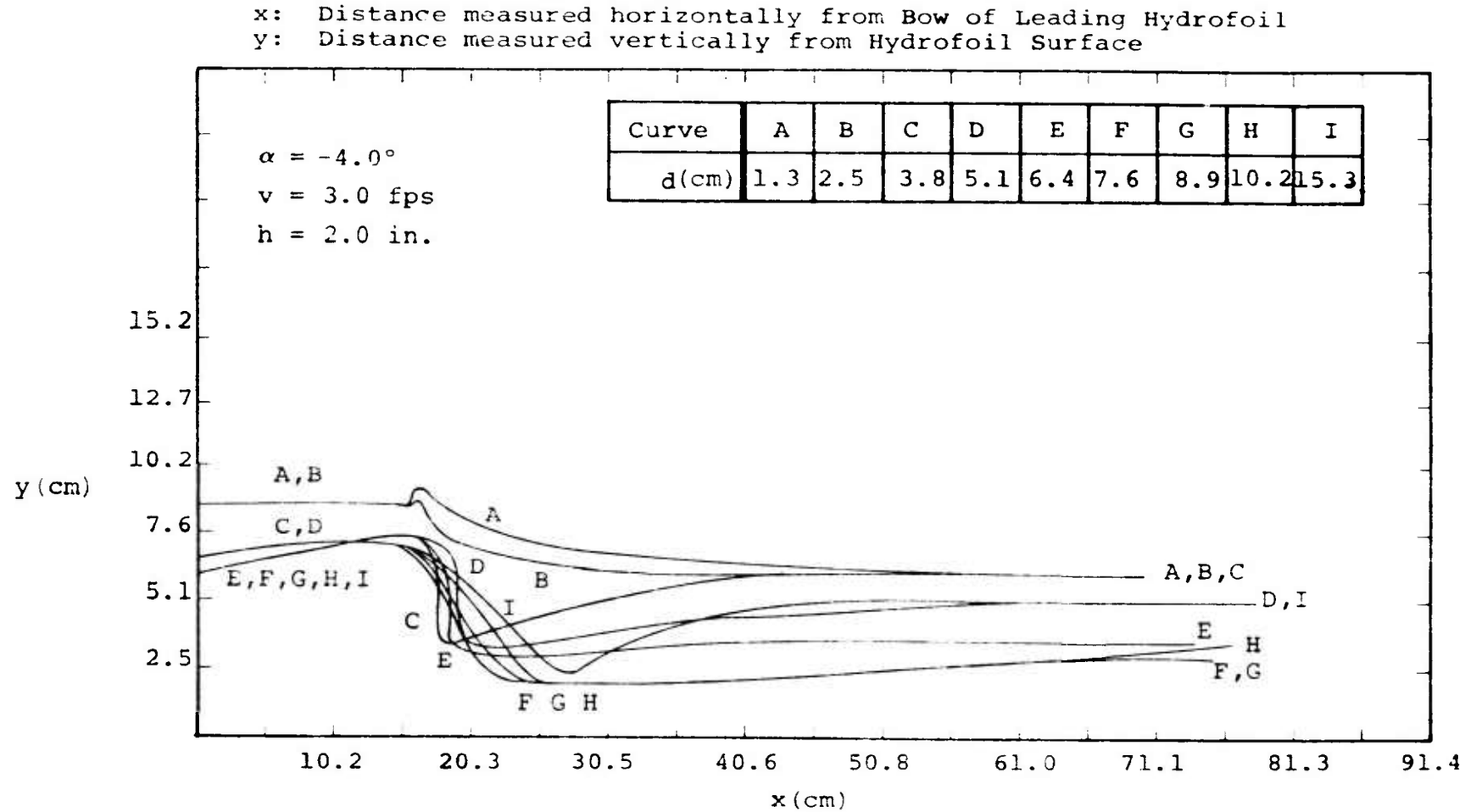

FIGURE 3.27: FREE SURFACE DIAGRAM: α = -4.0°; v = 3.0 fps; and h = 2.0 in.

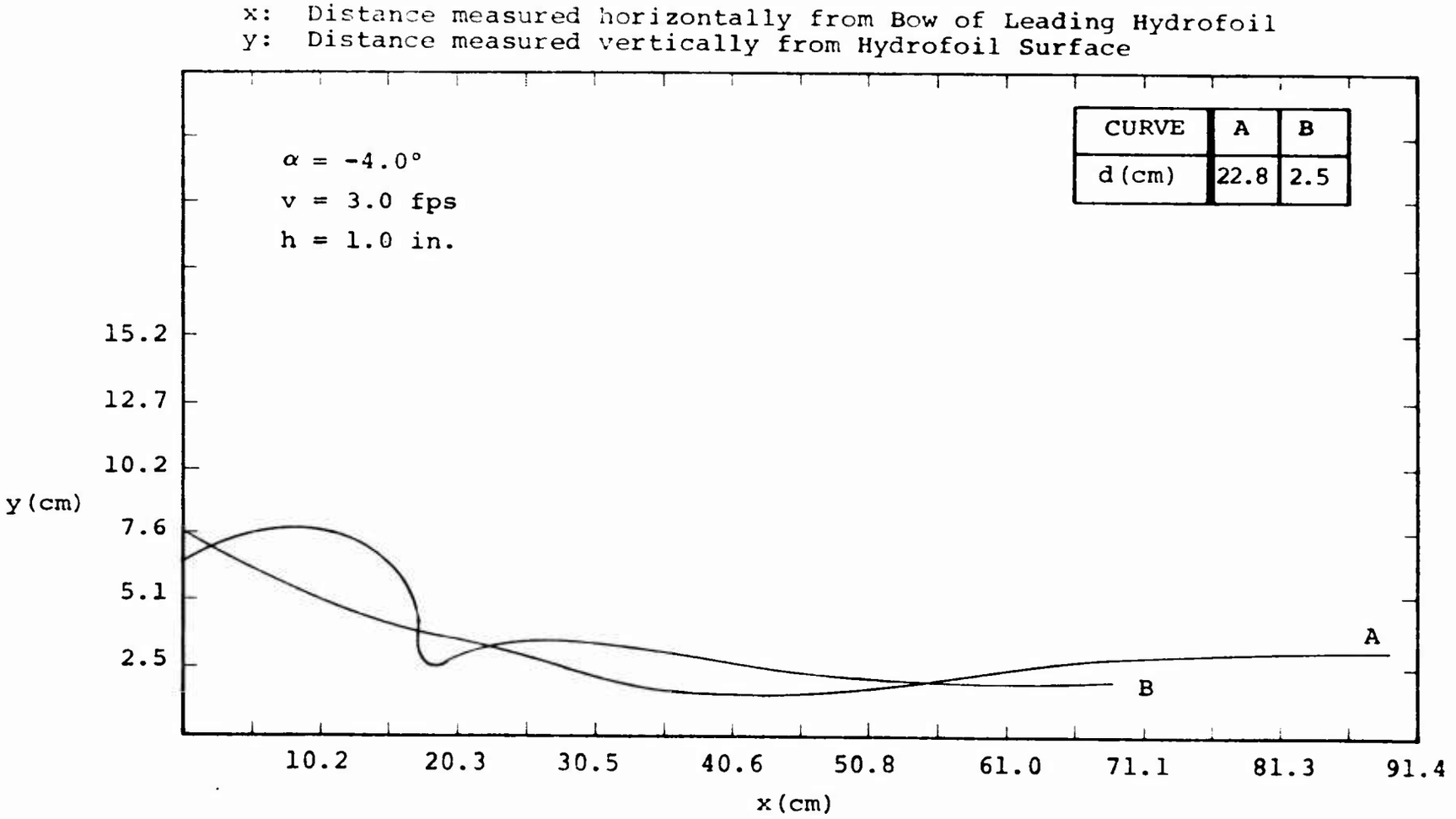

FIGURE 3.28: FREE SURFACE DIAGRAM: α = -4.0°; v = 3.0 fps; and h = 1.0 in.

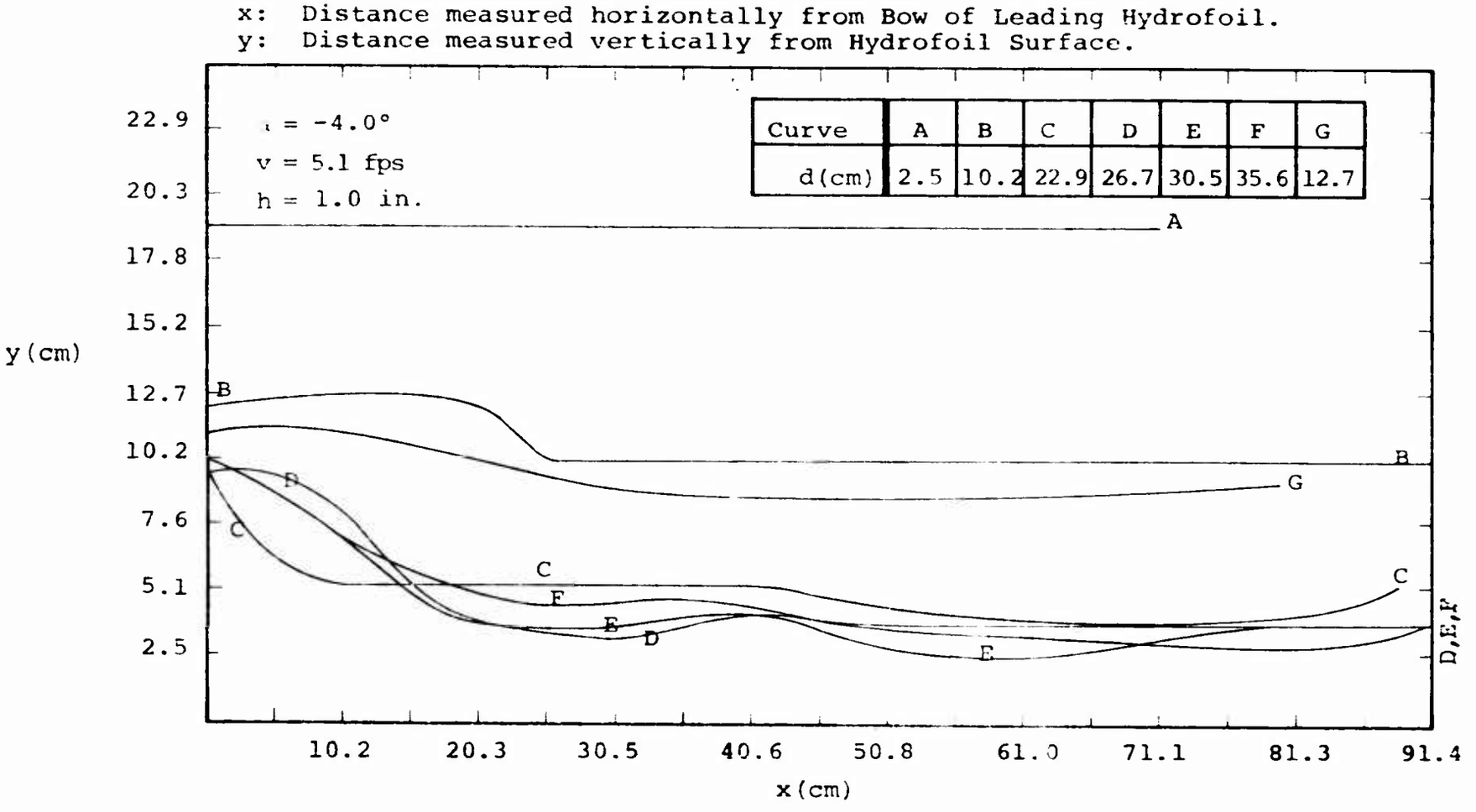

106

FIGURE 3.29: FREE SURFACE DIAGRAM: $\alpha = -4.0°$; v = 5.1 fps; and h = 1.0 in.

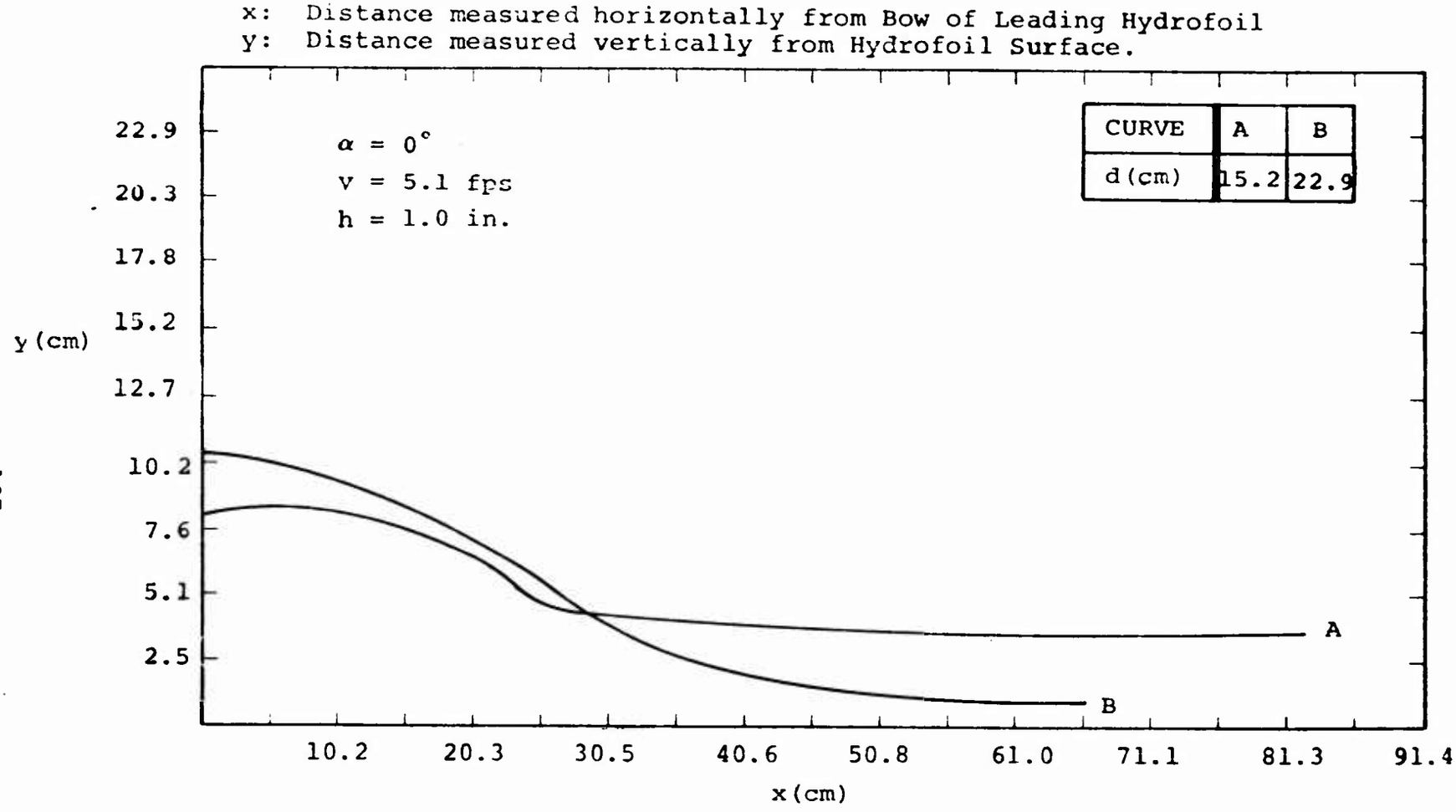

FIGURE 3.30: FREE SURFACE DIAGRAM: $\alpha = 0°$; v = 5.1 fps; h = 1.0 in.

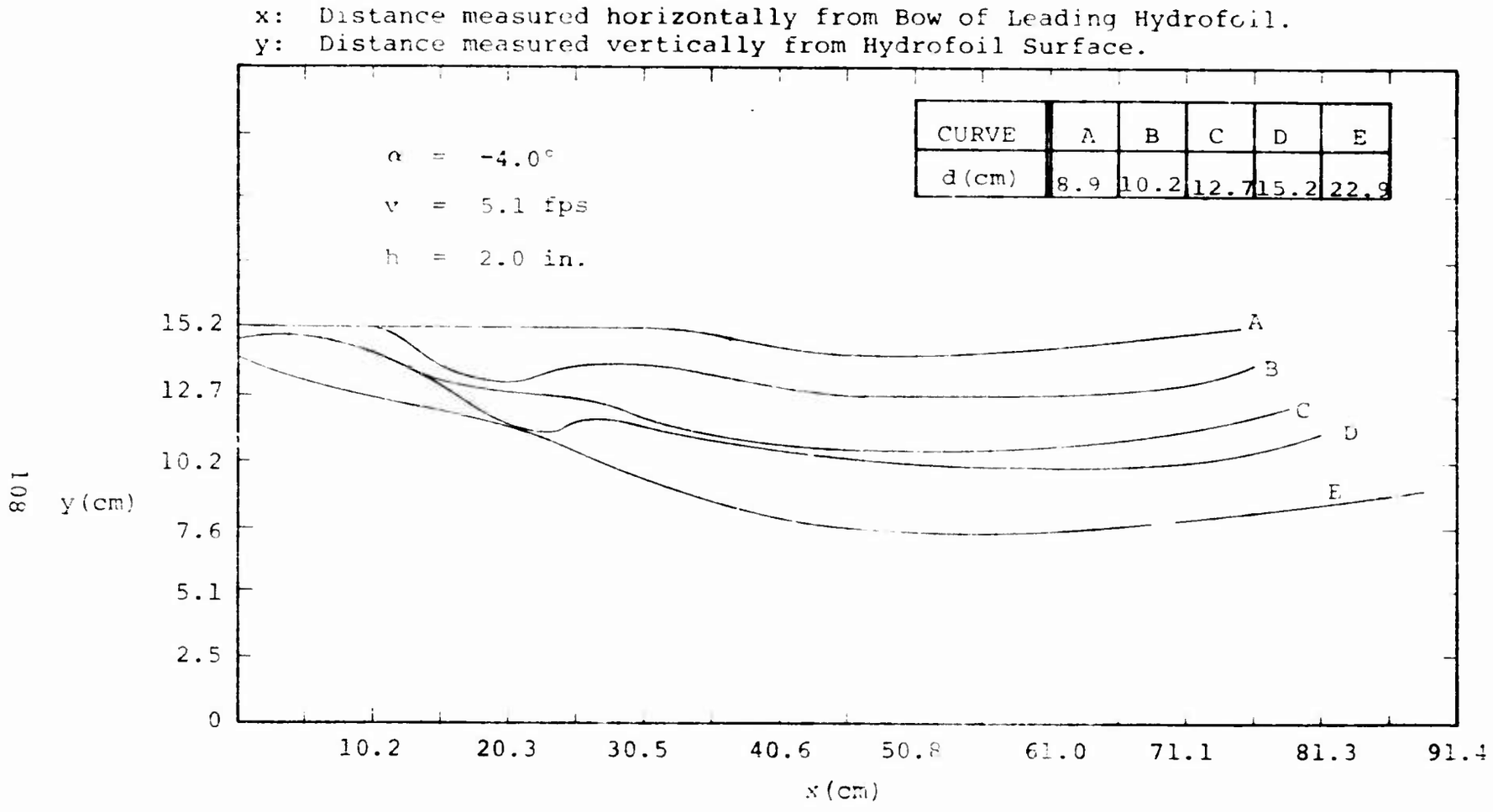

FIGURE 3.31: FREE SURFACE DIAGRAM: α = -4.0°; v = 5.1 fps; and h = 2.0 in.

x: Distance measured horizontally from Bow of Leading Hydrofoil.
y: Distance measured vertically from Hydrofoil Surface.

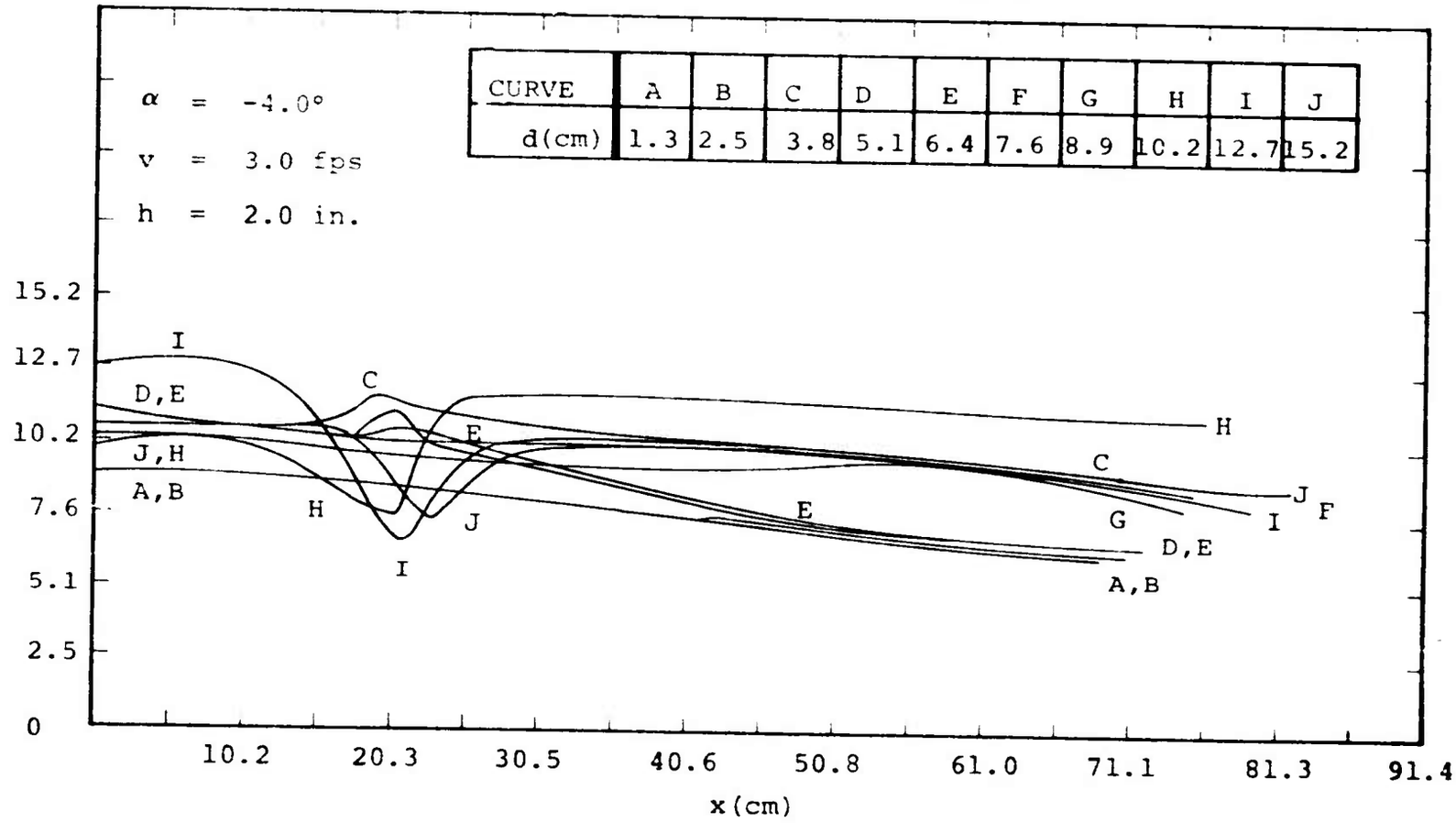

FIGURE 3.32: FREE SURFACE DIAGRAM: $\alpha = -4.0°$; v = 3.0 fps; and h = 2.0 in.

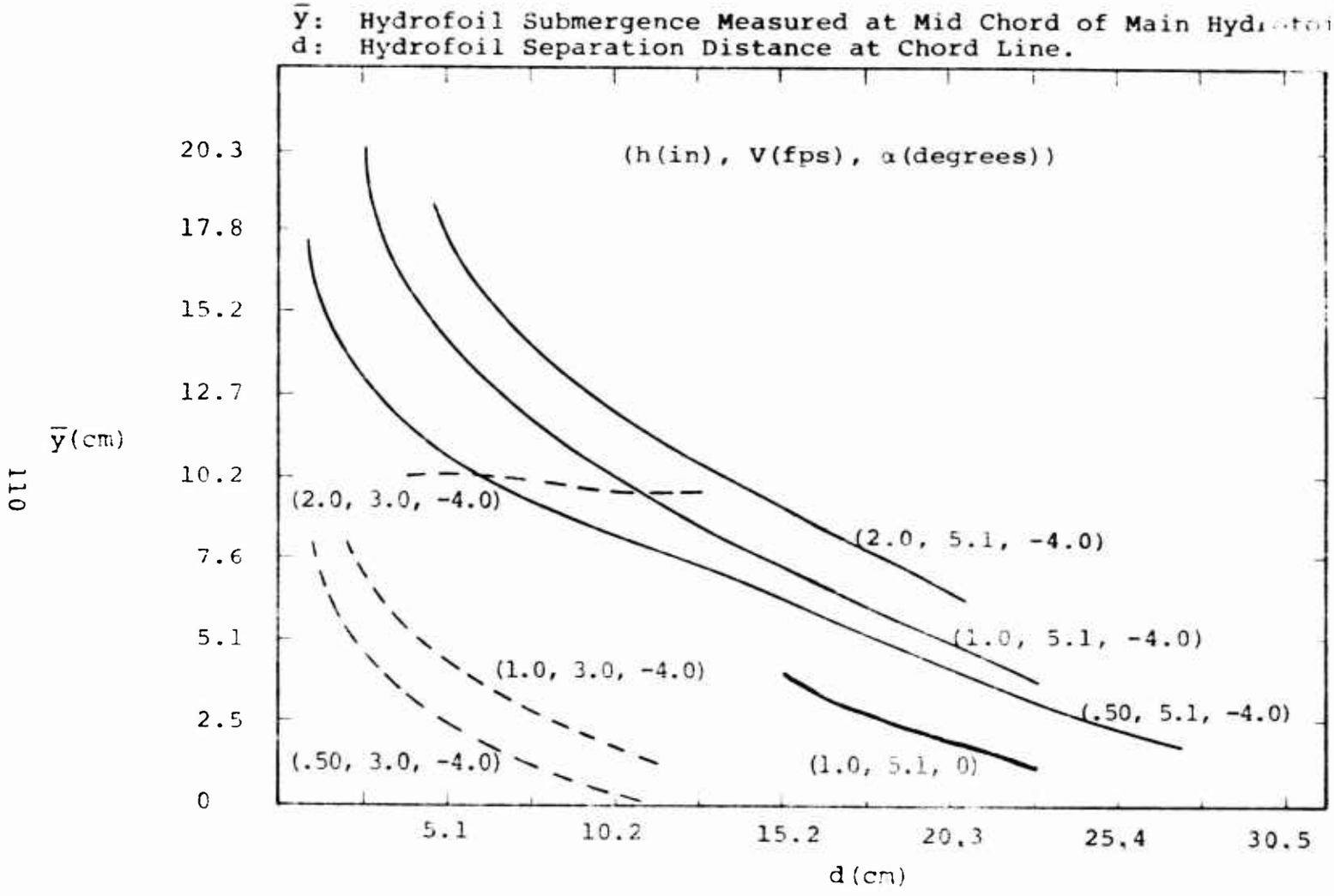

FIGURE 3.33: HYDROFOIL SUBMERGENCE DEPTH VERSUS HYDROFOIL SEPARATION DISTANCE

jumps or turbulent flow appeared on the rear of the main hydrofoil. These qualitative results also agree with the general observations made for the large scale hydrofoil in Reference 2.

It appears then that the current hydrofoil design has associated with it a critical velocity (between 0.9 and 1.6 m/sec), above which the free surface flow is non-turbulent. This operating condition is desirable, otherwise oil that is spread on the surface of the water may be emulsified prior to recovery. However, the recovery of oil would not be inhibited if turbulence were present during some portion of the flow over the hydrofoil. Thus, any number of operating points may be identified from the data reported in Figure 3.33. Generally, it is desirable to operate with the smallest depth of flow over the surface of the hydrofoil in order to minimize the quantity of water to be processed by the recovery system. However, when waves are present (in particular those for which the hydrofoil's flotation system cannot follow) a minimum flow thickness is desirable to allow for the loss of a portion of that flow through the vented slot. Therefore, an operating point must be found that represents a trade-off between the minimum flow thickness that can be realistically achieved by the hydrofoil operating in calm water and some maximum flow thickness for which the hydrofoil can operate under specified wave conditions and for which the recovery system's performance does not deteriorate due to the large quantities of water it must process.

The data reported in Figures 3.25 through 3.33 include the tests performed with waves (test numbers 58 through 76 in Table 3.6). The wave data reported represents the average

submergence at the points A through F for the duration of each individual test. This approximation may at first appear to be arbitrary; however, even in severe chop (with the exception of tests 75 and 76 for which no data were obtained) the variation of the flow thickness with time did not vary by more than $\pm$ 1.25 cm over the rear of the main hydrofoil. The bow of the lead hydrofoil reflects most of the wave forward resulting in a reduced amplitude and increased wave length wave over the remainder of the hydrofoil. The behavior of the bow of the lead hydrofoil effectively isolates the remainder of the hydrofoil from the deleterious effects of the waves, except for extremely choppy water conditions for which all of the fluid is periodically vented through the slot (tests 75 and 76). Moreover, the vented hydrofoil system did not experience any difficulty in operating in waves whose wavelength was relatively large (tests 58 through 68) or in moderate chop (tests 69 through 74). For the long period waves the flotation system was able to accomodate itself to the water surface, whereas for the moderately choppy water condition, the hydrofoil itself reflected the waves forward as previously discussed. Thus, the wave response characteristics of the vented hydrofoil system are strongly dependent upon the size and type of flotation provided.

Based on the previous discussions, it was found that a favorable operating condition for the vented hydrofoil system is at a depth of submergence (see Figure 3.33) greater than or equal to 2.50 cm for the current model design. This submergence depth allows the vented hydrofoil system to operate over a wide range of water surface conditions without seriously degrading its performance characteristics.

A limited amount of data was gathered for various angles of attack of the hydrofoil system; however, the data of Figure 3.33 clearly shows that it has a significant impact on the operating characteristics of the hydrofoil. In effect, for the same vented slot opening, a zero angle of attack hydrofoil will produce a lower depth of submergence than a negative angle of attack. Therefore, smaller slot openings would be required to achieve the same amount of venting provided by the negative angle of attack hydrofoil.

In conclusion, the vented hydrofoil concept has been shown to be a viable control device. The system has been operated successfully in calm, wavy and choppy water conditions. However, the vented hydrofoil has its limitation in extremely choppy water conditions, although this may be overcome to some degree with an improved design (see section 6). The hydrofoil also has a lower limit in its operating velocity (with the present design this is about 1.2 m/sec); however, an improved design (see section 6) will reduce this limit to about 0.76 m/sec. At velocities below 0.76 m/sec, the MARCO Filterbelt recovery system or one similar to it can be used without the hydrofoil in place (this is also discussed in section 6).

3.5.4 Hydrofoil/Ramp Experiments - The idea of using an air jet to separate the surface layer of oil and some water from the main hydrofoil was described in detail in section 3.5.2. However, the results of those tests indicated that the air jet was not a viable technique. Therefore, it was decided to add a small ramp to the rear of the main hydrofoil in the manner discussed in section 1.2.2. The purpose of the ramp is to direct the oil/water flow tangentially onto the polyurethane foam belt. In this manner, the

moving belt never experiences a high normal velocity which could cause the oil/water mixture to flow through without depositing the oil in the belt. Moreover, the ramp converts some of the kinetic energy of the flow into potential energy by raising its height above the surface of the hydrofoil. The configuration for the ramp is shown in Figures 3.16 and 3.17 of section 3.3 and consisted of a sheet of 0.16 cm thick aluminum 0.61 m wide and 10.0 cm long. The aluminum sheet was bent to form a cusped shape with its highest point 6.25 cm above the rear surface of the main hydrofoil at an angle of approximately 30°. The 6.25 cm height of the ramp was the minimum required to allow the flow to be directed tangentially onto the belt at its lowest point. Moreover, the ramp height is directly related to the minimum velocity for which the system can operate, through the formula for the ideal conversion of kinetic energy into potential energy:

$$\frac{V^2}{2} = gh$$

where V is the hydrofoil velocity, g is the acceleration of gravity and h is the ramp height. Therefore, for the present h = 6.25 cm; the minimum operating velocity of the system is 1.1 m/sec.

A number of tests were conducted with this configuration and many changes were made to the model design. These design modifications resulted in the final configuration shown in Figures 3.16 through 3.19 of section 3.3. The tests performed were documented with the video tape and are listed in Table 3.7 with the proper references to the video tape number and location on the tape. For clarity, a general discussion of all the tests outlined in Table 3.7 is presented rather than a detailed description of each

TABLE 3.7: SUMMARY OF VENTED HYDROFOIL TOW TANK TEST DATA (With Ramp)

Tape #/Footage	Test #	Test Description
4/2.4	81	10.0 cm high ramp test, 1.5 m/sec hydrofoil velocity
4/2.9	82	Same as #81 but with use of air jet, configuration (B)
4/3.6	83	6.25 cm high ramp test with air jet, configuration (B)
4/5.3	84	Same as #82
4/6.4	85	6.25 cm high ramp, 1.22 m/sec hydrofoil velocity
4/7.2	86	6.25 cm high ramp, 1.83 m/sec hydrofoil velocity
4/8.3	87	6.25 cm high ramp, 1.44 m/sec hydrofoil velocity
4/8.8	88	Same as #87 but with use of 15 GPM pump
4/9.8	89	Same as #88 but with use of oil
4/10.5	90	Same as #88

test. The reason for this is that in the short time that remained to perform these tests (prior to the University of Michigan test series), only qualitative observations of the new control/recovery configuration were made, and no detailed test data was obtained.

In general, the tests outlined in Table 3.7 can be classified into three groups: (1) ramp and air jet (2) velocity and (3) pump and oil. During the first series (test #81 through 84) two different ramp heights (10.5 and 6.25 cm) were tested and the air jet in configuration B was explored. The results of these tests indicated that the 10.5 cm high ramp converted too much of the flow's kinetic energy into potential energy as discussed previously. The air jet tests were no more successful than those described in section 3.5.2. The velocity tests (#85 through #87) indicated that at the lowest velocity, the water flowed smoothly up onto the polyurethane foam belt to a height of about 10.0 cm. As the velocity was further increased, the water flowed to the top of the belt and at the highest velocity it flowed over the belt. These results indicated that the belt length would have to be substantially increased to allow the control/recovery system to operate at the higher speeds (see section 6 for further discussion of this point). The final series of tests (#88 through #90) were conducted with a pump to remove the fluid from the collection sump during the test (this was not done in the previous tests). The addition of the pump to the system improved its performance greatly because none of the fluid that was processed by the belt was lost. The pump also served the purpose of maintaining the flotation equilibrium of the control/recovery device. At this stage of the system design, more flotation was required; however, not enough time remained to incorporate this modification. Therefore, the pump not only

removed the fluid from the system but prevented the rear of the device from sinking into the water. One of the final tests to be performed was that associated with the addition of some oil to the surface of the water. Although no measurements of the quantity of oil removed from the water was made, it appeared that the system was performing as expected within the limitations of the existing design (short belt, inadequate flotation, undersized pump, and a small volume sump).

It can generally be concluded that the results of these tests were quite encouraging. The final control/recovery system concept appeared to be one which could meet the requirements of operating in a fast current environment. Further experiments with a differently designed model would greatly improve the system's overall performance characteristics.

SECTION 4

Large Scale Flume Experimental Program

4.1 Introduction

The primary objective of the large scale flume experiments, conducted at the University of Michigan, was to demonstrate the oil control and recovery functions of the phase I fast current oil response system. The model used for this demonstration was that described at the end of section 3.3 and further discussed in section 3.5.4. The facility in which these tests were performed was a large recirculating water flume whose test section dimensions are 4.9 m in length, 1.75 m in width and 2.13 m in depth. The water depth in the test section at zero velocity was 1.83 m; however, at its maximum velocity of 2.13 m/sec, the water depth dropped to about 1.52 m. The flow conditions in the test section were generally turbulent and waves having an average wave length of 0.61 to 0.91 m and an amplitude of 7.5 cm to 15.0 cm were present throughout the velocity range of the facility. These conditions resulted in it being almost impossible to support the phase I model from a fixed point above the facility. Therefore, the flotation system used in the tow tank experiments was employed. Pivotable towing arms were fabricated and the model was attached to a catwalk which was placed over the top of the facility in much the same manner as was done during the tow tank experimental program. This installation allowed the phase I model to respond somewhat to the waves in the facility; however, the situation was far from optimum.

During each test sequence, oil was pumped from a central storage tank and spread over the surface of the water in front of and across the width of the control/recovery device. After processing by the phase I control/recovery system, the recovered oil/water mixture was pumped to another storage tank where the oil was separated for reuse. The primary parameters measured during each test were the oil delivery rate (GPM), slick thickness (inches), percent of oil in the oil/water mixture, total oil/water mixture flow rate (GPM), and the water current velocity (fps). These parameters were then reduced to five different types of graphs:

1. Average oil/water recovery rate (GPM) versus water current speed (fps)

2. Average recovery efficiency (percent) versus water current speed (fps)

3. Average oil recovery rate (GPM) versus water current speed (fps)

4. Average specific oil recovery rate (GPM) versus water current speed (fps)

5. Throughput efficiency (percent) versus water current speed (fps),

where these parameters are defined as follows:

a. Water current speed (fps): velocity of water flowing in the flume

b. Oil/water recovery rate (GPM): total rate of oil/water mixture being pumped from the phase I control/recovery device

c. Average recovery efficiency (percent): percent of oil in recovered oil/water mixture averaged over the duration of each test

d. Average oil recovery rate (GPM): (b) x (c)

e. Average specific oil recovery rate (GPM): (d) x $\frac{1 \text{ foot}}{\left(\begin{array}{l}\text{Width of} \\ \text{phase I} \\ \text{device(ft)}\end{array}\right)}$

f. Throughput efficiency (percent): (d)/oil delivery rate (GPM).

During the experimental program, three types of oils having the properties shown in Table 4.1 were used.

TABLE 4.1: PHYSICAL PROPERTIES OF THE OIL USED DURING THE UNIVERSITY OF MICHIGAN FLUME TESTS

Oil Type	10	51	64
Oil viscosity (centistokes)	10.1	264	361.5
Oil specific gravity	0.813	0.877	0.819

4.2 Discussion of Test Program

During the early portion of the experimental program, the phase I model was held in a rigid manner to a suspension system that was fixed to the sidewalls of the flume. In this configuration, it was just about impossible to adjust the depth of submergence of the hydrofoil (a critical parameter to the phase I system's operation) to its proper value because of the waves and variable water depth in the test facility. Therefore, it was decided that the only way to perform the tests would be to float the phase I model in a manner similar to that which was discussed in sections 3.3 and 3.5.2-4 for the tow tank experiments. Thus, the hydrofoil depth and angle of attack was easily

adjusted (without waves or changing water depth) prior to the test sequence. The latter mode of operation proved to be quite effective and allowed SAI to demonstrate its phase I model.

Several other problems were encountered during the test program which are more appropriately discussed before presenting the experimental data. These problems are those associated more with the physical deficiencies of the phase I model rather than the limitations of the control/recovery concept itself. These problems were alluded to in the discussion at the end of section 3.5.4. One of the most serious problems experienced during the test program was that associated with the length of the polyurethane foam belt. The phase I model was originally designed to operate in the air jet generated oil/water spray mode that was discussed in previous sections. The belt in this mode would not have to process the quantities of fluid that are associated with the present design concept, but the belt design was not changed due to a lack of time remaining prior to the University of Michigan test series. A belt length of somewhere between 3.0 and 4.6 m would be required in order to drain most of the water from the belt prior to squeezing. However, with the current belt length of 0.38 m, a large quantity of water is retained prior to squeezing, which results in a low oil to water ratio in the collected fluid samples. Therefore, the average recovery efficiency reported here is artificially low and reflects the capabilities of the current design and not that of the control/recovery system concept. The existing belt design also affects the total amount of fluid handled by the system since a longer belt would allow a high percentage of the water to drain out (while retaining the oil) and therefore

only the oil and a fraction of the water would be collected. Thus, the data reported for the average oil/control recovery rate is higher than it should be for a properly designed system. The final limitation of the short belt is associated with the maximum current speed that the system could attain. At speeds above approximately 4.0 fps the oil/water mixture would flow over the top of the belt and flood out the small (2 gallon) sump that was provided on the existing model; thus, the data collected during those tests did not truly represent the maximum efficiency of the system. Moreover, the pumping capacity provided for in the current model (50 GPM) was too small to handle the large volumes of fluid that were encountered. In addition, the pump motor experienced overheating problems during the test program, and would shut down in the middle of a test. Moreover, the characteristics of the test facility were such that only a nominal velocity of say 4.0 fps could be established, and variations of $\pm$ 0.50 fps about this value were experienced during an individual test run. These conditions produced surges of fluid over the model which caused the flow to pass over the top of the short belt and momentarily flood out the sump. The final problem associated with the belt was that of flow through its sides (because the width of the belt was too short). This problem was partially solved near the end of the test program by sewing on an additional strip of belt material. The increased oil recovery efficiency that resulted from this modification was very encouraging.

Another problem that was experienced during the test program was related to the minimum operating velocity of the system. This problem was discussed at length in section 3.5.3 and 3.5.4. Moreover, it was established that this

lower limiting velocity (for the current hydrofoil design) was in the vicinity of 3.5 fps. Therefore, the operating range for the present model was limited to a nominal velocity of 4.0 fps. One higher velocity (4.5 fps) is reported in the data; however, it can easily be seen that the efficiency of the system is greatly reduced for that operating condition.

Several other minor problems were also encountered during the University of Michigan test program. The first was related to the momentary venting of all the fluid passing over the lead hydrofoil through the slot and under the main hydrofoil. For several unrelated operating conditions, fluid was completely absent (for a short time period) from the main hydrofoil. This situation resulted from the system's inability to follow the short wavelength waves that existed in the test facility. However, this operating condition occurred infrequently, and, although it represented a loss, (and therefore a reduced efficiency) it was not considered a serious problem. The wave following characteristics of the hydrofoil are discussed in more detail in section 3.5.3. The last problem, which is completely related to the present model design, was associated with the inability to adjust the hydrofoil to a distance closer than 3.0 cm under the water surface. Therefore, all tests were conducted at that depth of submergence. However, this situation was not serious, since the results of section 3.5.3 indicate that a depth of submergence greater than or equal to 2.50 cm would be optimum. Additional buoyancy for the control/recovery system model would have been desirable for these tests; however, this did not limit its performance. Tests with the vented hydrofoil model (section 3.5.3) were conducted at two distinct angles of attack

(0° and -4.0°); however, neither of these angles were achieved during the University of Michigan test series. The angle of attack with respect to the hydrofoil's chord line and the free surface associated with the waves appeared to be approximately +5.0°, and the depth of water over the rear of the main hydrofoil was approximately 6.0 cm. This depth of submergence was achieved with a 13.75 cm vented slot opening (measured along the chord line). Unfortunately, no comparable tow tank test data (similar to that reported in Figure 3.33) was available for this angle of attack.

The foregoing discussion puts into perspective the results of the University of Michigan test program that are presented below in section 4.3.

4.3 Discussion of Test Data

The test data for the experiments described in sections 4.1 and 4.2 appear in Figures 4.1 through 4.12. In each graph the ordinate represents one of the quantities discussed in section 4.1 versus the current speed. Moreover, each individual graph represents a different oil, and two oil slick thicknesses. Several data points were repeated during the experimental program, primarily because of sump flooding, inadequate pumping capacity, and intermittent operation of the pump. However, all of the data has been included on the graphs.

The average oil/water recovery rate data is shown in Figures 4.1 through 4.3 for the three different types of oils. Some of this data, especially that in the vicinity of 50 GPM, represents near capacity operation of the pump and possibly some loss of fluid due to sump flooding. Other

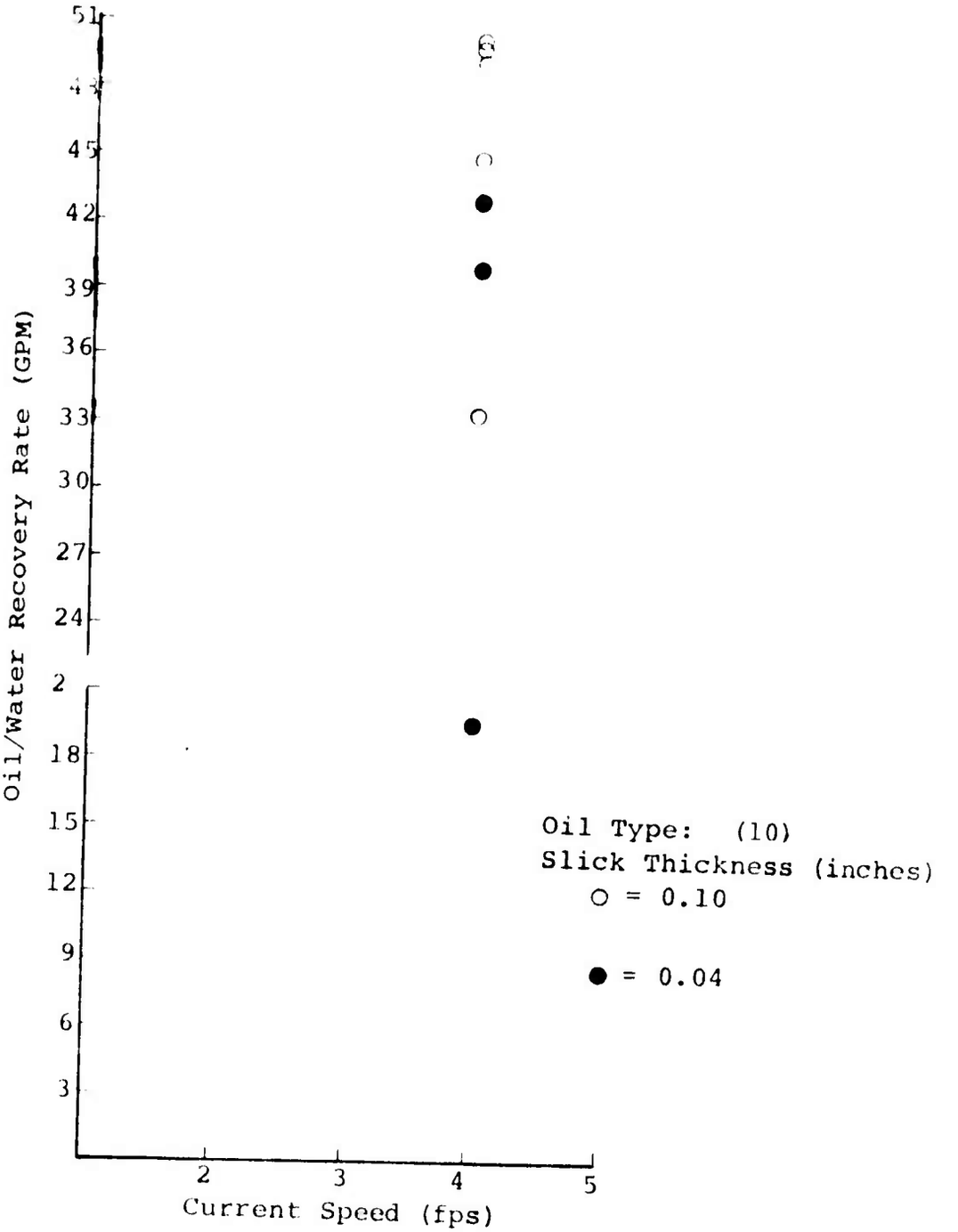

FIGURE 4.1. OIL/WATER RECOVERY RATE (GPM) VERSUS CURRENT SPEED (fps) FOR THE NUMBER 10 OIL

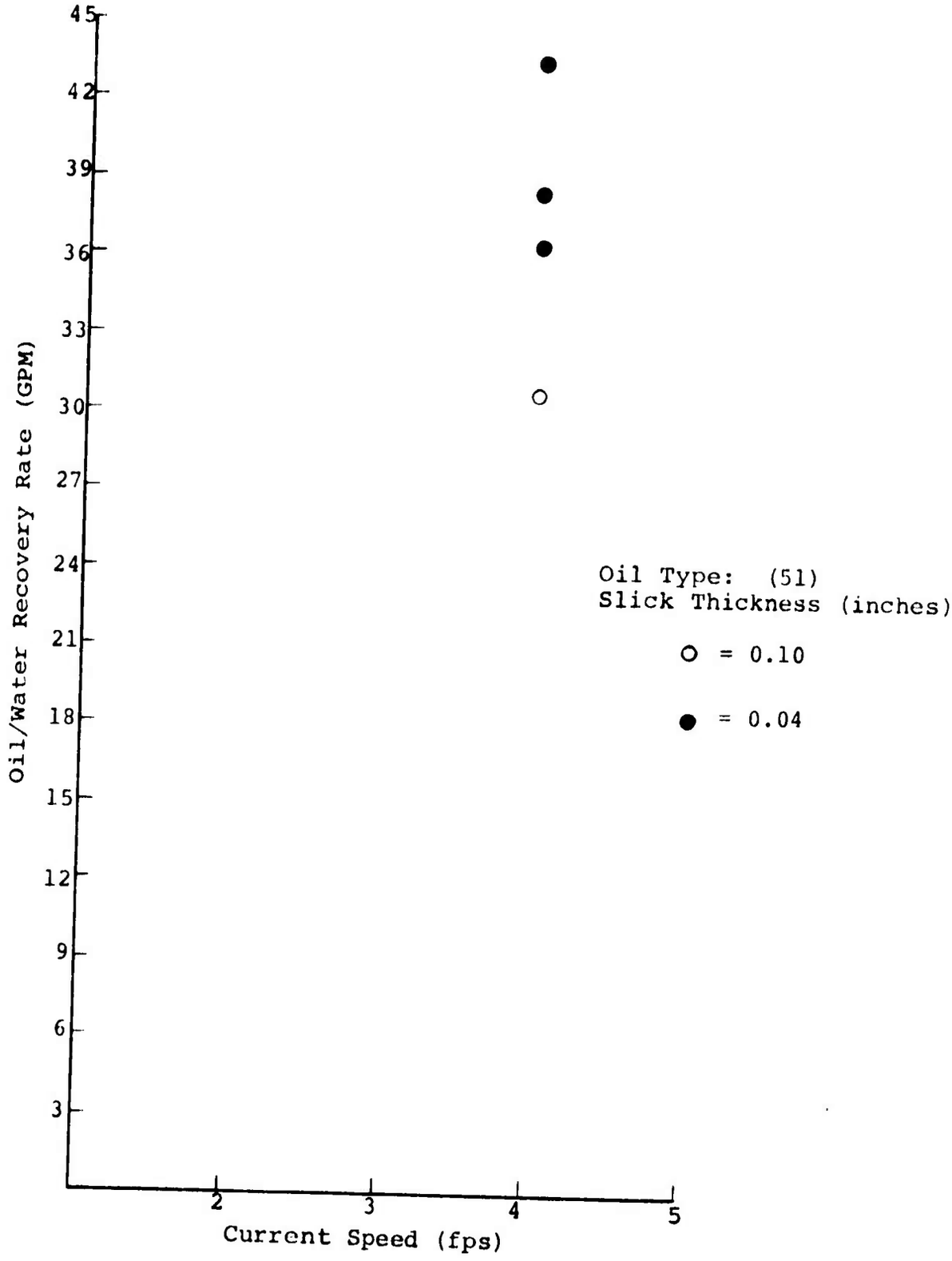

FIGURE 4.2. OIL/WATER RECOVERY RATE (GPM) VERSUS CURRENT SPEED (fps) FOR THE NUMBER 51 OIL

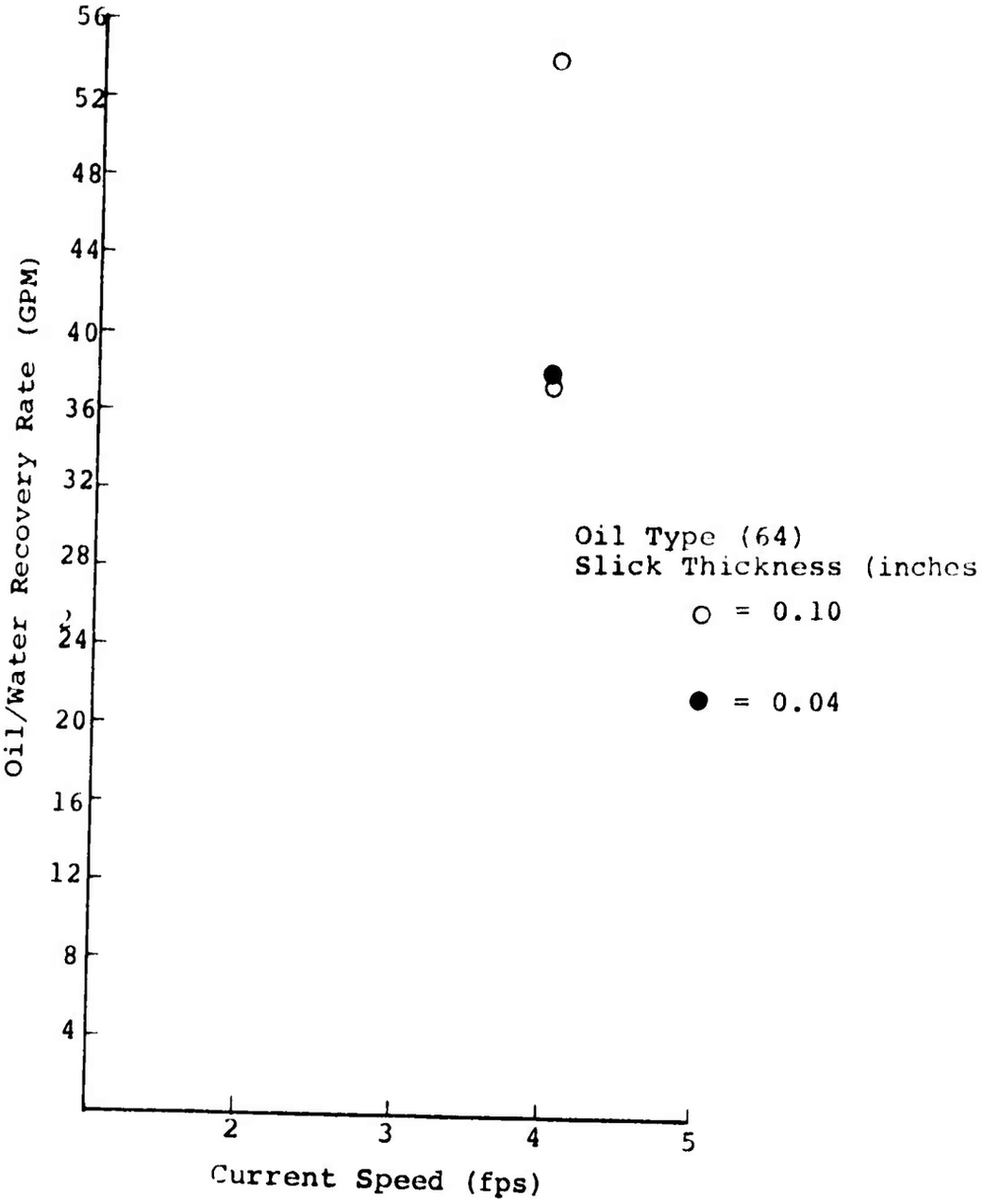

FIGURE 4.3. OIL/WATER RECOVERY RATE (GPM) VERSUS CURRENT SPEED (fps) FOR THE NUMBER 64 OIL

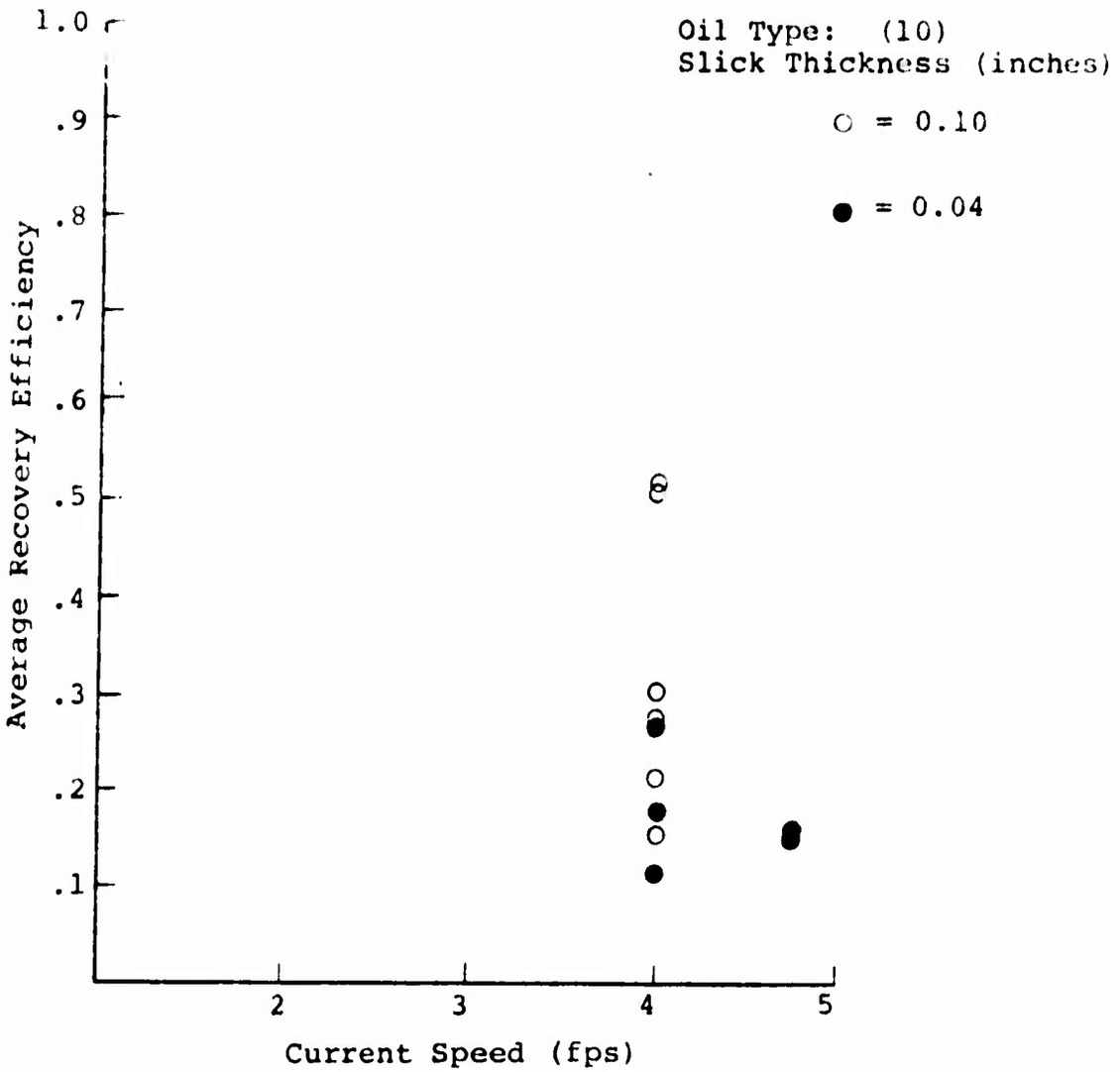

FIGURE 4.4. AVERAGE RECOVERY EFFICIENCY (PERCENT) VERSUS CURRENT SPEED (fps) FOR THE NUMBER 10 OIL

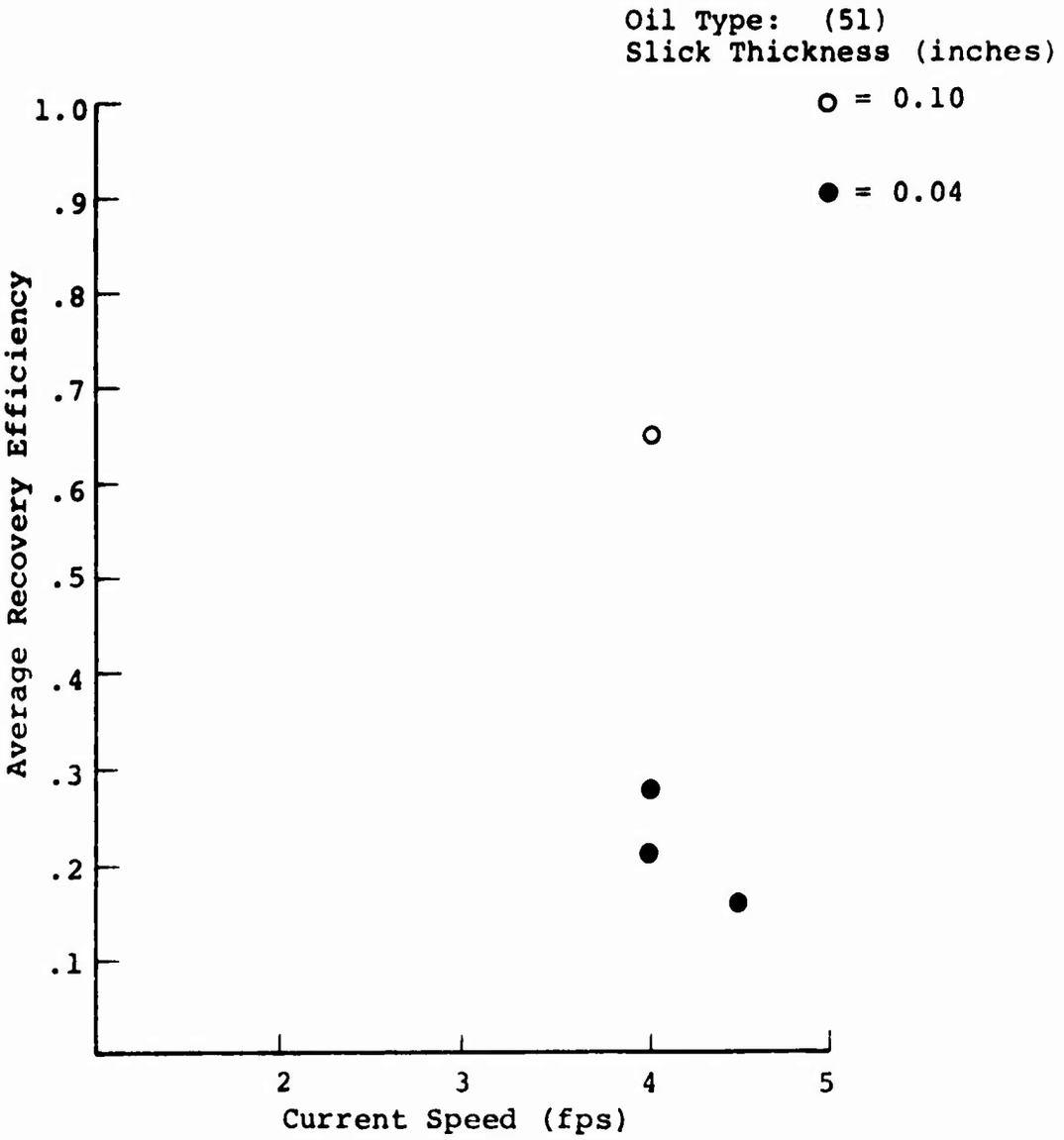

FIGURE 4.5. AVERAGE RECOVERY EFFICIENCY (PERCENT) VERSUS CURRENT SPEED (fps) FOR THE NUMBER 51 OIL

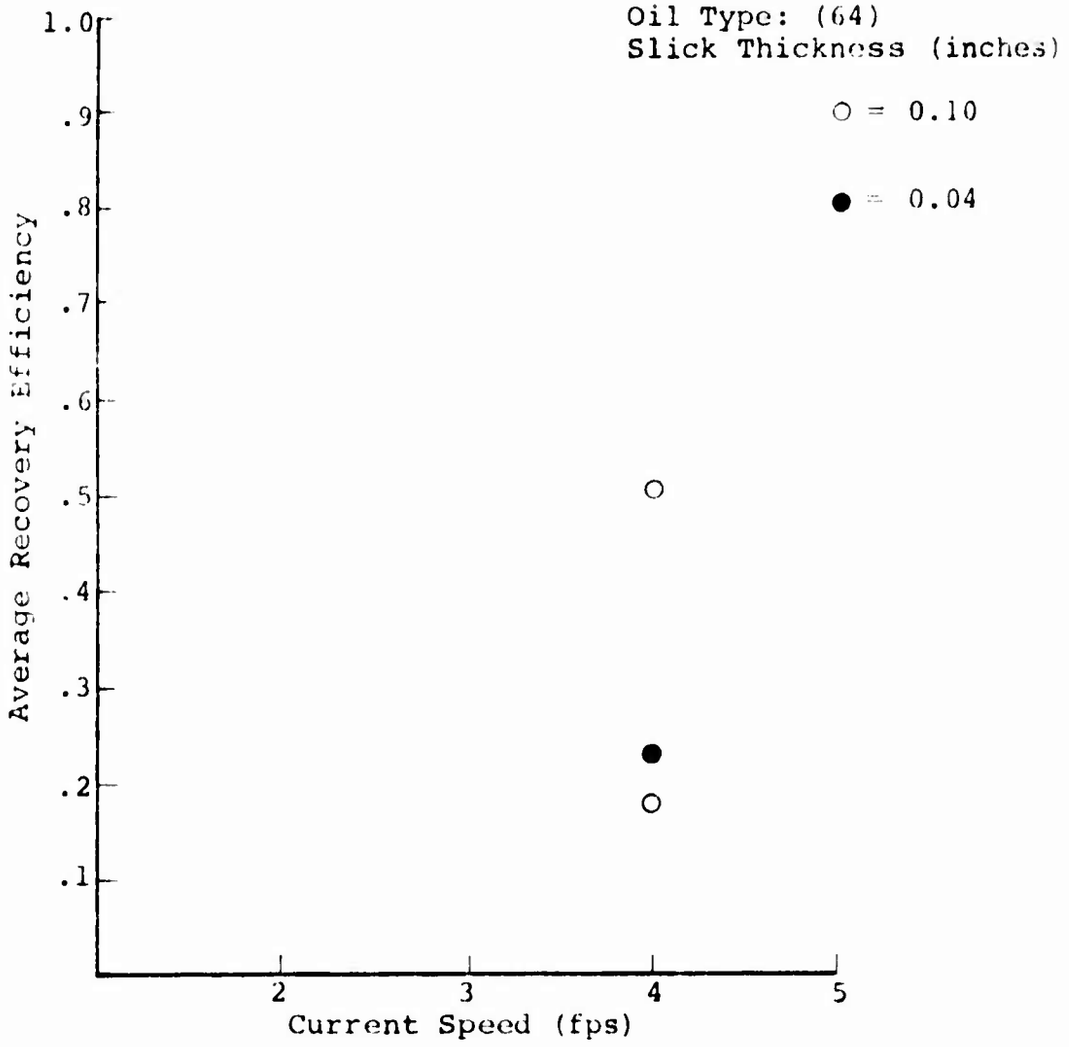

FIGURE 4.6. AVERAGE RECOVERY EFFICIENCY (PERCENT) VERSUS CURRENT SPEED (fps) FOR THE NUMBER 64 OIL

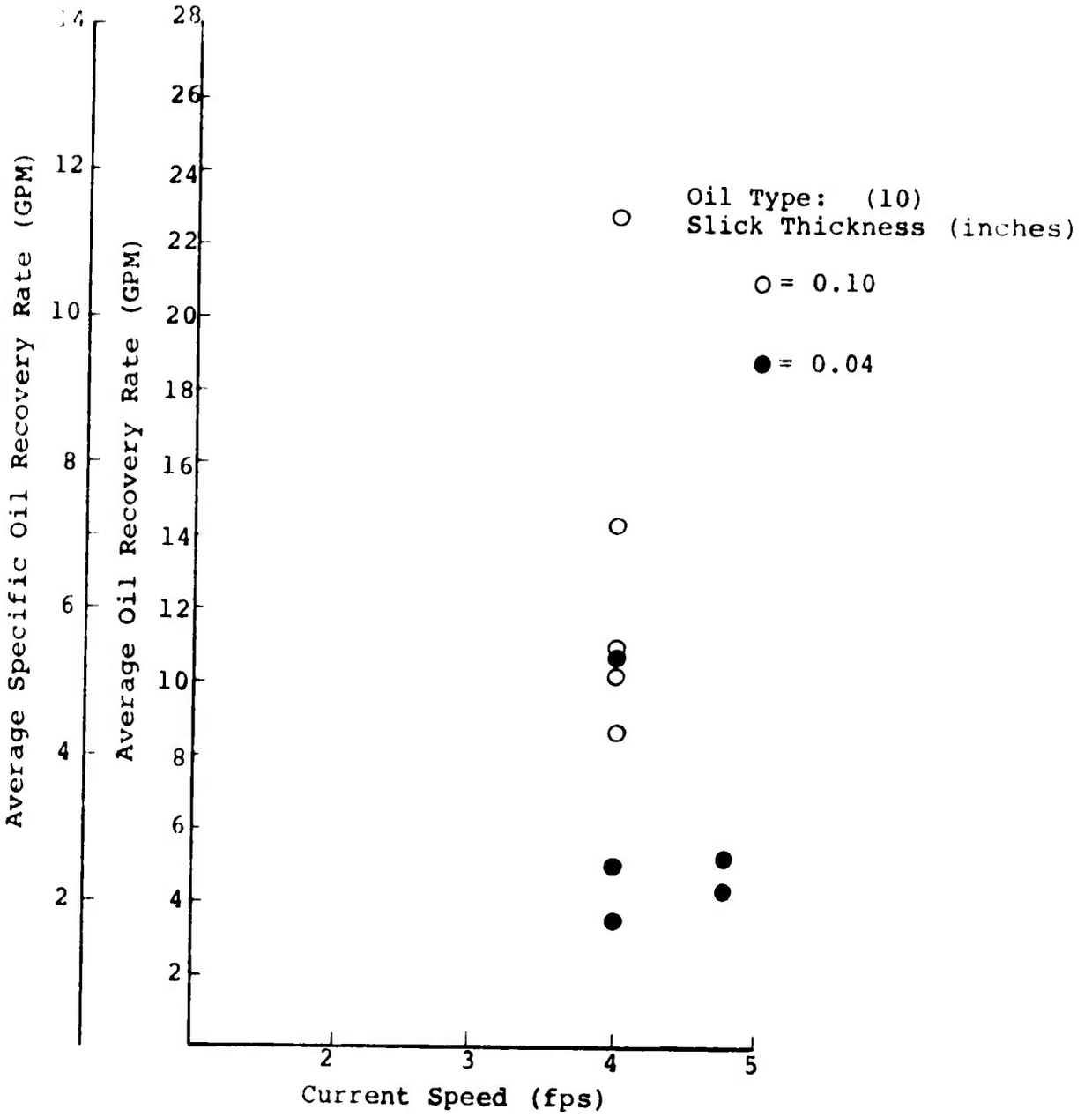

FIGURE 4.7. AVERAGE SPECIFIC OIL RECOVERY RATE (GPM) AND AVERAGE OIL RECOVERY RATE (GPM) VERSUS CURRENT SPEED (fps) FOR THE NUMBER 10 OIL

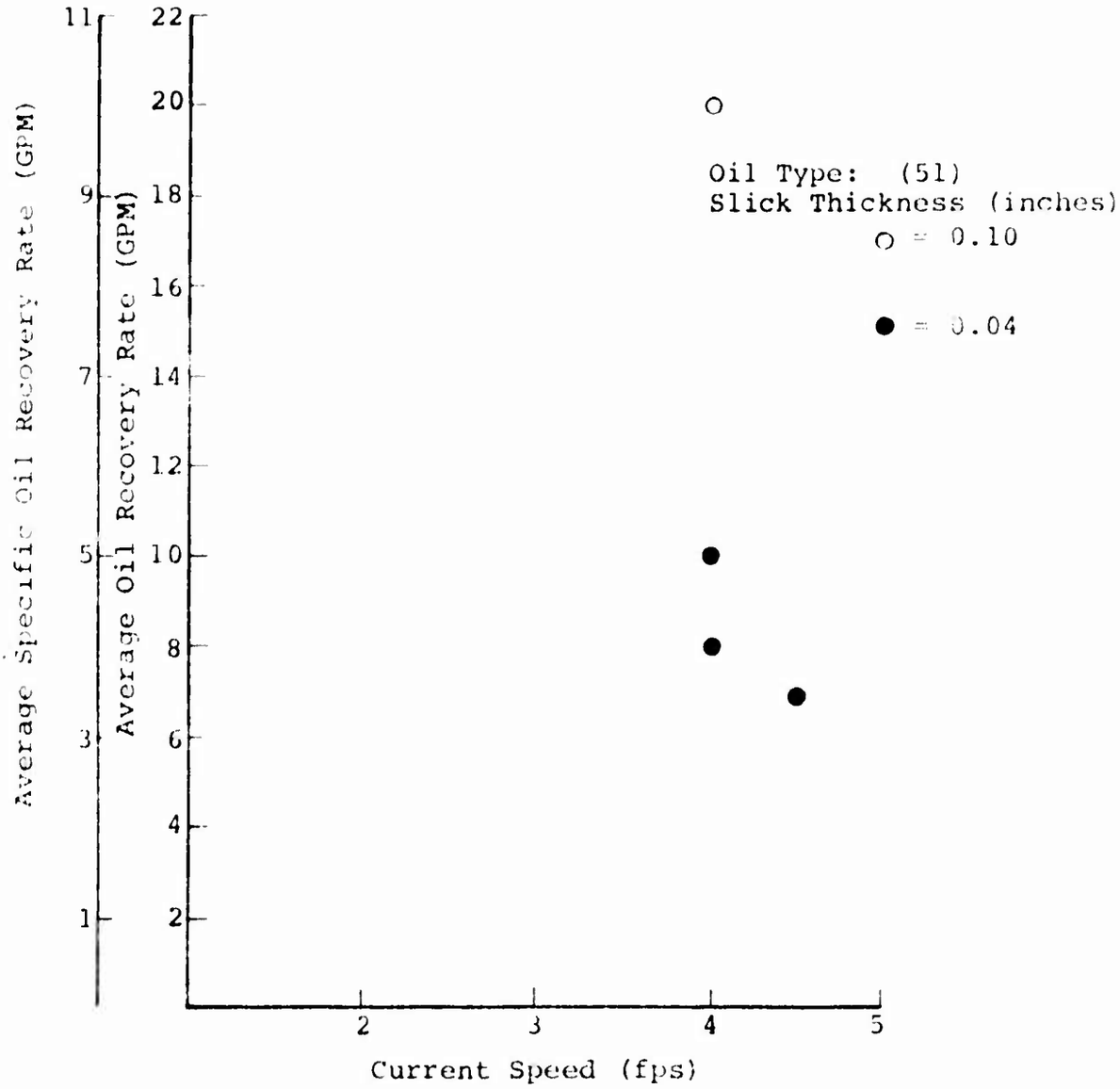

FIGURE 4.8. AVERAGE SPECIFIC OIL RECOVERY RATE (GPM) AND AVERAGE OIL RECOVERY RATE (GPM) VERSUS CURRENT SPEED (fps) FOR THE NUMBER 51 OIL

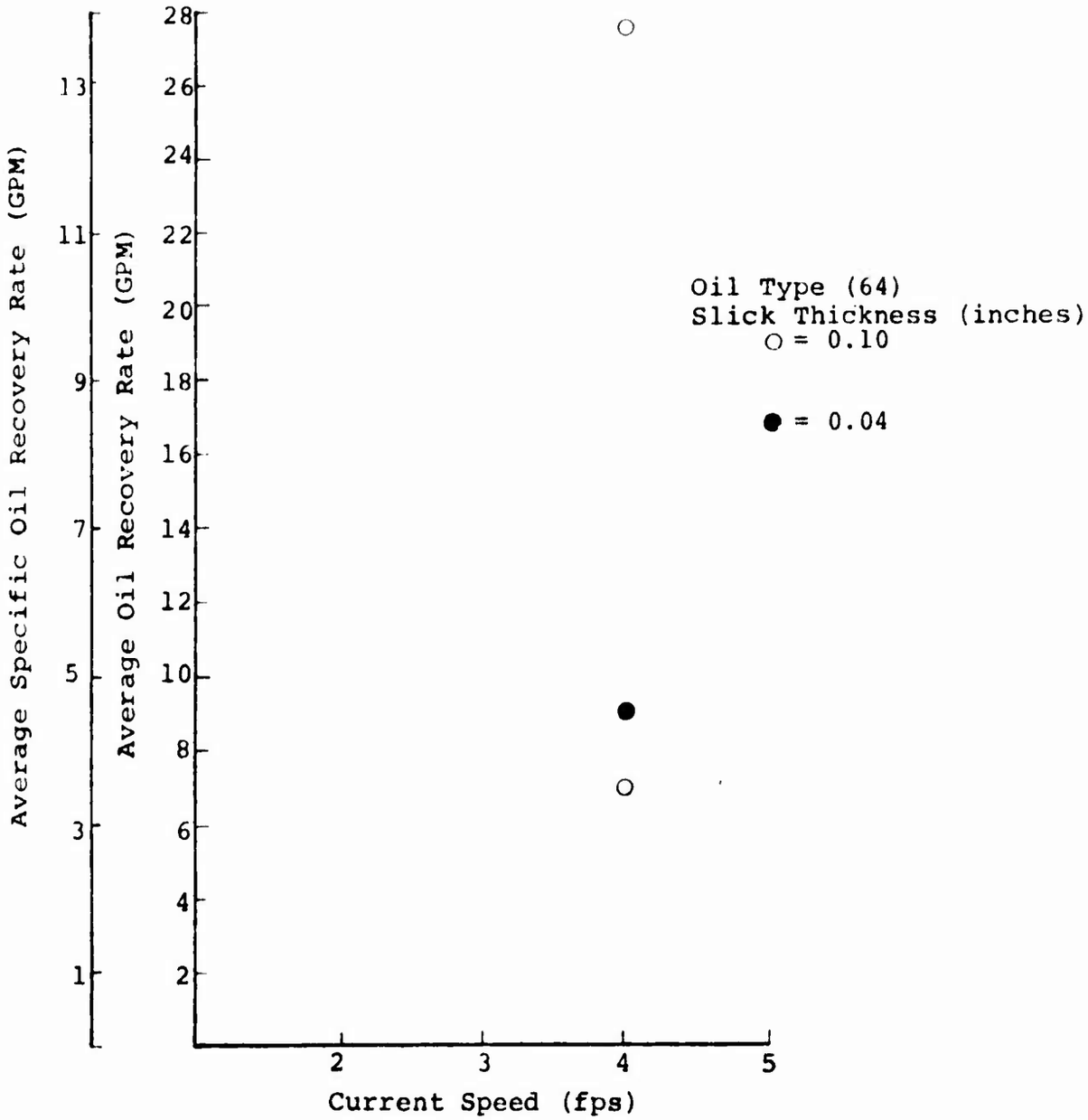

FIGURE 4.9. AVERAGE SPECIFIC OIL RECOVERY RATE (GPM) AND AVERAGE OIL RECOVERY RATE (GPM) VERSUS CURRENT SPEED (fps) FOR THE NUMBER 64 OIL

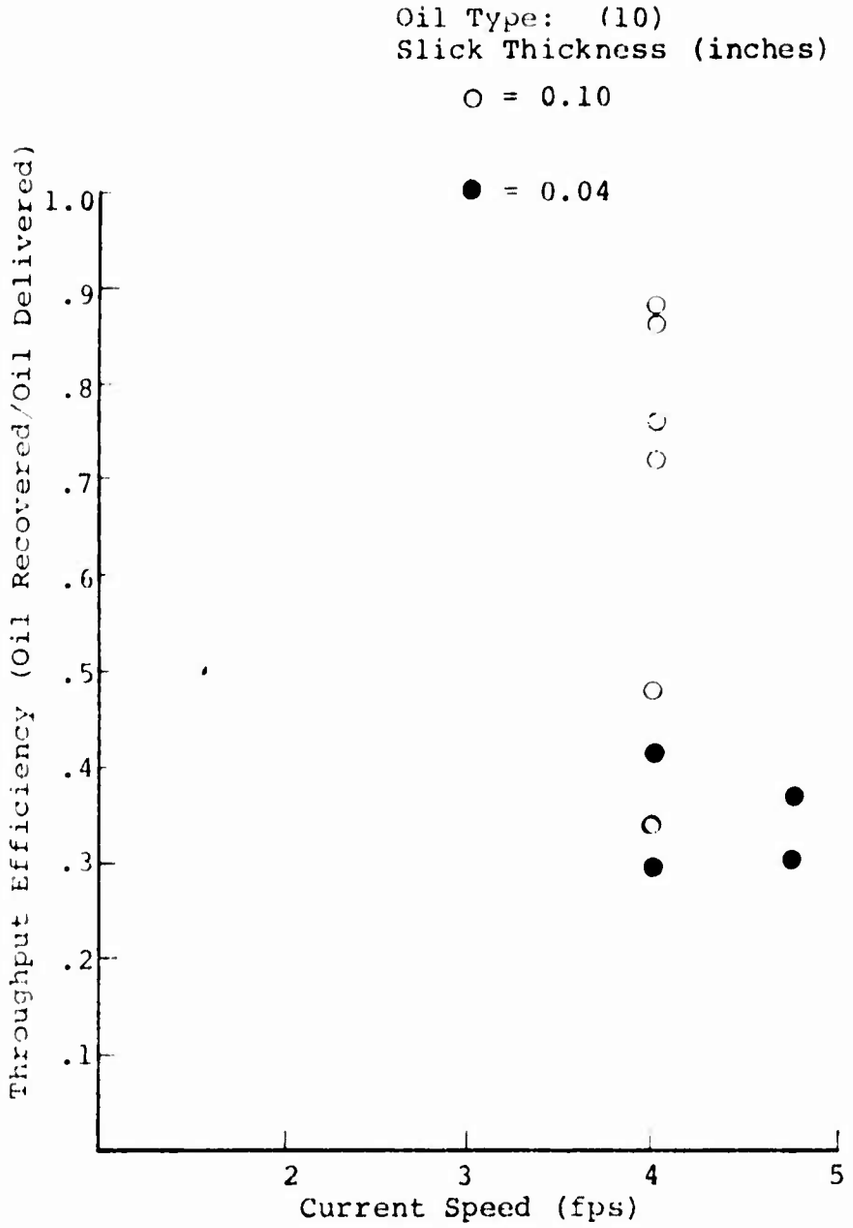

FIGURE 4.10. THROUGHPUT EFFICIENCY (OIL RECOVERED/OIL DELIVERED) VERSUS CURRENT SPEED (fps) FOR THE NUMBER 10 OIL

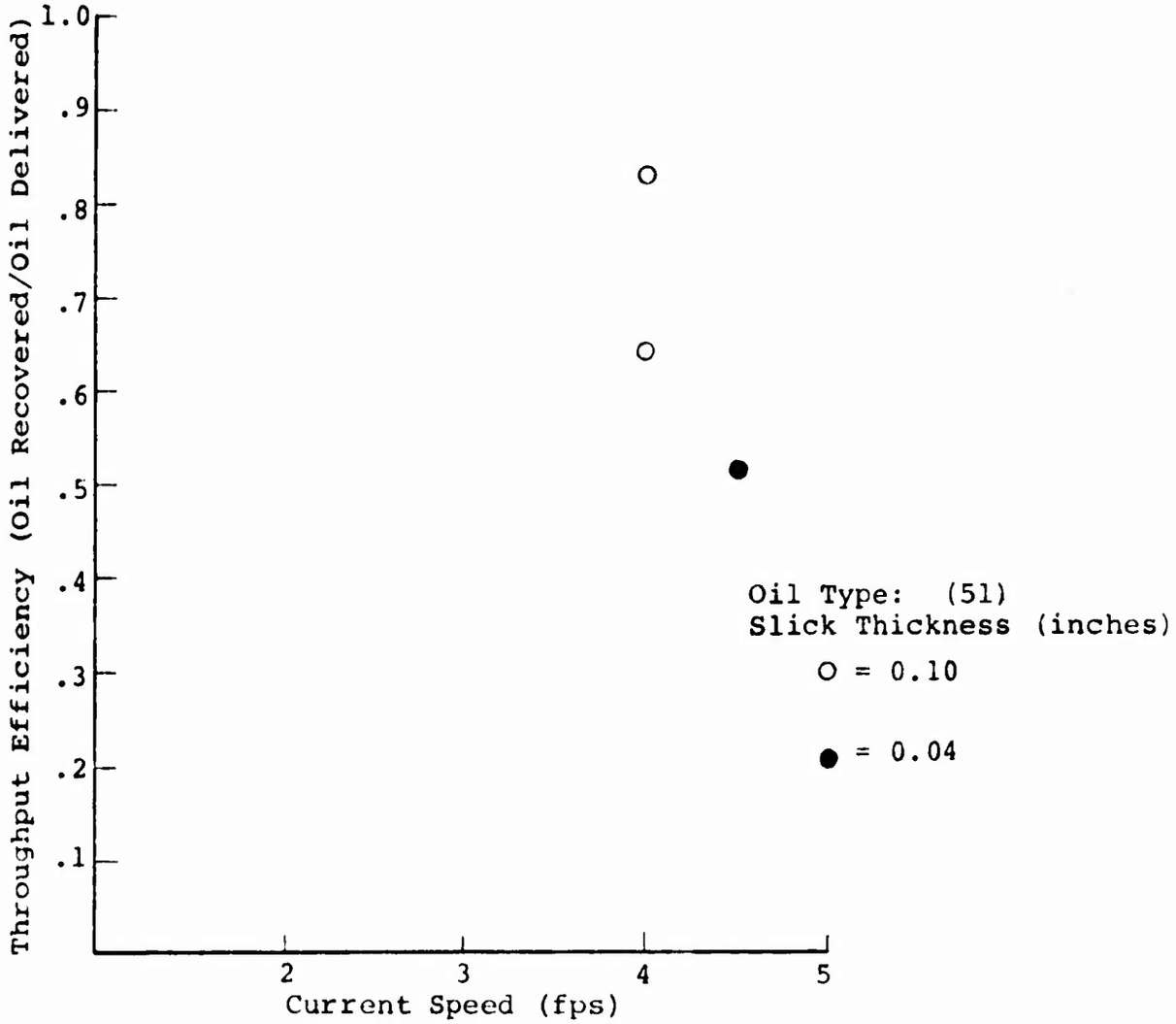

FIGURE 4.11. THROUGHPUT EFFICIENCY (OIL RECOVERED/OIL DELIVERED) VERSUS CURRENT SPEED (fps) FOR THE NUMBER 51 OIL

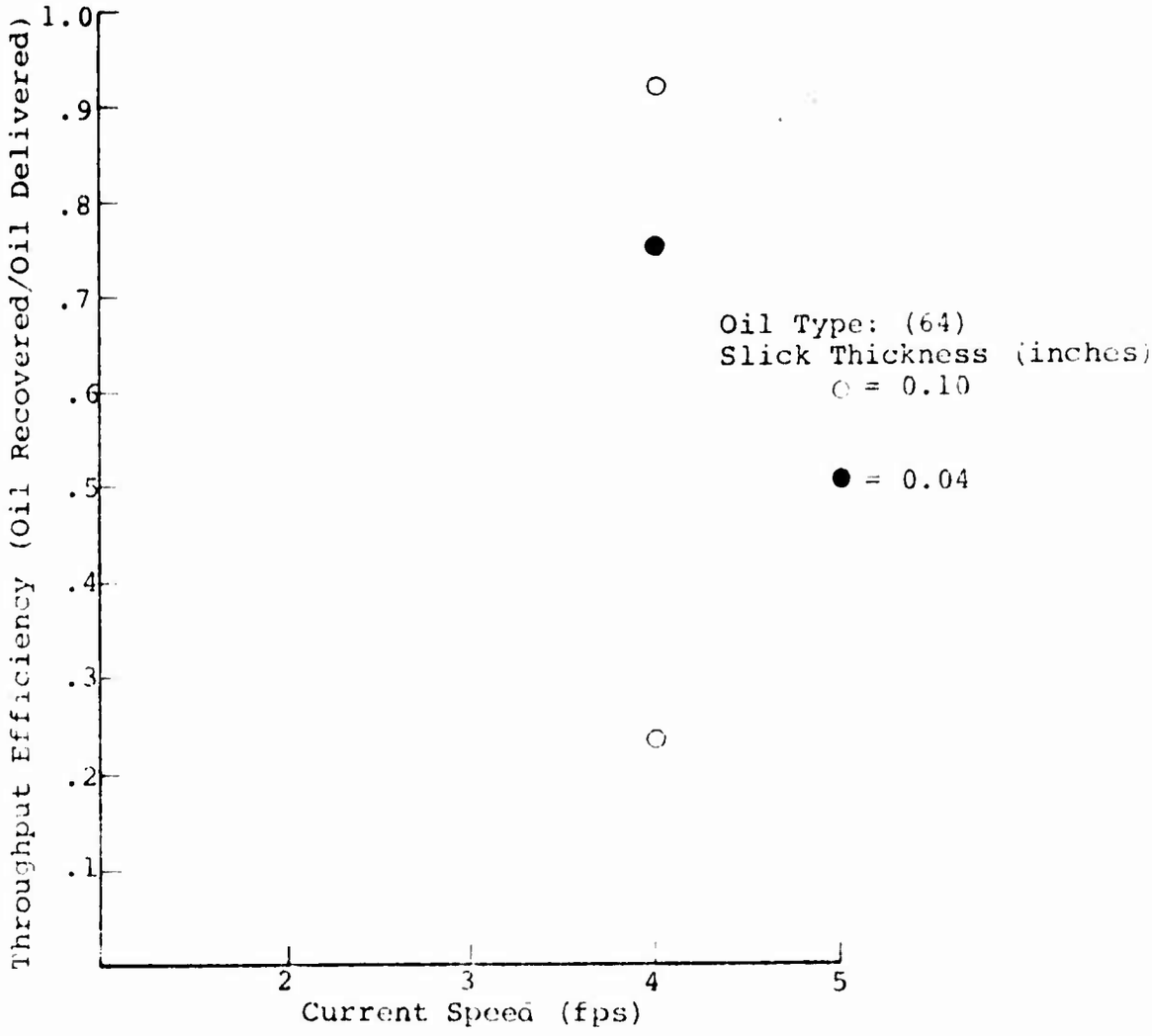

FIGURE 4.12. THROUGHPUT EFFICIENCY (OIL RECOVERED/OIL DELIVERED) VERSUS CURRENT SPEED (fps) FOR THE NUMBER 64 OIL

data points, in particular those representative of 4.75 fps, indicate a continuous loss of fluid from the system resulting from sump flooding or intermittent operation of the pump (automatic shutdown caused by overheating of the pump motor). Figures 4.4 through 4.6 represent the average recovery efficiency for each type of oil. These data generally show that samples of the fluid which were pumped from the control/recovery system's sump contained a large fraction of water. The reasons for this were discussed at length in section 4.2. The average specific oil recovery rate and the average oil recovery rate data are shown in Figures 4.7 through 4.9. This data is merely a combination of the previously mentioned Figures. The average oil recovery rate data is for the actual two foot wide model employed during the test program, whereas the average specific oil recovery rate data represent a scaling down of the data to reflect the operation of a one foot wide model.

The last series of data represent the oil throughput efficiency and are shown in Figures 4.10 through 4.12. This data is the most meaningful in the present series of experiments since it shows the percentage of oil recovered by the particular system. As mentioned previously, a number of the individual experiments were repeated several times in order to obtain a reasonable estimate of what the system's efficiency would be if the pump/transfer system were operating reasonably well. The data appear to fall into two general categories: (1) the data points that indicate a low efficiency represent cases where some pumping or other problems (described in section 4.2) were experienced during a test and (2) data points which represent a reasonably high efficiency indicate that the problems

discussed in section 4.2 were not as severe for those particular tests. The latter test data, if averaged over all conditions, show that approximately an 80% throughput efficiency was achieved for the 4.0 fps velocity tests. The 4.75 fps data indicate a much lower throughput efficiency; however, in those tests the problems discussed in section 4.2 were always present.

For all but two of the tests reported here, a 10 ppi polyurethane foam belt was employed; for the remaining two tests a 20 ppi belt was used. The reason for experimenting with two different foam belts was to determine the effect of pore size on the operating characteristics of the system. The results indicated that the throughput efficiency was identical; however, the average oil/water recovery rate was 20% higher for the 20 ppi foam. Thus, the increased water drainage provided by the 10 ppi foam results in a reduced fluid pumping requirement for the system.

It is unfortunate that more data at other current speeds could not be obtained for this control/recovery system. However, the 80% overall throughput efficiency achieved under these non-optimum conditions is a definite indication that this system is viable, and an improved design would result in a higher performance level.

SECTION 5

System Design and Performance Considerations

This section of the report has been divided into five parts. In the first part, the general philosophy behind the development of SAI Services Fast Current Oil Response System, regarding scaling, is discussed. The second part contains a review of the design goals based on the results of the Phase I program. In the third part, a discussion of the state of development of the ancillary functions is presented. The fourth part contains a detailed discussion of the performance characteristics of the large scale/prototype system. In the fifth part, a detailed preliminary design of the large scale system model is presented.

5.1 Scaling

The general philosophy behind the development of the SAI Services Fast Current Oil Response System has been to experiment with models that are full scale. In this manner, the problems associated with scaling a device over an order of magnitude are eliminated from the outset. Moreover, systems capable of dealing with larger oil throughputs can easily be developed by just increasing the width of the device.

The most important feature of the SAI Services device is that it is being developed to extend the capability of the MARCO Class 1 Filterbelt oil recovery system (or a similar system) to operate in faster currents. Presently, the MARCO device has not been operated successfully in currents in excess of 2.0 to 3.0 fps. The SAI Services control/recovery system has a lower limit of about 2.5 fps and no upper limit

to its ability to operate in fast currents. It is envisioned that the SAI Services control/recovery system can easily be incorporated into the MARCO[6] system or a similar system at a minimal cost, since all of the ancillary functions have been previously developed either under government contract or privately. Thus, the emphasis of this program as it relates to the SAI Services system is to stress the development of the control/recovery functions and to utilize the existing ancillary functions employed on the MARCO system. The end result of this program will be a device that is capable of operating over a wide range of currents and which results in a cost savings to the government since many of the ancillary functions need not be redeveloped.

5.2 Review of Design Goals Based on the Results of the Phase I Program

A revised list of design goals that fairly represent the capability of the SAI Services Fast Current Oil Response System are discussed below.

Areas of Operation - As mentioned earlier, the SAI Services Fast Current Oil Response System can be made in a number of sizes by increasing its width. This flexibility allows it to be used in a wide variety of oil spill operations such as in the U.S. coastal waters, bays, harbors, estuaries and coastal rivers.

Operational Environment - The results of the Phase I tests indicate, as previously discussed, that the system will be

---

[6]Moses, R. and Blackstone, S, "Filter Belt Oil Recovery System," USCG Report CG-D-82-74, December, 1971.

able to operate in currents in excess of about 1.5 knots. At the present time there does not appear to be an upper limit on the current in which the system can operate effectively; however, there may be a practical limit based on the length of belt required for currents in excess of 10 knots. For a fixed length of belt material, a larger water to oil ratio in the collected mixture will result beyond a certain design current.

From our experience during the Phase I program it appears that the device may have some difficulty in operating beyond a sea state 4 condition; however, actual tests will have to confirm this limit. Operation in winds of 20 knots does not appear to be a major problem at the present time; however, more experience with the proposed Phase II design will confirm this speculation also.

Survival Environment - There does not appear to be any serious survival problem in sea state 6 in combination with 40 knot winds since the hydrofoil system and belt can be retracted and secured on the craft under these conditions. The only limitation would be on the catamaran or similar type of craft to be used on the final design of the system.

Oil Quantity and Thickness - If a correctly sized device is used to clean up a particular oil spill, there does not appear to be any limitation of the oil thickness or quantity on its operating characteristics.

Oil Type - For a given porosity belt (such as 10 ppi), the device will operate more efficiently as the viscosity of the oil is increased. That is, a larger oil to water ratio will result in the collected mixture. However, if several types (ppi) of belts are carried with the device, the proper ppi belt can be used for the particular oil to be cleaned up. In general, then, there does not appear to be

any really serious limitation on the oil type that can be recovered with the SAI Services system.

Tides - If the current changes direction the device must be turned in the same direction as the current in order to operate.

Sea Temperature - Water temperature has no effect on the operation of the device, except as it affects the oil viscosity (discussed under oil type).

Air Temperature - Air temperature has no effect on the operation of the device, except as it affects the oil viscosity (discussed under oil type).

Mode of Operation - The design is very flexible and therefore the system can either be moored in a fast moving current and/or towed or propelled through the water.

Transportation from Central Storage to Nearest Port - There does not appear to be any reason why a C-130 aircraft cannot be used to transport almost any size of the SAI Services system, since the device will most probably be modular and can be assembled on site.

Transportation from Nearest Port to Scene - The system, as stated above, is not sensitive to the method of delivery.

Power Supply - Gasoline driven systems will be the preferred mode of power; however, other power systems can be substituted if necessary.

Fuel Supply - There does not appear to be any limitation on the fuel supply so that the system can operate for a period of 12 hours.

System Integrity - There does not appear to be any problem in choosing materials that will withstand the expected environment.

Cleanability - There does not appear to be any problem here either.

System Support - The overall system is reasonably simple and therefore will not have any unusual support requirements.

Control Function - The hydrofoil system has proven to be very effective in reducing the quantity of water that contacts the belt as well as reducing the speed of the incoming flow prior to impacting the polyurethane foam belt.

Oil Recovery Function - Tests at the University of Michigan during Phase I indicated that approximately 80% of the oil was recovered (throughput efficiency). However, there were very real limitations due to polyurethane foam belt length, sump capacity and pumping capacity that SAI Services believes can be easily overcome in the Phase II design. Therefore, 95% recovery efficiency does not appear to be a limitation for the system.

For the same reasons stated above, it is believed that a maximum of 25% water in the recovered mixture does not appear to be out of the operating range of the proposed system.

The GPM rate of recovery is basically controlled by the current velocity, slick thickness and width of the hydrofoil/polyurethane foam belt system. The Phase II system has been designed to handle up to approximately 200 GPM. However, a wider hydrofoil and belt can recover up to the 1,000 GPM limit. The scaling on width of the device is linear with respect to the maximum GPM allowable, so no real problem exists there.

Debris Handling/Protection Functions - These functions will be performed in the same manner as is currently accomplished with the MARCO Class 1 Filterbelt Oil Recovery

system. During the Phase I tests some small debris was successfully recovered; however, further work on this problem will be performed during Phase II.

Pump and Transfer Function - Again these functions will be accomplished in the same manner as in the MARCO Class 1 Filterbelt Oil Recovery system.

Temporary Storage Function - There does not appear to be any problem in this area.

5.3 Discussion of the State of Development of the Ancillary Functions

A visualization of the Phase II system in actual operation is shown in Figure 5.1 and a top view of the overall preliminary design is shown in Figure 5.2. The design is full scale and consists of two basic components, the control/recovery function (hydrofoil system and rotating belt of polyurethane foam) and the support craft/ancillary functions (catamaran hulls and the pump-transfer, temporary storage, debris protection and power supplies). This version of the system is meant to be towed; however, a self powered unit can easily be incorporated into the design. The device operates on the same principle as the Phase I system; however, in that system the hydrofoils and the foam belt were floated as a unit on 1.68 m long pontoons. This system had the disadvantage of not being able to adequately respond to short wavelength waves (~0.60 to 0.90 m). In the current design, this problem has been solved by having the polyurethane foam belt articulated in such a manner as to be capable of following the short wavelength waves (discussed in section 5.5). The only problem

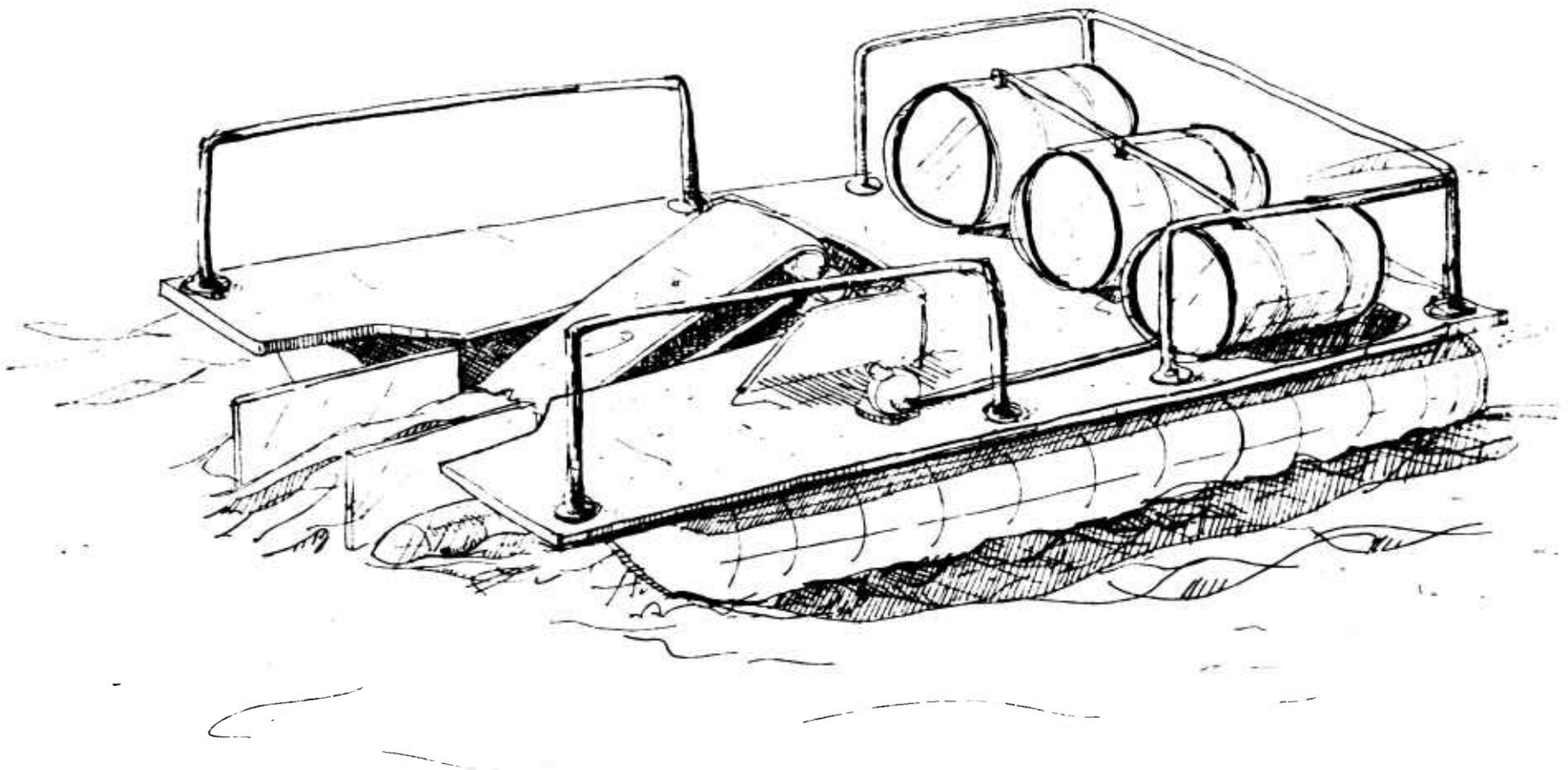

FIGURE 5.1: VISUALIZATION OF THE PHASE II SYSTEM

FIGURE 5.2: TOP VIEW OF PHASE II SYSTEM

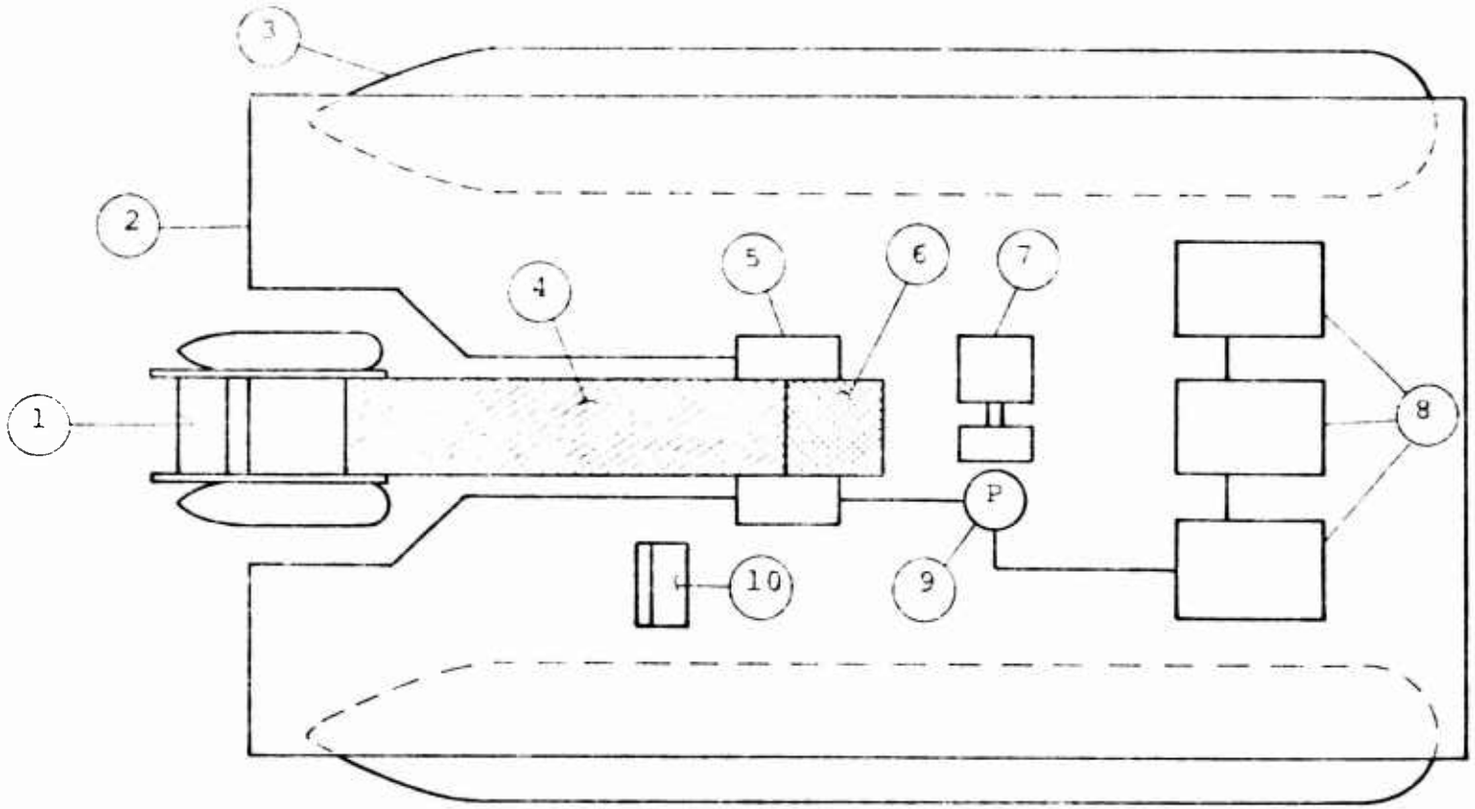

1. Hydrofoil Assembly
2. Catamaran Deck (10 feet wide and 24 feet long)
3. Catamaran Pontoons
4. Polyurethane Foam Belt (1 foot wide and 10 to 15 feet long)
5. Oil Collection Sump (25 gallon capacity)
6. Wire Screen Debris Collection Bin
7. Gasoline Engine Driven Hydraulic Power Unit
8. Oil Collection Reservoir (three 55 gallon steel drums)
9. 100 GPM Oil Collection Pump from Sump to Reservoir
10. Operator's Control Station

that remains is the determination of the method of connecting the hydrofoils to the polyurethane foam belt in a manner that allows the hydrofoils to respond to the waves and yet remain in close proximity to the belt (this will be addressed in section 5.5).

The state of development of the ancillary functions are now discussed in detail:

Control (Hydrofoils)- During the first part of Phase II, further work on the hydrofoil design will be performed. The purpose of this work is to optimize the design of the leading and main hydrofoils so that the minimum operating velocity of the hydrofoil system can be reduced from 4.0 to 2.5 fps. Moreover, the reduction of the remaining oil/water layer over the top surface of the main hydrofoil to a minimum thickness is also a goal of this work. Responding to waves having 0.60 to 0.90 m wavelengths can also be achieved with the Phase II design, thereby minimizing the potential for loss of fluid through the venting slot in choppy water conditions.

Recovery (Rotating Polyurethane Foam Belt)- A completely redesigned foam belt will be employed in the Phase II program. This belt will be approximately 3.65 m in length and will be modeled after the MARCO Class 1 Filterbelt design. As stated previously, the problem of connecting the hydrofoil system to the belt will be addressed during the first part of the Phase II test program (see section 5.5).

The ancillary functions of pump and transfer, temporary storage, debris protection, power supply and seakeeping requirements have all been modeled after the MARCO Class 1 Filterbelt Oil Recovery System for the Phase II program and therefore do not require further discussion at this time. However, during the Phase III program, a MARCO Class 1 unit will be used in conjunction with the SAI Services developed hydrofoil system. The reason for not purchasing the MARCO system at this time is primarily one of cost and flexibility. The cost of the MARCO system is in the neighborhood of $45,000 and does not allow us the flexibility to easily alter its design to an extent which is as yet to be determined during the Phase II program.

5.4 Factors Affecting the Performance of the Large Scale-Prototype System

There are several specific parameters that significantly affect the performance of the large scale-prototype control/recovery functions. These parameters are outlined below and will be addressed during the Phase II program.

Current - Operation in fast currents is the primary requirement for this program. During Phase I, the SAI Services Fast Current Oil Response System was limited to a very small range of currents (4.0 ± 0.5 fps). As explained previously, the lower limit of velocity can be extended to about 2.5 fps by slightly modifying the hydrofoil design. Moreover, at the upper end of the velocity scale, the device can be made to operate efficiently by increasing the polyurethane belt length, sump volume and pumping capacity. These problems have been addressed in the proposed large scale-prototype system design for Phase II (see section 5.5).

Waves - During the Phase I program, the control/recovery device was subjected to waves in the EPA 30.5 m long tow tank as well as in the University of Michigan flume. The only difficulties experienced were with 7.5 to 15.0 cm amplitude chop at wavelengths of approximately 0.3 to 1.80 m. At all other wavelengths larger than 1.8 m, the device was able to conform to the water surface. However, it must be remembered that the control/recovery device was supported by 1.68 m long pontoons, which limited its response capability. In the large scale-prototype design, the hydrofoils will be supported independently of the main portion of the articulated polyurethane foam belt on much smaller pontoons (0.6 to 0.9 m in length), and therefore will be able to respond to the shorter wavelengths. The connection of the hydrofoil system to the polyurethane foam belt then will be a key problem to be addressed with respect to the wave response characteristics of the control/recovery concept. This specific influence has been addressed in the large scale-prototype design.

Oil Film Thickness - This parameter will be addressed again in a more comprehensive manner during Phase II. However, there does not appear to be any problem with encountering varying thicknesses of oil.

Oil Properties - The most important oil related parameter with respect to the SAI Services system is the viscosity of the oil. As the polyurethane foam belt ppi rating increases, this appears to favor the less viscous oils and results in a lower water to oil ratio in the collected samples. For the more viscous oil, a lower ppi foam belt rating is desirable. These facts do not alter the utility of the proposed concept since the foam belt is easily changeable and can be chosen for particular oil spill situations. Additional work will

be performed during the Phase II program with various polyurethane foam belt ppi ratings.

Oil/Water Emulsification - During Phase II, the problem of emulsification will be carefully monitored. However, this did not appear to be a factor in Phase I. Any emulsification that occurred appeared to be a direct result of the pump that was used to drain the oil collection sump. There was also excess water present in the sump during the Phase I tests because of the nonoptimum design of the foam belt system - this will not occur in Phase II.

Debris - Small debris on the order of the width of the polyurethane foam belt is picked up by the moving belt. A system similar to that used by MARCO will be employed to separate and recover that debris. Larger debris that has the potential for damaging some of the system components either will have to be manually diverted from the system, or some protection will have to be provided for the device. This problem will also be addressed during Phase II.

Wind - The problem of the effects of wind on the control/recovery functions has not been addressed to date. However, it is anticipated that as long as the catamaran hull can maintain some level of stability, that there will not be any problem associated with moderate winds.

Sea and Air Temperature - There does not appear to be any problem associated with these parameters other than their influence on the oil viscosity which was addressed earlier.

5.5 Preliminary Design of the Large Scale Model

A visualization of the preliminary design of the large scale fast current oil response system appears in Figure 5.1. This design is full scale and consists of two basic components, the control/recovery function (hydrofoil system and rotating belt of polyurethane foam) and the support craft/ancillary functions (catamaran hulls and pump-transfer, temporary storage, debris protection and power supplies). A top view of the fast current oil response system with its major components and subsystems is shown in more detail in Figure 5.3.

The most important features of the system are items 10 and 11 listed on Figure 5.3. These subsystems comprise the control/recovery function for which some detailed preliminary design has been performed. The remainder of the components (items 1 through 9 on Figure 5.3) are standard off-the-shelf items, and will not be discussed in detail in this report.

The recovery system design consists of the rotating belt of polyurethane foam and its support equipment. After eliminating a number of belt concepts, an articulated belt design (in conjunction with the hydrofoil system) was chosen as the only feasible way to insure that the hydrofoil system would be able to respond to short wavelength waves. The overall design for the articulated belt is shown in Figure 5.4. The details of the belt tensioning device and the articulated-joint belt tensioning slide are shown in Figures 5.5 and 5.6 respectively.

FIGURE 5.3: TOP VIEW OF FAST CURRENT OIL RESPONSE SYSTEM
LARGE SCALE MODEL

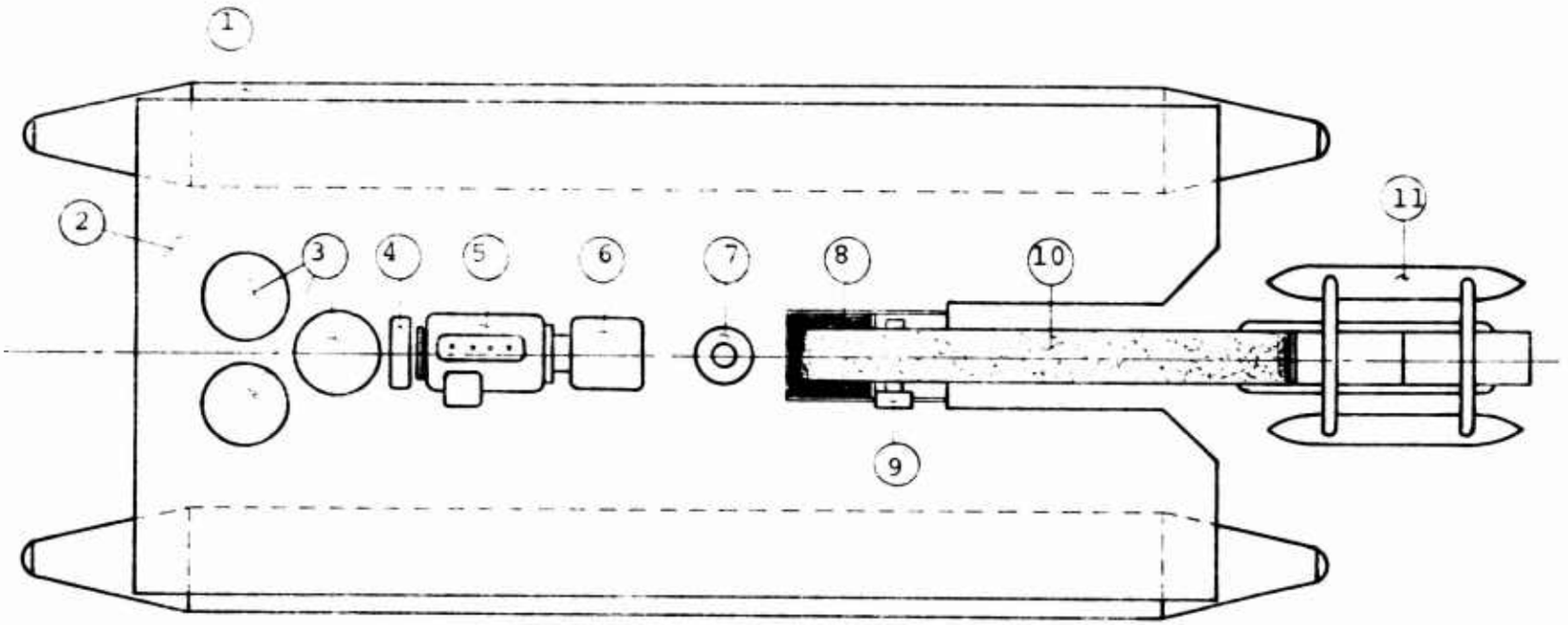

(1) 24'x23" pontoons. Rated capacity=3260 lbs; 10 ft.wide outside dimensions.
(2) Catamaran deck of structural aluminum framework and stretched steel covering.
(3) Oil collection holding tanks (3-55 gal.steel drums).
(4) Radiator.
(5) Diesel engine for all catamaran-skimmer power
(6) Hydraulic power pump.
(7) Sump pump (100 GPM) powered by hydraulic motor.
(8) ~25 gal.sump which doubles as belt boom support frame.
(9) Hydraulic motor for belt.
(10) Control function (Polyurethane foam belt).
(11) Recovery function (hydrofoil system).

0 2 4

FEET

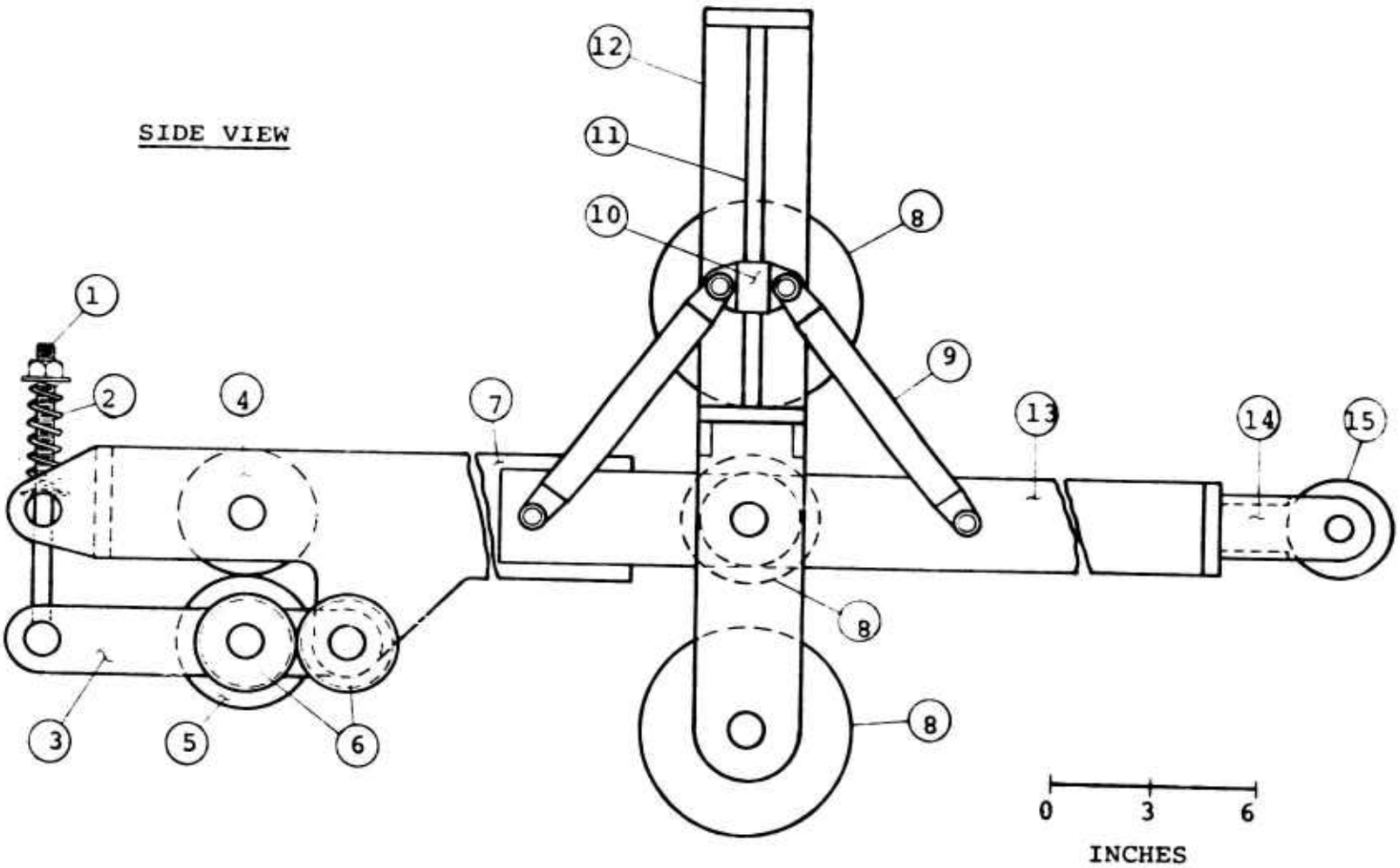

FIGURE 5.4: ARTICULATED POLYURETHANE FOAM BELT PRELIMINARY DESIGN

(See Next Page for Note Descriptions)

NOTE DESCRIPTIONS FOR FIGURE 5.4.

(1) Squeeze roller compression adjustment rod.

(2) Adjustment rod compression spring (~100 lbs/in).

(3) Squeeze roller compression arm.

(4) Drive roller (by chain drive from hydraulic motor on upper boom - not shown for clarity).

(5) Squeeze roller.

(6) Squeeze roller drive gear pair (driver gear at compression arm's pivot is driven by chain drive from drive roller - not shown for clarity).

(7) Upper belt boom (two 4" wide aluminum channel beams internally braced; boom also contains integral belt tensioning device).

(8) Articulation rollers to restrain belt when boom bends (two 6" dia. rollers and one 4" dia. roller).

(9) Articulation rollers' pitch control arm.

(10) Pitch control slide.

(11) Slide bar.

(12) Articulation rollers' support frame.

(13) Lower belt boom.

(14) Forward (or lower) roller support.

(15) Forward roller (3" dia.).

Not Shown: Belt tensioning device placed on upper belt boom.

FIGURE 5.5: BELT TENSIONING DEVICE

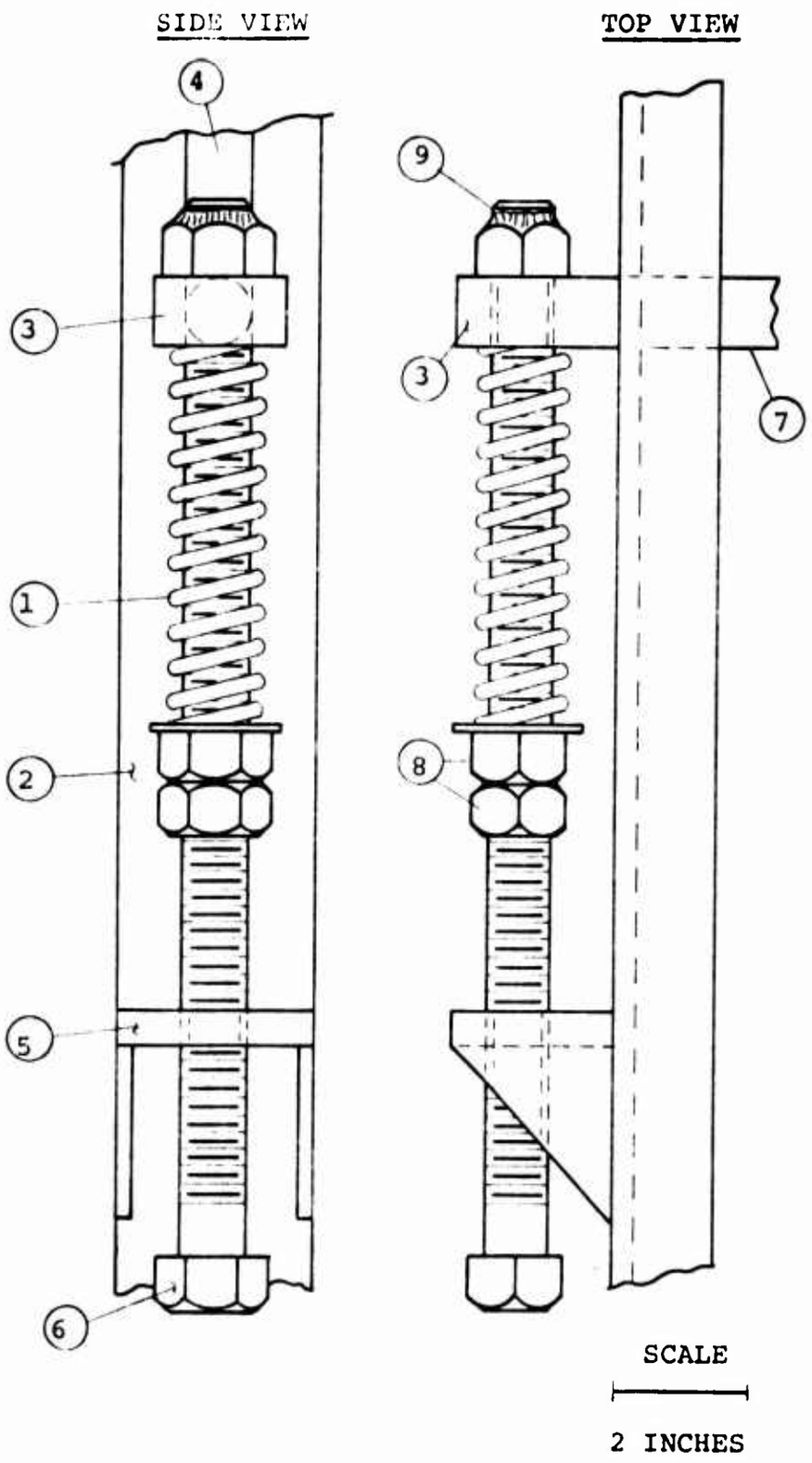

(See Next Page for Note Descriptions)

NOTE DESCRIPTIONS FOR FIGURE 5.5.

(1) Compression spring.

(2) Upper belt boom channel.

(3) Compression spring push block.

(4) Push bar guide slot in channel.

(5) Adjustment screw support (internally threaded).

(6) Adjustment screw.

(7) Push bar.

(8) Positioning jamnuts for compression spring.

(9) Nut welded to end of adjustment screw.

FIGURE 5.6: ARTICULATED-JOINT BELT TENSIONING SLIDE

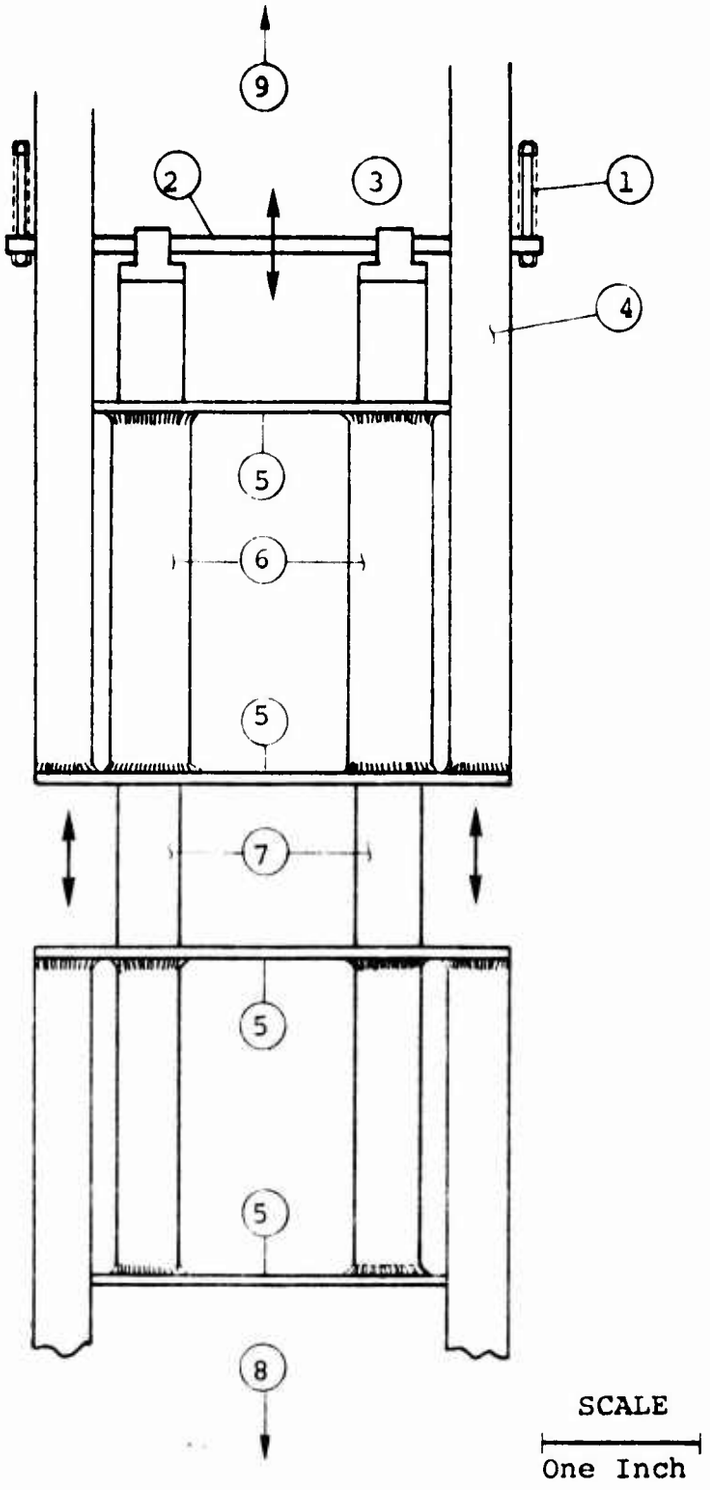

(See Next Page for Note Descriptions)

NOTE DESCRIPTIONS FOR FIGURE 5.6.

(1) Belt tension adjustment springs.

(2) Push bar.

(3) Push bar yoke.

(4) Aluminum channel of upper belt boom.

(5) Support tracing.

(6) Telescoping guide tubes.

(7) Push tubes.

(8) Toward articulation rollers.

(9) Toward drive rollers.

The next major component of the fast current oil response system is the vented hydrofoil system design. The overall design of this device is shown in Figures 5.7(a and b) which are side and top views of the hydrofoils and its support frame. The side view drawing indicates the allowable motion of the lead and main hydrofoils. The overall design of the control/recovery system from the lead hydrofoil to the pivot point on the polyurethane foam belt is shown schematically in Figure 5.8.

Two methods of connecting the pivoted foam belt to the hydrofoil system have been considered. The first technique consists of having the lower portion of the pivoted belt permanently fixed to the hydrofoil system. In this configuration, the hydrofoil's flotation system would support a portion of the foam belt's weight (see Figure 5.9). Moreover, the angle between the main hydrofoil's surface and the foam belt's pivoted section always remains constant. In the second method of connection, the foam belt and the rear of the hydrofoil system are both free to pivot (see Figure 5.10). The flotation system required for this configuration is shorter than that needed in the first method of connection, and is concentrated mainly at the front of the hydrofoil system. However, in this connection scheme, the rear of the hydrofoil must be kept in the vicinity of the foam belt with a flexible connection as shown in Figure 5.11.

The preliminary design for the large scale fast current oil response system has been presented in Figures 5.3 through 5.11. However, the details of this system were addressed only for the control/recovery functions. The reason for this is that they are the most unique in the present system

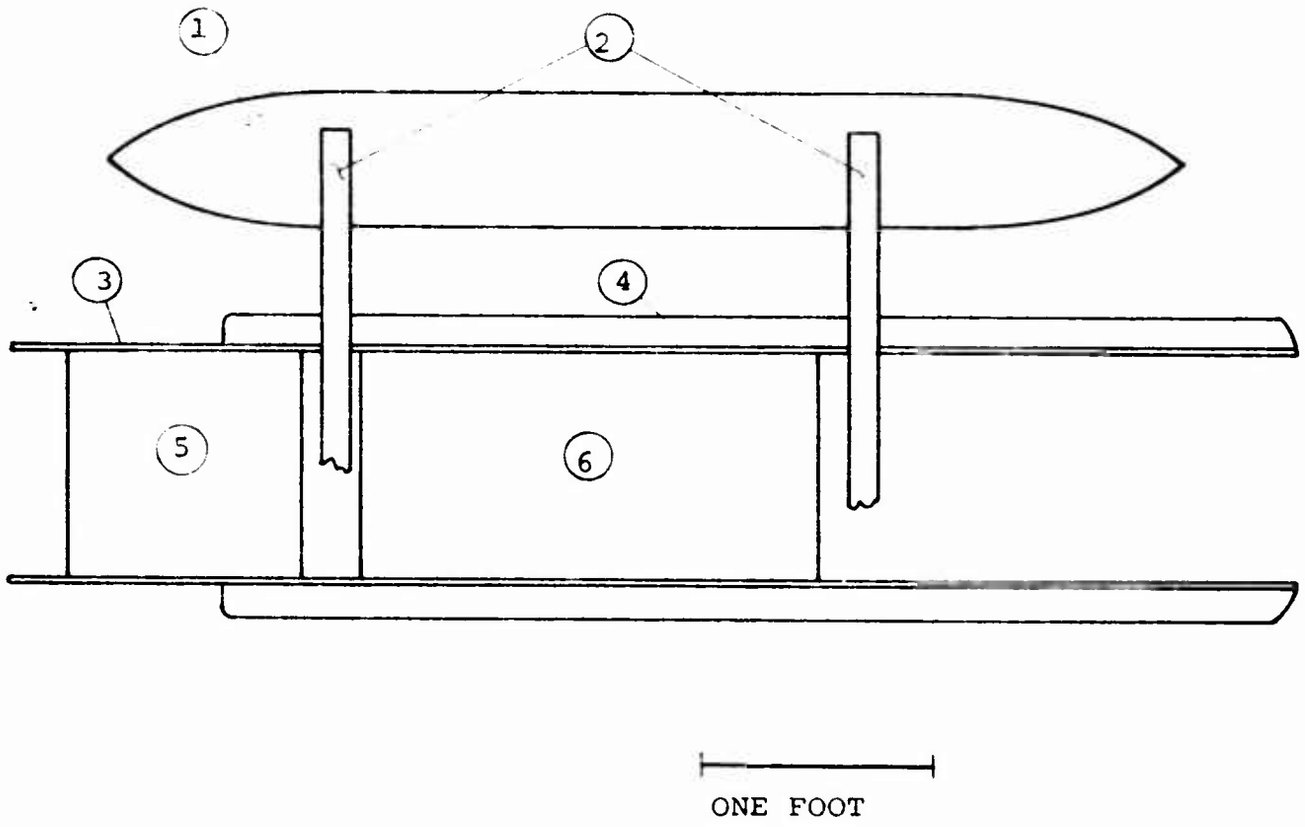

FIGURE 5.7a: OVERALL SCHEMATIC DRAWING OF THE HYDROFOIL SYSTEM (TOP VIEW)

(See Next Page for Note Descriptions)

NOTE DESCRIPTIONS FOR FIGURE 5.7(a).

(1) Float hull.

(2) Hydrofoil to float hull support arms.

(3) Sidewall

(4) Sidewall reinforcement beam.

(5) Lead hydrofoil.

(6) Main hydrofoil.

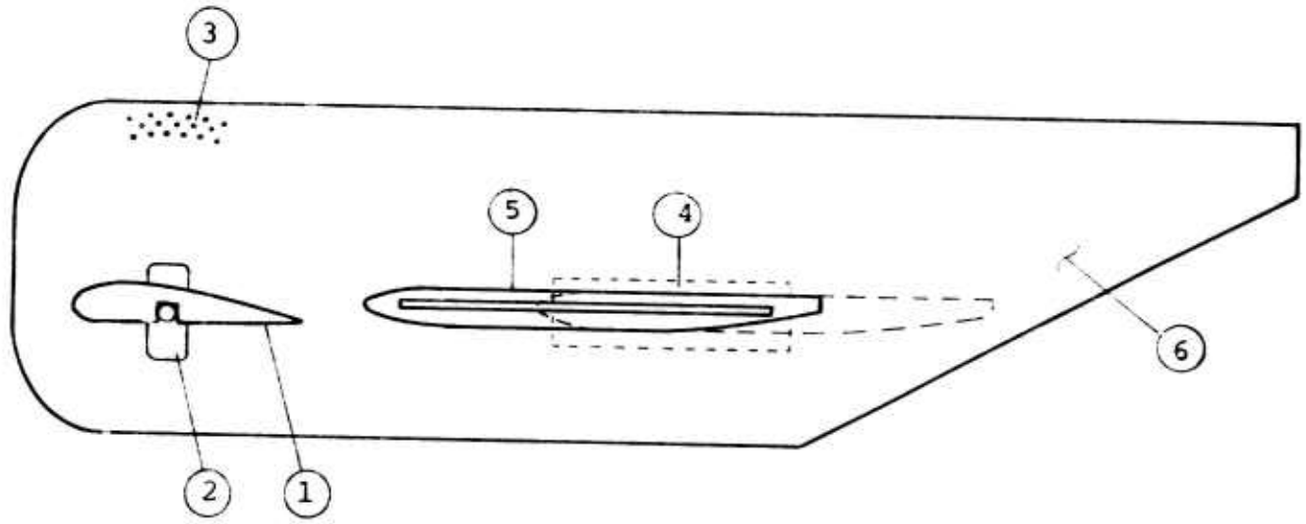

ONE FOOT

FIGURE 5.7b: OVERALL SCHEMATIC DRAWING OF THE HYDROFOIL SYSTEM (SIDE VIEW)

(See Next Page for Note Descriptions)

NOTE DESCRIPTIONS FOR FIGURE 5.7(b).

(1) Lead hydrofoil.

(2) Lead hydrofoil vertical adjustment device ($\pm$ 2.6 in).

(3) Lead hydrofoil angle of attack adjustment ($\pm$10°) holes for locking attack angle adjustment arm.

(4) Main support and horizontal adjustment device.

(5) Maximum limits of main hydrofoil horizontal travel (1.0 to 15 inch separation between foils along the chord lines).

(6) 0.25 in. thick aluminum plate sidewall.

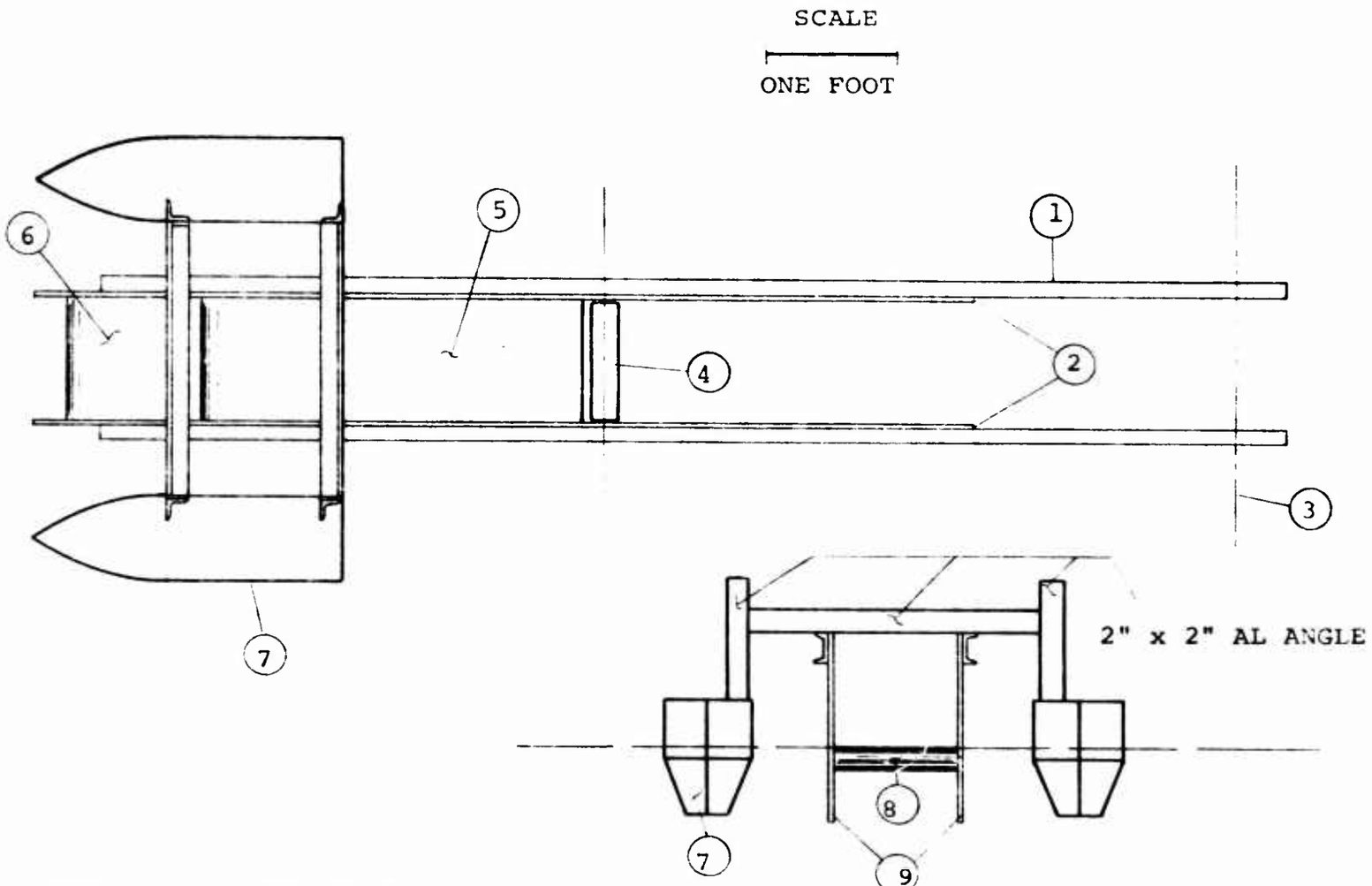

FIGURE 5.8: SCHEMATIC DRAWING OF CONTROL/RECOVERY SYSTEM FROM THE LEAD HYDROFOIL TO THE PIVOT POINT ON THE POLYURETHANE FOAM BELT
(See Next Page for Note Descriptions)

NOTE DESCRIPTIONS FOR FIGURE 5.8.

(1) Skimmer support beam.

(2) Aft end of sidewalls.

(3) Pivot axis.

(4) Forward belt roller position.

(5) Main hydrofoil.

(6) Lead Hydrofoil.

(7) Floats for this configuration.

(8) Hydrofoils.

(9) Sidewalls.

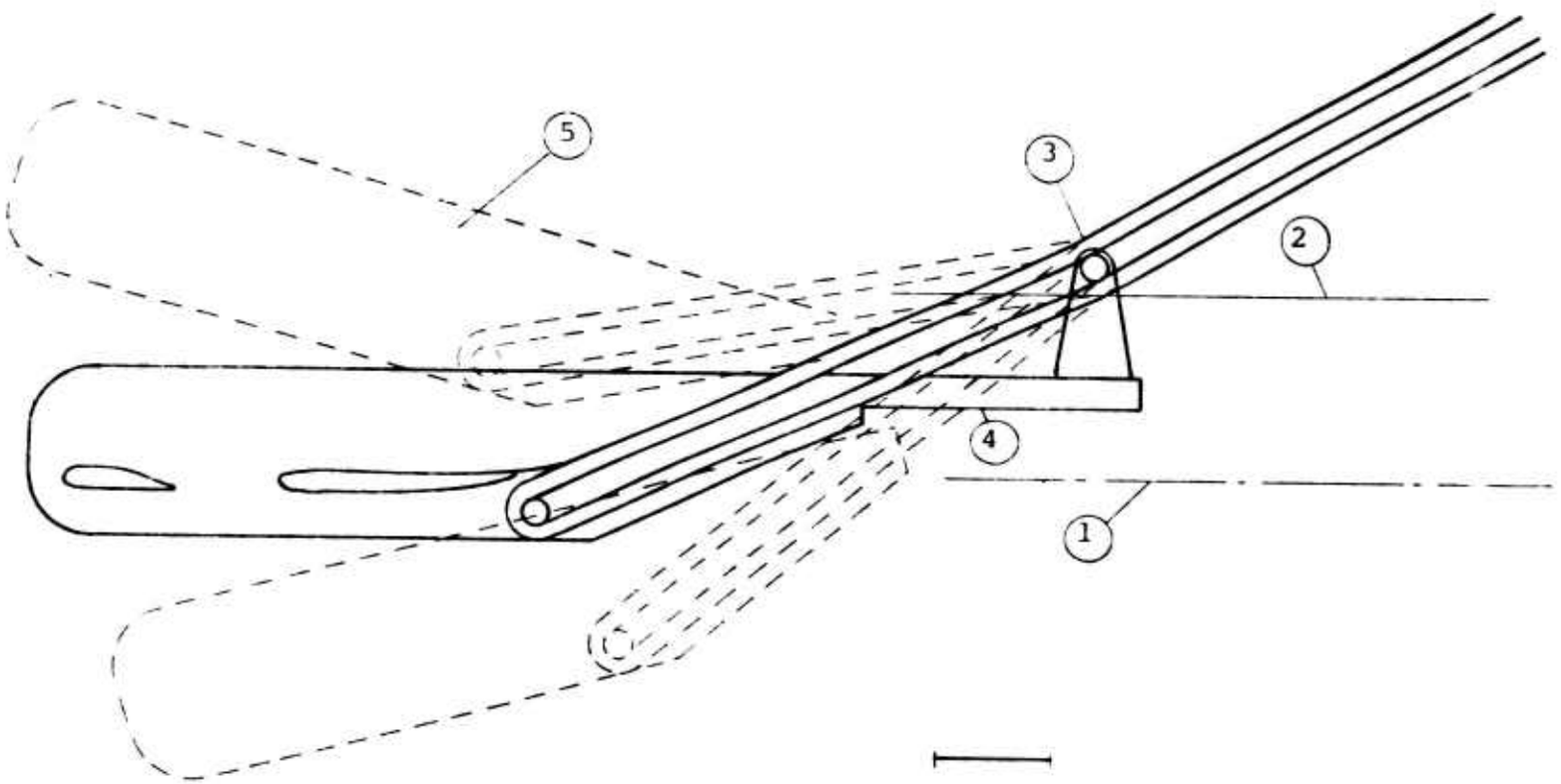

FIGURE 5.9. SCHEMATIC DRAWING OF FIXED-PIVOT CONTROL/RECOVERY SYSTEM

(See Next Page for Note Descriptions)

Note Descriptions for Figure 5.9

1. Normal still water line

2. Approximate deck level (≈ 20 in. from water line)

3. Articulated joint about which the hydrofoil system pivots

4. Foam belt support boom

5. Maximum limits of hydrofoil system travel relative to catamaran (±15°)

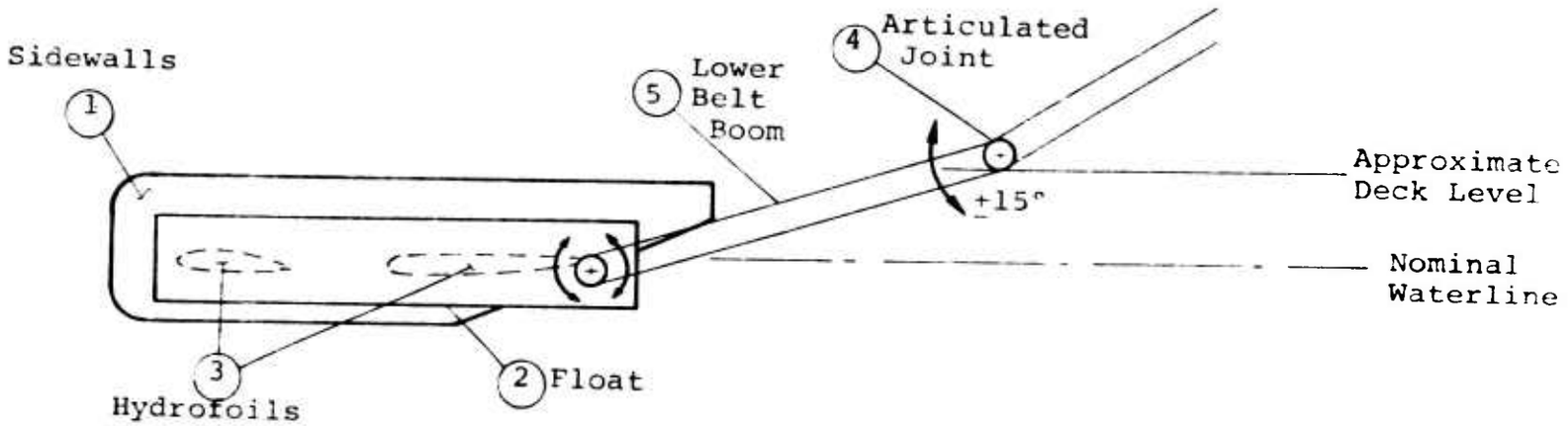

FIGURE 5.10. SCHEMATIC DRAWING OF PIVOT-PIVOT CONTROL RECOVERY SYSTEM

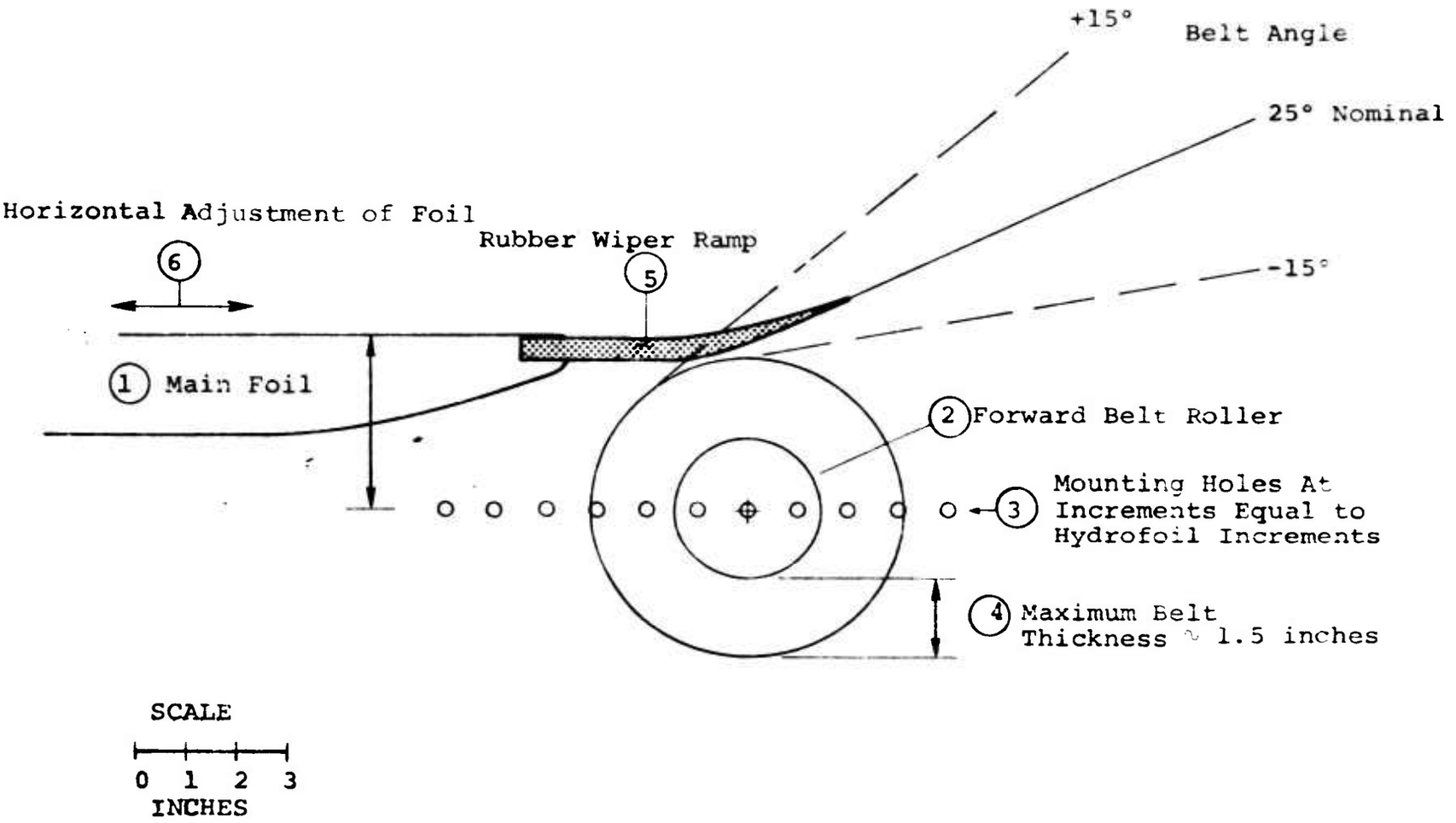

FIGURE 5.11: CONNECTION OF REAR OF HYDROFOIL TO FOAM BELT IN THE PIVOT-PIVOT MODE

and require the most attention. The overall dimensions and specifications for the ancillary functions were described, but not in detail, since they mainly consist of "off-the-shelf" hardware and do not require a detailed design.

SECTION 6

Conclusions

The results of this study have led to the following conclusions for the small scale model hydrofoil experiments:

(1) The important hydrofoil scaling parameters are:

$$F = V/\sqrt{gT} \qquad \text{and} \qquad G_B = gB/V^2$$

(2) Operation of the hydrofoil at high positive freeboard produces a turbulent bow wave and a small amount of flow over the hydrofoil.

(3) Operation of the hydrofoil at lower freeboards causes a transition to a smooth bow wave and increases the flow rate over the hydrofoil.

(4) The point of transition from turbulent to smooth bow wave is determined by model shape and scaling parameters.

(5) Slots in the hydrofoil can bypass some flow from the upper side to the lower side of the hydrofoil, thus reducing the amount of fluid passing over the model's rear portion.

(6) The flow through a slot increases with slot width.

(7) Slot position does not appear to be of major importance in determining total flow through it; however, slot geometry is a significant parameter in this respect.

(8) Operation with an open slot, in some cases, allows a smooth bow wave to form at higher freeboards, whereas with the slot closed, a turbulent bow wave would normally result.

The results of the tow tank experimental program for the full scale control/recovery system lead to these conclusions:

(1) The use of an air jet from either above the hydrofoil surface or from the hydrofoil surface is not effective in producing a directed spray that can be collected by some simple means.

(2) The vented or slotted hydrofoil is very effective in reducing the quantity of flow over the rear of the main hydrofoil in calm, wavy and choppy water conditions.

(3) Momentary venting of all the flow through the slot occurred in very choppy water conditions. However, this is a function of the wave response characteristic of the hydrofoil-pontoon system and can be greatly improved over the Phase I design.

(4) A ramp placed at the rear of the main hydrofoil in combination with the polyurethane foam belt proved to be a very effective control/recovery system.

The data obtained from the University of Michigan test sequence resulted in the following conclusions:

(1) The short polyurethane foam belt restricted the system from operating at velocities much above 4.0 fps. At

the lower end of the velocity spectrum, the system was limited to about 3.5 fps by the particular hydrofoil design. The upper end of the velocity range can be greatly improved (to approximately 10.0 knots) by increasing the length of the belt and the lower end can be reduced to about 1.5 knots by redesigning the hydrofoil.

(2) Insufficient oil/water sump volume combined with a low volume capacity pump inhibited the control/recovery systems performance.

(3) Low oil to water ratio resulted in the collected samples because of the short belt not being able to drain the water through prior to squeezing.

(4) However, an overall throughput efficiency of approximately 80% was achieved with this non-optimum system.

(5) Most of the components of an operational control/recovery system were incorporated in the Phase I design; however, some were undersized as the results of the tests indicate.

(6) This control/recovery system concept appears to be one which can meet the requirements of operating in a fast current environment.

SECTION 7

Recommendations

Based on the extensive experimental program undertaken during Phase I, the following recommendations are made:

(1) Improve the design of the control/recovery system based on the conclusions outlined in section 6.

(2) Perform further testing with the full scale device; in particular, attention should be addressed to operating over a wider range of currents and in waves.

(3) Install the improved control/recovery system on a catamaran hull and demonstrate the feasibility of the control/recovery system and the ancillary functions in an environment respresentative of an actual oil spill.

SECTION 8

References

1. Hale, L. A., Norton, D. J., and Rodenberger, C. A., "The Effects of Currents and Waves on an Oil Slick Retained By a Barrier," USCG Report CG-D-53-75, April, 1974.

2. Wooten, D. C., "Mechanical Control of Oil Spills Utilizing a Streamlined Boom," Proceedings of Joint Conference on Prevention and Control of Oil Spills, March 13-15, 1973, Washington, D.C., pages 383-389 and EPA Report under contract 68-01-0128, December, 1972.

3. Parkin, B. R., Perry, B. and Yao-tsu Wu, T., "Pressure Distribution on a Hydrofoil Running Near the Water Surface," Journal of Applied Physics (1956), Vol. 27, No. 3, pages 232-240.

4. Laitone, E. V., "Limiting Pressure on Hydrofoils at Small Submergence Depths," Journal of Applied Physics (1954), Vol. 25, No. 5, pages 623-626.

5. Abbott, I., von Doenhoff, A., and Stivers, L. S., "Summary of Airfoil Data," NACA Report No. 824, 1945.

6. Moses, R., and Blackstone, S., "Filter Belt Oil Recovery System," USCG Report CG-D-82-74, December, 1971.

GPO 892-394